Christoph Englert

Spin 1 Resonances in Vector Boson Fusion Processes in Warped Higgsless Models

Spin 1 Kaluza-Klein Resonanzen in Vektorboson-Fusionsprozessen in höherdimensionalen Modellen ohne Higgs Boson

Diplomarbeit

Institut für Theoretische Physik
Universität Karlsruhe (TH)

Juli 2007

Referent: Prof. Dr. D. Zeppenfeld
Korreferent: Prof. Dr. U. Nierste

Ich versichere, dass ich diese Arbeit selbständig verfasst und keine anderen als die angegebenen Hilfsmittel benutzt habe.

Christoph Englert
Karlsruhe, den 23. Juli 2007

Als Diplomarbeit anerkannt.

Prof. Dr. Dieter Zeppenfeld
Karlsruhe, den 23. Juli 2007

Contents

Chapter 1
Introduction

The Standard Model of Particle Physics consistently unifies Quantum Chromodynamics (QCD) and Electroweak Theory in terms of a local, spontaneously broken and chiral quantum field theory, based on the gauge group $SU(3)_C \times SU(2)_L \times U(1)_Y$. Up to the accessible energy and length scales, the Standard Model has withstood all experimental tests. The existence of neutral current interactions, the fermion family structure, that is motivated from the theory's anomaly freeness, and the relations between gauge boson masses and couplings are just few examples of Standard Model predictions that agree with measurements to utmost precision. Hence, the Standard Model is widely accepted as the low energy limit of a more fundamental theory, which may be formulated as a spontaneously broken gauge theory.

One crucial increment of the Standard Model, the Higgs boson, a scalar relict of electroweak symmetry breaking that guarantees unitarity in scattering processes, has remained undiscovered so far. This may be considered as the most striking argument against Standard-Model-like symmetry breaking until the Higgs particle's discovery, but there are numerous other flaws that arise along with the Higgs. These caveats have led to a plethora of models 'beyond the Standard Model'.

Besides the 'classical' solutions to electroweak symmetry breaking like the Standard Model, the Minimal Supersymmetric Standard Model and strongly coupled, extended Technicolor models, Little Higgs models and models with extra dimensions gained a lot of theoretical attention. Most radical proposals remove the Higgs completely from the theory's spectrum and leave geometrical constraints that trigger symmetry breaking. These models evade some of the flaws arising from the Higgs mechanism and bear solutions to other Standard Model issues, e.g. the flavour hierarchy. Within this framework, unitarity violation is postponed by the exchange of heavier copies of $W^{\pm}$ and Z bosons to a considerably higher scale compared to the Standard Model without the Higgs particle. The appearance of these particles at the TeV scale, along with their characteristic signatures, can be tested at the *Large Hadron Collider* (CERN).

The subject of this thesis are the Higgsless model's predictions for vector boson fusion processes at the LHC. These processes are sensitive to the mechanism of electroweak symmetry breaking and offer a good signal-to-background ratio after appropriate phase space cuts. Chapter 2 reviews the basics of Standard Model's Higgs sector, stressing the need for a custodial $SU(2)$ and points out solutions to the Standard Model's naturalness problem involving extra dimensions. Chapter 3 introduces gauge symmetry breaking from extra compactified dimensions without fundamental scalars. A realistic model of higgsless electroweak symmetry breaking on an anti-de Sitter background is presented and its UV-completion is discussed. Chapter 4 is devoted to longitudinal gauge boson scattering in the Higgsless model, the model's parameter space is analyzed, and unitary violation bounds are discussed. The Higgsless cross sections are compared to the Standard Model. Chapter 5 covers the phenomenology of Weak Boson Fusion processes (WBF) and comments on the models' implementation into the parton-level Monte Carlo program Vbfnlo, while chapter 6 presents the numerical results of the model's LHC phenomenology. Furthermore, QCD in the Higgsless framework is discussed briefly, and next-to-leading order QCD corrections to weak boson fusion processes in the Higgsless model are presented and discussed. Chapter 7 gives a summary.

Chapter 2
The Minimal Standard Model

2.1 Standard Model Higgs mechanism

The Standard Model of Particle Physics is a chiral product group gauge theory $SU(3)_C \times SU(2)_L \times U(1)_Y$, free of anomalies. Gauge boson masses are incorporated by spontaneous symmetry breaking of the electroweak gauge group $SU(2)_L \times U(1)_Y$ to the gauge group of Quantum Electrodynamics (QED) $U(1)_Q$. The theory's covariant derivative originates from local invariance with respect to gauge transformations (color interactions are neglected in the following)

$$D_\mu = \partial_\mu - igt^a W_\mu^a - ig' Y \mathbb{1} B_\mu \tag{2.1}$$

with $t^a = \sigma^a/2$ for doublets, the generators of the $\mathfrak{su}(2)$ algebra. To trigger spontaneous symmetry breaking, a scalar Higgs field that carries Y-charge $1/2$ and transforms as a doublet under $SU(2)_L$ is introduced.

$$\Phi = \begin{pmatrix} \phi_1 \\ \phi_2 \end{pmatrix}$$

A $SU(2) \times U(1)$ invariant, renormalizable Higgs potential is given by

$$V(\Phi) = \mu^2 \Phi^\dagger \Phi + \lambda (\Phi^\dagger \Phi)^2$$

For $\mu^2 > 0$, this is just a massive gauge-coupled scalar field that is subject to ϕ^4 interaction. There is only the trivial minimum $|\Phi_0| = 0$ and all gauge bosons remain massless. However, if $\mu^2 < 0$, there is going to be a local maximum $|\Phi_0| = 0$ and a non-trivial minimum

$$|\Phi_0| = \left(-\frac{\mu^2}{\lambda}\right)^{1/2} \equiv \frac{v}{\sqrt{2}}$$

A common parametrization of of the fluctuations of Φ around Φ_0 is given by

$$\Phi(x) = \frac{1}{\sqrt{2}} \mathrm{e}^{i\pi^a(x) t^a / v} \begin{pmatrix} 0 \\ v + H(x) \end{pmatrix} \tag{2.2}$$

Linear combinations of the three would-be Goldstone bosons π^a turn into the massive gauge bosons' longitudinal degrees of freedom. In doing so, they decouple from the theory's spectrum: a suitably chosen local $SU(2)$ transformation rotates the Goldstone fields away in (2.2). Gauge transformations along $t^3 + \mathbb{1}$ leave the vacuum invariant, signalizing an unbroken $U(1)$ gauge symmetry associated with this direction. The corresponding gauge field remains massless and will be interpreted as the physical photon. Inserting (2.2) into the kinetic term of the Higgs field yields

$$|D_\mu \Phi_0|^2 = \frac{1}{2}(\partial_\mu H)^2 + \frac{g^2}{4}(v+H)^2 W_\mu^+ W^{-\mu} + \frac{g^2+g'^2}{8}(v+H)^2 Z_\mu Z^\mu \tag{2.3}$$

with

$$W_\mu^\pm = \frac{1}{\sqrt{2}}\left(W_\mu^1 \mp i W_\mu^2\right) \qquad Z_\mu = \frac{1}{\sqrt{g^2+g'^2}}(g W_\mu^3 - g' B_\mu)$$

From (2.3) one can infer the gauge boson masses

$$m_W = \frac{gv}{2} \qquad m_Z = \frac{\sqrt{g^2+g'^2}\,v}{2}$$

(W_μ is a complex, Z_μ is a real field). The linear combination orthogonal to Z_μ

$$A_\mu = \frac{1}{\sqrt{g^2+g'^2}}(g' W_\mu^3 + g B_\mu)$$

is massless according to (2.3), as expected. Written in terms of the mass eigenstates, the covariant derivative reads

$$\begin{aligned} D_\mu = \partial_\mu - \frac{ig}{\sqrt{2}} t^+ W_\mu^+ - \frac{ig}{\sqrt{2}} t^- W_\mu^- - \frac{i}{\sqrt{g^2+g'^2}}(g^2 t^3 + g'^2 Y \mathbb{1}) Z_\mu \\ - \frac{igg'}{\sqrt{g^2+g'^2}}(t^3 + Y\mathbb{1}) A_\mu \end{aligned}$$

with $t^\pm = t^1 \pm i t^2$. The coupling of the massless A_μ can be identified as the QED coupling

$$e = \frac{gg'}{\sqrt{g^2+g'^2}} \qquad Q = t^3 + Y\mathbb{1} \tag{2.4}$$

Thus, $W^\pm, Z$, and A carry $Q = \pm 1, 0$, respectively, as they are eigenstates of $t^3_{\text{adj}} = \text{diag}(-\sigma^2, 0)$ and $Y(W^a, B) = 0$. The transformation $\{W_\mu^3, B_\mu\} \to \{Z_\mu, A_\mu\}$ is a twodimensional, real isometry that is fixed by the single electroweak mixing angle

$$\cos\theta_w = \frac{g}{\sqrt{g^2+g'^2}} \qquad \sin\theta_w = \frac{g'}{\sqrt{g^2+g'^2}}$$

With the definition of θ_w the covariant derivative can be written

$$D_\mu = \partial_\mu - \frac{ig}{\sqrt{2}}(t^+ W_\mu^+ + t^- W_\mu^-) - \frac{ig}{\cos\theta_w}(t^3 - Q\sin^2\theta_w) Z_\mu - ieQA_\mu \tag{2.5}$$

The Higgs' mass and self-interaction can be read off the potential

$$V(H) = -\frac{\lambda v^2}{2}(v+H)^2 + \frac{\lambda}{4}(v+H)^4 = V_0 + \lambda v^2 H^2 + \lambda v H^3 + \frac{\lambda}{4} H^4 \tag{2.6}$$

The Euler-Lagrange equations only contain derivatives with respect to the fields, so constants V_0 do not contribute to the theory's dynamics and can be dropped in (2.6). The Higgs' mass is $\sqrt{2}\lambda v$, its charge, according to (2.4), is zero.

2.2 Gauge boson masses and custodial $SU(2)$

As a result of spontaneous symmetry breaking the gauge boson masses obey

$$\rho = \frac{m_W}{m_Z \cos\theta_w} \equiv 1 \tag{2.7}$$

This relation, with small corrections by loop effects, along with predictions of the charged- and neutral-current interactions (2.5) have been confirmed experimentally with a precision better than a permille [1]. A theory that contains the Standard Model as a limit should reproduce (2.7) in a natural fashion. (2.7) is a consequence of a global $SU(2)$ symmetry of the Higgs sector after symmetry breaking, referred to as 'custodial' $SU(2)$. This symmetry can be anticipated from the form of Higgs potential and Higgs kinetic term, written in terms of the real components of the doublet, e.g.

$$\Phi^\dagger\Phi = (\Re\{\phi_1\})^2 + (\Im\{\phi_1\})^2 + (\Re\{\phi_2\})^2 + (\Im\{\phi_2\})^2$$

The Higgs sector is invariant under the action of the group of orthogonal, fourdimensional transformations $O(4)$. Whereas this Lie group is not simple, it's Lie Algebra is isomorphic to the Lie Algebra of the simple group $SU(2)\times SU(2)$. After the Higgs has acquired a vacuum expectation value, the $O(4)$ gets broken down to $O(3) \simeq SU(2)$, leaving $SU(2)$ as a global symmetry. More technically, the twodimensional representation of $SU(2)$ is symplectic, that is, fundamental and complex conjugate module are isomorphic and there is an invariant, two-component, anti-symmetric tensor ε that transforms the modules into each other [2]. Conventionally, this tensor is chosen to be the twodimensional Levi-Cività $\varepsilon = i\sigma^2$. Both $\varepsilon\Phi^\star$ and Φ are vectors of the fundamental representation (but $\varepsilon\Phi^\star$ carries hypercharge $-1/2$) and every normalized combination of them transforms accordingly. Thus, there is a global $SU(2)$ that mixes the vectors. With the definition

$$\mathcal{H} = (\varepsilon\Phi^\star, \Phi) = \begin{pmatrix} \phi_2^\star & \phi_1 \\ -\phi_1^\star & \phi_2 \end{pmatrix}$$

$\Phi^\dagger\Phi$ is equal to $\mathrm{Tr}(\mathcal{H}^\dagger\mathcal{H})$. Neglecting constants $\sim v^2$, the Higgs potential (2.2) reads

$$V(\mathcal{H}) = \lambda\left(\mathrm{Tr}\{\mathcal{H}^\dagger\mathcal{H}\} - \frac{v^2}{2}\right)^2$$

which is now manifestly invariant under $SU(2)_L \times SU(2)_R$

$$\mathcal{H} \to U_L \mathcal{H} U_R^\dagger$$

The vacuum expectation value of the Higgs field $\mathrm{diag}(v, v)$ breaks the symmetry down to the diagonal group $SU(2)_D$, all gauge boson masses m_{W^a} are identical, as they form a triplet under the diagonal transformations. And as the Z mass eigenstate is rotated by θ_w with respect to W^3, (2.7) follows immediately.

$SU(2)_R$ is actually *not* exact. Φ and $\varepsilon\Phi^\star$ have different hypercharges, thus gauging $U(1)_Y$ will break $SU(2)_R$. In addition, Φ and $\varepsilon\Phi^\star$ are used to assign different masses to up- and down-type fermions, which also leads to an explicit breaking of custodial symmetry by the Yukawa sector. For the Yukawa couplings and g' being small, the breaking is only small, and (2.7) is still satisfied approximately.

The relation of tree-level W/Z mass-ratio and custodial $SU(2)$ is not characteristic to the Higgs mechanism, but it is generic to the symmetry breaking pattern $(SU(2)_L \times SU(2)_R)/SU(2)_D$, which is generally analyzed in terms of a non-linear sigma model. The breaking is triggered by the field

$$\mathcal{H} = \frac{v}{\sqrt{2}} \mathrm{e}^{i\pi^a\sigma^a/v} \begin{pmatrix} 1 & 0 \\ 0 & 1 \end{pmatrix} \tag{2.9}$$

The Goldstone fields are parametrized by the unitary matrix $\Sigma = \exp(i\pi^a\sigma^a/v)$, the non-linear sigma field. Under the unbroken transformations $SU(2)_D$, $\mathcal{H}$ transforms

$$\mathcal{H} \to U_D \mathcal{H} U_D^\dagger = U_D \Sigma U_D^\dagger U_D \mathcal{H}_0 U_D = U_D \Sigma U_D^\dagger \mathcal{H}_0 = \exp\left\{ iU_D \pi U_D^\dagger \right\} \mathcal{H}_0$$

with $\mathcal{H}_0 = \mathbb{1}v/\sqrt{2}$. This implies for the Goldstone fields

$$\pi^a \to \frac{1}{2} \mathrm{Tr} \left\{ U_D t^b U_D^\dagger t^a \right\} \pi^b = R^{ab} \pi^b$$

with $R \in SO(3)$, that is, they form a triplet under $SU(2)_D$. Under the broken, non-diagonal transformations one has

$$\Sigma \to U_L \Sigma U_R^\dagger = U_L \Sigma U_L^\dagger U(\vec{\alpha})$$

where the group properties have been used. Thus, to linear order

$$\vec{\pi} \to R\vec{\pi} + \vec{\alpha}$$

that is the π^a transform non-linear under the broken transformations, which forbids Goldstone masses. Using the covariant derivative (2.1) with $U(1)_Y \subset SU(2)_R$, the σ-field kinetic term expanded into powers of the πs reads

$$\begin{aligned} &\frac{v^2}{4} \mathrm{Tr}\{D_\mu \Sigma^\dagger D^\mu \Sigma\} \\ &\quad = \frac{1}{2} \partial_\mu \vec{\pi}^\dagger \partial^\mu \vec{\pi} + \frac{v^2 g^2}{8} W_\mu^a W^{a\mu} - \frac{v^2 g g'}{4} W_\mu^3 B^\mu + \frac{v^2 g'^2}{8} B_\mu B^\mu \\ &\quad + \text{higher orders} \end{aligned}$$

Diagonalizing yields the desired W/Z mass ratio.

2.3 Standard Model fine-tuning

The Standard Model exhibits numerous flaws. For example, electroweak symmetry breaking is not explained but ad hoc realized by introducing a scalar field with quartic coupling and tachyonic mass. The vacuum energy density inferred from the Higgs'

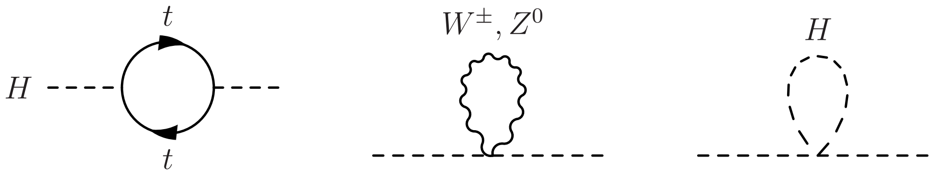

Figure 2.1: Dominant Feynman graphs for the radiative corrections to the Higgs-two-point-function at next-to-leading order perturbation theory.

vacuum expectation value shows a mismatch with measurements of the cosmological constant at a level of 10^{54}, which can not be overcome by merely redefining the energy's zero [3]. Despite those reasons, the main motivation for building models beyond the Standard Model is constructing solutions to the so-called 'strong fine-tuning problem' that arises from generic radiative instability of fundamental scalars in non-supersymmetric theories. Naively, as the mass dimension of the Higgs field is $[H] = 1$, the Higgs two-point-function is quadratically divergent. The dominant contributions at next-to-leading-order stem from top quark, $SU(2)$ gauge bosons and the Higgs itself (figure 2.1). If a cut-off Λ is used to regularize the divergent loop integrals, the quadratic Higgs mass will be shifted by

$$m_H^2 - m_H^{0\,2} = \frac{3g^2}{32\pi^2}\frac{\Lambda^2}{m_W^2}\left(2m_W^2 + m_Z^2 + m_H^2 - 4m_t^2\right) \tag{2.10}$$

If $\Lambda \sim M_{\mathrm{Pl}} \approx 10^{19}$GeV [1], stabilizing the electroweak scale $v \approx 246$GeV requires the right side to be tuned to the 32nd digit. And as there is no symmetry of the Standard Model that guarantees the cancellation of (2.10), electroweak symmetry breaking at the TeV scale from a fundamental scalar field seems to be unnatural [4]. Approaches to solve the observed hierarchy $M_{\mathrm{Pl}} \gg v$ can be anticipated from the condition (2.10): Supersymmetric extensions of the Standard Model guarantee such cancellations due to an enlarged particle spectrum with identical couplings arising from Bose-Fermi-symmetry [5]. The realization of the Higgs boson as a pseudo-Nambu-Goldstone boson that acquires mass from radiative and collective symmetry breaking in Little Higgs models does not suffer from quadratic divergences and has only a logarithmic dependence on the cut-off scale [6].

Another possibility to get rid of the Hierarchy problem is to dilute the fundamental cut-off scale to the TeV region by introducing extra dimensions. This is done using a larger number of flat extra dimensions (known as the ADD-scenario [7]) or only one additional dimension with a non-factorizable anti-de Sitter (AdS) background geometry (known as the RS-scenario [8]). As nature is manifestly fourdimensional at the accessible energy scales, higherdimensional Lorentz invariance has to be broken down to its $4d$ subgroup. That is, the extra dimensions are not allowed to be infinite but have to be compact. The fundamental, higherdimensional Planck scale will be lowered as result of a large compactified volume (ADD) or will only appear to be large because of an AdS-suppressed coupling of gravity to matter, that is, the RS-scenario states that

[1]The effects of gravitation, becoming sizable at the Planck scale at the latest, must not be neglected and the Standard Model has to be UV-completed.

gravity is strongly located in an inaccessible region of the higherdimensional space. The main features of these proposals are based upon the the ideas of Theodor Kaluza and Oskar Klein, who tried to unify fourdimensional gravity and electromagnetism to a higherdimensional theory of gravity [9].

Arkani-Hamed Dimopoulos Dvali models (ADD)

Based on Klein's idea of compactifying the extra dimensions on circles S^1, making them invisible to experiments at distances larger than the compactification radii r_c by Gauss' law

$$V(r) \sim \begin{cases} -\dfrac{m_1 m_2}{M_{\mathrm{Pl},4+n}^{2+n} r_c^n}\dfrac{1}{r} & r \gg r_c \\ -\dfrac{m_1 m_2}{M_{\mathrm{Pl},4+n}^{2+n}}\dfrac{1}{r^{n+1}} & r \ll r_c \end{cases}$$

Arkani-Hamed, Dimopoulos and Dvali embedded the Standard Model strictly localized on an 3+1 dimensional subspace ('3-brane') in the higherdimensional spacetime $M^4 \times T^n$. As gravity is the consequence of spacetime symmetry, it will propagate in all $4+n$ dimensions. Hence, the action divides into a Einstein-Hilbert bulk and a Standard Model brane piece

$$\int\limits_{M^4\times T^n} \mathrm{d}(x,y)\sqrt{-g_{4+n}}\left\{M_{\mathrm{Pl},4+n}^{(n+2)} R_{4+n} + \mathcal{L}_{\mathrm{SM}}\delta\left((x,y)-\{M^4\}\right)\right\}$$

where g_{4+n} is the determinant of the metric g_{MN} $(M,N = 1,\ldots,4+n)$ and R_{n+4} is the higherdimensional Ricci scalar. In the linearized approximation

$$\mathrm{d}s^2 = (g_{\mu\nu}+h_{\mu\nu})\mathrm{d}x^\mu \mathrm{d}x^\nu - r_c^2 \mathrm{d}\Omega_{(n)} \tag{2.11}$$

after integrating out the compactified directions, the bulk action reads

$$\int\limits_{M^4\times T^n} \mathrm{d}(x,y)\sqrt{-g_{4+n}} M_{\mathrm{Pl},4+n}^{n+2} R_{4+n} = M_{\mathrm{Pl},4+n}^{n+2}(2\pi r_c)^n \int\limits_{M^4} \mathrm{d}x\,\sqrt{-\bar{g}_4}\bar{R}_4(\bar{g}_4) + \ldots \tag{2.12}$$

that is a fourdimensional Einstein-Hilbert action with Planck mass

$$M_{\mathrm{Pl},4}^2 = M_{\mathrm{Pl},4+n}^{n+2}(2\pi r_c)^n$$

Compactification on a torus allows for an expansion of the metric into a Fourier series, and in (2.12) only the zero-mode of the $h_{\mu\nu}$ is given [10]. The Hierarchy problem will disappear, if the fundamental Planck scale (the ultimate cut-off in (2.10)) $M_{\mathrm{Pl},4+n} \sim \mathcal{O}(1\mathrm{TeV})$ and the compactified volume is large enough to have $M_{\mathrm{Pl},4} \sim \mathcal{O}(10^{19})\mathrm{GeV}$. Of course, the Hierarchy problem is more hidden in the choice of r_c than solved, the ADD-model still needs a mechanism that stabilizes the size of the extra dimensions in (2.11).

Provided such a mechanism exists, a single extra dimension $r_c = 3\times 10^{12}\mathrm{m}$ is ruled out by solar system observations; a recent analysis of gravity's inverse square law [1] yields $r_c < 0.22\mathrm{mm}$, $M_{\mathrm{Pl},6} \geq 1.1\mathrm{TeV}$ for two equal-sized extra dimensions.

Randall Sundrum models (RS)

The model of Randall and Sundrum takes a different approach. The main assumption is a single extra dimension compactified on an $S^1/\mathbb{Z}_2$ orbifold (the extra dimension exhibits the symmetry properties $y \sim y + 2\pi r_c$ and $y \sim -y$), with two 3-branes located at the orbifold fixed points 0 and πr_c that extend in x^μ direction and support fourdimensional Lorentz-invariant field theories. The Standard Model is located on the TeV-brane πr_c (the visible brane in RS language), so there is again a gravity-only bulk

$$
\begin{aligned}
S &= S_{\text{bulk}} + S_{\text{TeV}} + S_{\text{hid}} \\
S_{\text{bulk}} &= \int \mathrm{d}^4x \int \mathrm{d}y \sqrt{-g}\left\{-\Lambda + M_{\text{Pl},5}^3 R_5\right\} && \text{(2.13a)} \\
S_{\text{TeV}} &= \int \mathrm{d}^4x \sqrt{-g_{\text{TeV}}}\left\{\mathcal{L}_{\text{SM}} + V_{\text{TeV}}\right\} && \text{(2.13b)} \\
S_{\text{hid}} &= \int \mathrm{d}^4x \sqrt{-g_{\text{hid}}} V_{\text{hid}} && \text{(2.13c)}
\end{aligned}
$$

The bulk and boundary cosmological terms are needed for the solution to respect $4d$ Lorentz invariance. Using the Einstein equations to match $g_{\text{TeV}} = g(x^\mu, \pi r_c)$, $g_{\text{hid}} = g(x^\mu, 0)$, Randall and Sundrum obtained a metric which turned out to be a slice of a fivedimensional anti-de Sitter space [8]

$$\mathrm{d}s^2 = \mathrm{e}^{-2kr_c\phi} g_{\mu\nu}\mathrm{d}x^\mu \mathrm{d}x^\nu - r_c^2 \mathrm{d}\phi^2 \tag{2.14}$$

k, the $5d$ curvature, is a free parameter in the model. With the TeV-metric $g_{\text{TeV}} = \mathrm{e}^{-kr_c\pi} g_{\mu\nu}$, the Standard Model action reads

$$S_{\text{SM}} \supset \int \mathrm{d}^4x \left\{ D^\mu \tilde{H} D_\nu \tilde{H} - \lambda\left(\tilde{H}^2 - \left[\mathrm{e}^{-kr_c\pi} v\right]^2\right)\right\} \tag{2.15}$$

To have the Higgs field canonically normalized, it has been rescaled $\tilde{H} = \mathrm{e}^{-kr_c\pi} H$. The result of (2.13)-(2.15) is that TeV-brane-located mass parameters get 'warped down' by an exponential factor $\tilde{m} = \mathrm{e}^{-k\pi r_c} m$, whereas the $4d$ effective Planck scale remains almost unchanged

$$M_{\text{Pl},4}^2 = M_{\text{Pl},5}^3 \frac{1 - \mathrm{e}^{-2k\pi r_c}}{k} \tag{2.16}$$

Given a suitable size of the extra dimension (e.g. stabilized by the Goldberger-Wise mechanism [11]), all fundamental parameters of the theory can be $\mathcal{O}(M_{\text{Pl}})$. For a TeV-brane-located observer, nevertheless, the mass parameters seem to be $\sim$TeV because gravity is weakly coupled to matter there.

The coordinate transformation $y = \mathrm{e}^{kr_c\phi}/k$ yields another, often-used parametrization of the AdS_5-metric (2.14)

$$\mathrm{d}s^2 = \frac{1}{k^2 y^2}\left(g_{\mu\nu}\mathrm{d}x^\mu \mathrm{d}x^\nu - \mathrm{d}y^2\right) \tag{2.17}$$

Chapter 3

Higgsless Symmetry Breaking

3.1 Symmetry breaking from extra dimensions

3.1.1 Gauge theories with extra compactified dimensions

Starting point is a pure fivedimensional, non-abelian gauge theory in flat space that includes a single compactified dimension[1]. Compactification (thereby breaking of higherdimensional Lorentz invariance) is obtained by choosing a closed, real-valued interval as fifth dimension.

$$S_5 = \int_{M^4} \mathrm{d}^4x \int_R^{R'} \mathrm{d}y \left\{ -\frac{1}{4} F^{aMN} F^a_{MN} \right\} = \int \mathrm{d}^5x \left\{ -\frac{1}{4} F^{a\mu\nu} F^a_{\mu\nu} - \frac{1}{2} F^{a\mu 5} F^a_{\mu 5} \right\} \tag{3.1}$$

F^a_{MN} is the five-dimensional analog of the familiar fourdimensional field strength tensor

$$F^a_{MN} = \partial_M A_N(x,y) - \partial_N A_M(x,y) + g_5 f^{abc} A^b_M(x,y) A^c_N(x,y)$$

The $5d$ vector field decomposes under the action of the unbroken $4d$ Lorentz group into a $4d$ vector A^a_μ and a $4d$ scalar A^a_5, mixing between them has been made explicit in (3.1). Just as in $4d$, pure gauge theories in $5d$ are ill-defined unless the gauge is fixed. Technically, this is because the free theory's defining functional

$$\mathcal{Z}_0[J] = \int \mathcal{D}A^a_M \exp\left\{ iS_{\mathrm{cl}}[A^a_M]\big|_{\mathrm{quadratic}} + i \int \mathrm{d}^n x\, J^{aM}(x) A^a_M(x) \right\} \tag{3.2}$$

which is required to solve the interacting theory perturbatively, comprises integration over gauge-equivalent field configurations. The standard method to overcome this obstacle, known as De Witt-Faddeev-Popov-approach, is to define a section on the gauge orbit (that is 'fixing the gauge') [12], which is strictly speaking only possible in the perturbative regime. Doing so, the integration over the gauge group in (3.2) will factorize and one defines a new generating functional by omitting the gauge group integration. This new generating functional is 'well-defined', but there are remnants of the gauge fixing, occurring as additional terms in the action of (3.2): so-called ghost fields and the section's definition. The ghost fields are indispensable in quantized non-abelian gauge theories as they serve as negative degrees of freedom to cancel the unphysical polarizations of the gauge bosons, but they do not occur as asymptotic states of the S-matrix.

[1] A generalization to an arbitrary number of extra dimensions is straightforward.

In quantized abelian gauge theories they are redundant as there are gauge fixing conditions, which allow to integrate out the ghosts, so that they no longer participate in the theory's dynamics.

In (3.1), however, one is dealing with an additional *compactified* dimension, so finding a section that simplifies the calculations is slightly more involved than it is with pure $4d$ gauge theories. It was already mentioned that the $5d$ theory on the interval involves mixtures of $4d$ vectors and scalars. Fortunately, the situation is quite similar to the one encountered in the Standard Model, where Fujikawa-Lee-Sanda R_ξ gauges [13] are used to cancel the mixing of the would-be Goldstone and the gauge fields. Hence, mimicking the Standard Model's fixing hints at a solution. In the following the ghosts are neglected, they decouple in unitary gauge $\xi \to \infty$ except for loop effects, which are not discussed. The mixing of A^a_μ and A^a_5, quadratic in the fields, suppressing integration, reads

$$-\frac{1}{2}\left(\partial_\mu A^a_5 - \partial_5 A^a_\mu\right)\left(\partial^\mu A^{a5} - \partial^5 A^{a\mu}\right) = -\frac{1}{2}\left(\partial_\mu A^a_5 \partial^\mu A^{a5} + \partial_5 A^a_\mu \partial^5 A^{a\mu}\right) + \partial_5 A^a_\mu \partial^\mu A^{a5}$$

The term in the last line turns out to be more handy after partial integration

$$\int \mathrm{d}^5x\, \partial_5 A^a_\mu \partial^\mu A^{a5} = -\int \mathrm{d}^5x\, \partial_\mu A^{a\mu}\partial_5 A^a_5 + \int \mathrm{d}^4x\, [\partial_\mu A^{a\mu} A^a_5]^{R'}_R$$

In the spirit of R_ξ gauges the bulk-gauge fixing action

$$S_{\mathrm{gf,bk}} = -\int \mathrm{d}^5x\, \frac{1}{2\xi}\left(\partial_\mu A^{a\mu} - \xi \partial_5 A_5\right)^2$$

is introduced. The bulk gauge-fixed action, that mixes $4d$ scalar and vector fields is now

$$\begin{aligned} S_{2,\mathrm{mix}} + S_{\mathrm{gf,bk}} = & -\frac{1}{2}\int \mathrm{d}^5x\, \{\partial_\mu A^a_5 \partial^\mu A^{a5} + \partial_5 A^{a\mu}\partial^5 A^a_\mu + 2\partial_\mu A^{a\mu}\partial_5 A^a_5 \\ & + \frac{1}{\xi}\partial_\mu A^{a\mu}\partial_\nu A^{a\nu} - 2\partial_\mu A^{a\mu}\partial_5 A^a_5 + \xi \partial_5 A^a_5 \partial_5 A^a_5\} \\ & + \int \mathrm{d}^4x\, [\partial_\mu A^{a\mu} A^a_5]^{R'}_R \\ = & -\frac{1}{2}\int \mathrm{d}^5x\, \left\{A^a_5\left(\partial_\mu\partial^\mu - \xi\partial_5^2\right)A^a_5 + A^{a\mu}\left(g_{\mu\nu}\partial_5^2 - \xi^{-1}\partial_\mu\partial_\nu\right)A^{a\nu}\right\} \\ & + \frac{1}{2}\int \mathrm{d}^4x\, \left[2\partial_\mu A^{a\mu}A^a_5 + A^a_\mu \partial_5 A^{a\mu} - \xi A^a_5 \partial_5 A^a_5\right]^{R'}_R \end{aligned}$$

The mixing cancels as desired. After the $4d$ vector part of the squared field strength tensor is added to the action

$$\begin{aligned} S_5 + S_{\mathrm{gf}}|_{2,\mathrm{bk}} = & \frac{1}{2}\int \mathrm{d}^5x\, A^{a\mu}\left\{g_{\mu\nu}(\partial_\varepsilon\partial^\varepsilon - \partial_5^2) - (1-\xi^{-1})\partial_\mu\partial_\nu\right\}A^{a\nu} \\ & -\frac{1}{2}\int \mathrm{d}^5x\, A^a_5\left\{\partial_\varepsilon\partial^\varepsilon - \xi\partial_5^2\right\}A^a_5 \end{aligned}$$

an invertible kinetic operator for the $4d$ vector, which has acquired a mass given by the negative curvature along the fifth dimension, and a $4d$ scalar with mass proportional to the vector mass and the gauge fixing parameter ξ are left. There is still mixing on the boundaries that can be cancelled by another gauge fixing procedure. Introducing the boundary-localized gauge fixing action

$$S_{\mathrm{gf},\partial} = \int \mathrm{d}^5x \left\{ \frac{1}{2\zeta_1}(\partial_\mu A^{a\mu} - \zeta_1 A_5^a)^2 \delta(y-R') \right. \\ \left. + \frac{1}{2\zeta_2}(\partial_\mu A^{a\mu} + \zeta_2 A_5^a)^2 \delta(y-R) \right\} \tag{3.3}$$

the boundary part reads

$$S|_\partial = \frac{1}{2}\int \mathrm{d}^5x \left\{ A^{a\mu}\left(\partial_5 A_\mu^a - \zeta_1^{-1}\partial_\mu\partial^\nu A_\nu^a\right) + A_5^a\left(\zeta_1 A_5^a - \xi\partial_5 A_5^a\right)\right\}\delta(y-R') \\ - \frac{1}{2}\int \mathrm{d}^5x \left\{ A^{a\mu}\left(\partial_5 A_\mu^a + \zeta_2^{-1}\partial_\mu\partial^\nu A_\nu^a\right) - A_5^a\left(\zeta_2 A_5^a + \xi\partial_5 A_5^a\right)\right\}\delta(y-R)$$

from which the boundary equations of motion in ζ-unitary gauge can be inferred[2]

$$\text{at } y = R, R': \qquad \partial_5 A_\mu^a = 0 \qquad\qquad A_5^a = 0 \tag{3.4}$$

Performing ξ-unitary gauge, the A_5s decouple ($m_{A_5} \to \infty$) and one is left with a theory that contains only $4d$ vector fields $A_\mu^a(x,y)$. The $4d$ scalars resemble the Standard Model would-be Goldstone bosons as they have become the longitudinal polarizations of the massive $4d$ vectors.

Recapitulatory, starting from a pure gauge theory with an extra compactified dimension, one ends with bulk equations of motion and a simple set of boundary conditions for the fields in unitary gauge, which define a regular Sturm-Liouville-Problem. Its solutions form a Hilbert space, that is, they are complete and orthogonal, in particular. For example, in Feynman gauge $\xi = 1$, the solutions (referred to as 'Kaluza-Klein decomposition') of the unperturbed theory can be written

$$A_\mu^a(x,y) = \sum_k A_\mu^{(k)a}(x) f_k(y) \tag{3.5}$$

$$A_5^a(x,y) = \sum_k A_5^{(k)a}(x) g_k(y) \tag{3.6}$$

The wave functions with respect to y-direction are kernels of the operator $\partial_y^2 + m_k^2$, while $\Box_4 A_M^{(k)a} - m_k^2 A_M^{(k)a} = 0$. The eigenvalues m_k are determined by the boundary conditions of (3.4)

$$m_k = \frac{k\pi}{R' - R}$$

[2] One can also allow for the variation of the fields δA_M^a to vanish on the boundaries. This is fully consistent with (3.3) but would lead to explicit symmetry breaking [14].

Integrating out the fifth dimension leads to a $4d$ effective theory with a tower of massive states. The set of boundary conditions (3.4) allows for a zero-mode solution of the $4d$ vector, revealing an unbroken gauge symmetry of the effective theory (due to Dirichlet boundary conditions there is no non-trivial zero-mode for A_5^a). In order to incorporate full symmetry breaking of the $4d$ gauge theory, thus promoting the higherdimensional approach to a full symmetry breaking mechanism, one has to allow for a generalized set of boundary conditions, namely allow Dirichlet conditions for the vectors and Neumann conditions for the scalars. Dirichlet conditions expel the vectors from the corresponding 3-brane, and gauge symmetry is broken explicitly. But this is just the result of adding an infinite gauge boson mass term to the boundary in unitary gauge, yielding a modified version of (3.4): $A^{a\mu} \sim m^{-2}\partial_5 A^{a\mu} \to 0$. The lesson learned from the minimal Standard Model's Higgs mechanism is how to UV-complete these gauge boson masses by adding scalar fields with non-trivial vacuum expectation values to the theory.

3.1.2 Symmetry breaking and boundary-localized scalars

After the last section's final remarks the boundary action

$$S_\mathrm{h} = \int \mathrm{d}^5x \left\{ D_\mu\Phi^\dagger D^\mu\Phi - \lambda\left(\Phi^\dagger\Phi - \frac{v^2}{2}\right)\right\}\{\delta(y-R)+\delta(y-R')\} \tag{3.7}$$

is added. Using the analog of (2.2), one expands the action to quadratic order in the fields ($\vec{e}_v$ denotes the Higgs vacuum expectation values' direction)

$$\begin{aligned} 2D_\mu\Phi^\dagger D^\mu\Phi\big|_2 &= \vec{e}_v^{\,\top}\left[(\partial_\mu H - i\partial_\mu\pi^b t^b + ig_5 v A_\mu^a t^a)\times \text{h.c.}\right]\vec{e}_v \\ &= \partial_\mu H\partial^\mu H - g_5 v\partial_\mu\pi^a A^{b\mu}\mathrm{Tr}\left\{\{t^a,t^b\}\vec{e}_v\vec{e}_v^{\,\top}\right\} \\ &\quad + \left(\partial_\mu\pi^a\partial^\mu\pi^b + g_5^2v^2A_\mu^aA^{b\mu}\right)\mathrm{Tr}\left\{t^at^b\vec{e}_v\vec{e}_v^{\,\top}\right\} \end{aligned}$$

Focusing on $SU(2)$ symmetries (or products of $SU(2)$s), this is

$$D_\mu\Phi^\dagger D^\mu\Phi\big|_2 = \frac{1}{2}\partial_\mu H\partial^\mu H + \frac{1}{2}\partial_\mu\pi^a\partial^\mu\pi^a - g_5v\partial_\mu\pi^aA^{a\mu} + \frac{g_5^2v^2}{2}A_\mu^aA^{a\mu} \tag{3.8}$$

After partial integration the mixing between A_μ^a and π_μ^a reads $+g_5v\pi^a\partial_\mu A^{a\mu}$, so substituting $A_5^a \to A_5^a \pm g_5v\pi^a$ in (3.3) will cancel all the boundary mixings, leaving the bulk equations of motion for the vectors and scalars unaltered. In addition, there is the boundary-localized motion of the Goldstones

$$\partial_\mu\partial^\mu\pi^a - \zeta_{1,2}g_5^2v^2\pi^a \mp \zeta_{1,2}g_5vA_5^a\big|_{R',R} = 0$$

With $\partial^2\pi^a = -m^2\pi^a$, where m is the mass of a combination of A_5^a and π^a that does not decouple in ξ-unitary gauge

$$\pi^a = \frac{\mp\zeta_{1,2}g_5v}{\zeta_{1,2}g_5^2v^2+m^2}A_5^a \tag{3.9}$$

There are modified boundary conditions

$$\partial_5A_\mu^a \mp \zeta_{1,2}^{-1}\partial_\mu\partial^\nu A_\nu \pm g_5^2v^2A_\mu^a = 0, \quad \partial_5A_5^a \mp \frac{\zeta_{1,2}}{\xi}\left(\frac{m^2/\zeta_{1,2}}{g_5^2v^2+m^2/\zeta_{1,2}}\right)A_5^a = 0 \tag{3.10}$$

that is Neumann conditions for the scalars in unitary gauge $\xi \to \infty$, if $v \neq 0$. In the limit $v \to \infty$, the boundary conditions for the A^a_μ will be Dirichlet, and the Higgs that has acquired a mass $\sqrt{2}\lambda v$ (2.6) from (3.7) decouples. The same argument holds for the Goldstone fields (3.9) that vanish from the theory's spectrum as well. Higgsing only one boundary leads to wave functions that obey Dirichlet on one, and Neumann conditions one the other boundary, resulting in only trivial zero-modes for the vectors *and* the scalars.

This, in fact, admits general symmetry breaking patterns, without having or relying on relicts of a Higgs mechanism. However, as mentioned in section 2.2, a realistic model of electroweak symmetry breaking should contain a custodial symmetry that accounts for the W/Z mass ratio. A toy-$SU(2)$ model with Neumann conditions for one, and mixed Neumann and Dirichlet conditions for the other two vectors (with boundary conditions for the scalars flipped accordingly) contains a massless 'photon', a 'Z-boson' as the first massive Kaluza-Klein excitation of the photon-tower, and 'W-bosons' as first modes of the charged Kaluza-Klein tower:

$$m^k_{\gamma,Z} = \frac{k\pi}{R' - R}, \quad m^k_W = \frac{(2k+1)\pi}{2(R' - R)} \quad k \in \mathbb{N} \cup \{0\} \tag{3.11}$$

Besides yielding a mass ratio 0.5, the model predicts additional Zs and Ws with masses 180 GeV and 240 GeV, respectively, which is ruled out experimentally. Current bounds on Standard Model-like Ws and Zs are $\gtrsim$ 800 GeV at 95% confidence level [1].

3.2 Realistic electroweak symmetry breaking

The remark at the end of the last section pointed out the difficulties in finding a model that is realistic in the sense that it is compatible with electroweak precision data at tree level. Picking up the need for a custodial $SU(2)$ in the model, a straightforward guess is to put $SU(2)_L \times SU(2)_R \times U(1)$ into the bulk [14] (QCD interactions are neglected) and Higgs fields on the boundaries in the decoupling limit that provide symmetry breaking patterns $SU(2)_R \times U(1) \to U(1)_Y$ and $SU(2)_L \times SU(2)_R \to SU(2)_D$. This yields the Standard Model gauge boson content for low energies described in the previous section. However, one is still going to find an unacceptable $\rho \approx 1.1$ that arises from a sizeable overlap of the gauge boson wave functions with this brane that is not $SU(2)_R$-invariant. A way out is to modify the fermion sector [15] or to add large boundary-localized gauge-kinetic terms that may arise from bulk loops [16] and repel the gauge bosons from the brane. Another, theoretically more favored approach is to give up the flat space geometry and work on an RS-type background. Besides that the gauge bosons are repelled from the 'bad' brane by the metric, an anti-de Sitter background allows for a dual description in terms of a strongly coupled Conformal Field Theory (CFT) by exploiting the AdS/CFT conjecture [18, 19].

AdS/CFT - correspondence

Viewed in the light of AdS/CFT, the fifth dimension in fig. 3.1 corresponds to the CFT's energy scale, which clarifies the labelling of the model's branes and arises from

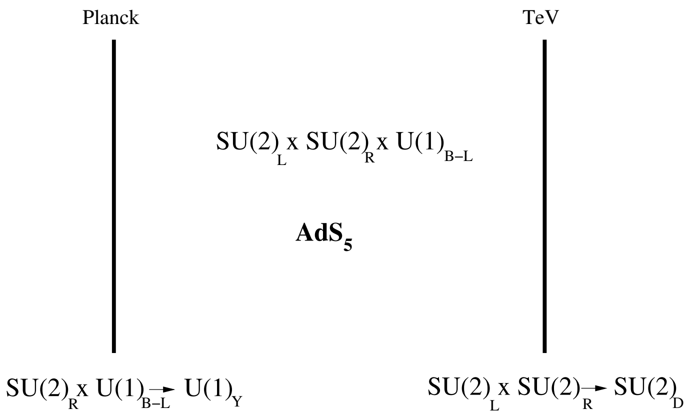

Figure 3.1: Sketch and symmetry breaking pattern of the Higgsless model [20]. The symmetry breaking pattern on the TeV brane is achieved by a bidoublet Higgs $(2,2)_0$. The Higgs on the Planck brane is similar to the Standard Model one $(0,2)_{1/2}$.

the AdS's metric scaling invariance $x^M \to \alpha x^M$. The Planck brane is related to the CFT's UV cut-off but the interpretation of the TeV- or IR-brane is more abstract: it's very existence marks the spontaneous breaking of conformal invariance by CFT dynamics [19]. The gauge fields in the bulk correspond to global symmetries of the CFT that will be weakly gauged if they remain unbroken by boundary conditions on the Planck brane. This is because if one expels the gauge field from the Planck brane, i.e. Dirichlet conditions on the UV- and Neumann conditions on the IR-brane, the first mode will have a mass of roughly $\mathcal{O}(M_{\mathrm{Pl}})$ and does not affect the theory at the TeV scale. Therefore one still has to consider the UV-broken symmetry as global. Flipping the boundary conditions results in a mass of the order of the CFT's IR cut-off for the mode[3]: CFT's strong dynamics has also broken a weakly gauged symmetry, and the Kaluza-Klein bosons are to be identified as CFT bound states. It is not a big surprise that an AdS_5 background will ensure $\rho \approx 1$ as there is a global $SU(2)$ symmetry in the CFT picture. Yet, $S \approx 0$ still requires a modified fermion sector.

3.2.1 The model

To have the symmetry breaking pattern sketched in fig. 3.1, one has to assign the boundary conditions

$$\text{at } y = R' \qquad \begin{cases} \partial_5(g_{5R}A_\mu^{La} + g_{5L}A_\mu^{Ra}) = 0, g_{5L}A_\mu^{La} - g_{5R}A_\mu^{Ra} = 0 \\ \partial_5 B_\mu = 0, g_{5L}A_5^{La} + g_{5R}A_5^{Ra} = 0 \\ \partial_5(g_{5R}A_5^{La} - g_{5L}A_5^{Ra}) = 0, B_5 = 0 \end{cases} \tag{3.12a}$$

$$\text{at } y = R < R' \quad \begin{cases} \partial_5 A_\mu^{La} = 0, A_\mu^{R1,2} = 0, \partial_5(g_{5R}B_\mu + \tilde{g}_5 A_\mu^{R3}) = 0 \\ \tilde{g}_5 B_\mu - g_{5R}A_\mu^{R3} = 0, A_5^{R,La} = 0, B_5 = 0 \end{cases} \tag{3.12b}$$

In order to have consistency with measurements of the oblique corrections [21] (that is mainly the S-parameter), TeV brane-localized kinetic terms that will affect (3.12) and a sizeable ratio g_{5R}/g_{5L} are needed. The immediate consequence is a heavier Kaluza-Klein mass spectrum that is incapable to restore partial wave unitarity at energies

[3]That is the mass eigenstate defining equation changes from $\tilde{R}_0 = R_1$ to $R_0 = \tilde{R}_1$, see (3.15)

higher than 2TeV [15], chapter 4. For this reason in the following $g_{5R} = g_{5L} \equiv g_5$ is assumed and brane-localized terms are neglected. The discussion on consistency with precision data is postponed to a later point in this section.

Gauge boson masses

If one works through (3.1)-(3.10) with the AdS$_5$ metric (2.17) taken into account, i.e. contractions comprise additional factors R/y, and an additional $\sqrt{g}$ for the tensor weight d^5x, the bulk equations of motion for the unperturbed gauge fields along the fifth direction read

$$\partial_y^2\psi^{(A)} - \frac{1}{y}\partial_y\psi^{(A)} + {m^{(A)}}^2\psi^{(A)} = 0$$
$$\longrightarrow \quad \psi_k^{(A)} = y\left(a_k^{(A)}J_1(m_k^{(A)}y) + b_k^{(A)}Y_1(m_k^{(A)}y)\right) \tag{3.13}$$

The boundary conditions (3.12) signalize an unbroken $U(1)$ gauge symmetry associated with the direction $t_R^3 + t_L^3 + \mathbb{1}$ and they also lead to heavy mixing of the $5d$ gauge fields. This implies that a single $4d$ mode will live in different $5d$ modes, which then can only differ by their wave functions along the compactified direction. The boundary conditions are to be met independently of x^μ for each Kaluza-Klein index k, cf. (3.5). The solution of the free theory is required to obey the equations of motion of a four-dimensional vector for each eigenvalue. So written in terms of these fields, that only differ by their mass eigenvalues, charge and $SU(2)_D$ assignments, the Kaluza-Klein decomposition reads

$$B_\mu(x,y) = g_5 a A_\mu + \sum_{k\geq 1}\psi_k^B(y)Z_\mu^{(k)}(x) \tag{3.14a}$$

$$A_\mu^{L3}(x,y) = \tilde{g}_5 a A_\mu + \sum_{k\geq 1}\psi_k^{L3}(y)Z_\mu^{(k)}(x) \tag{3.14b}$$

$$A_\mu^{R3}(x,y) = \tilde{g}_5 a A_\mu + \sum_{k\geq 1}\psi_k^{R3}(y)Z_\mu^{(k)}(x) \tag{3.14c}$$

$$A_\mu^{L\pm}(x,y) = \frac{1}{\sqrt{2}}\left(A_\mu^{L1} \mp iA_\mu^{L2}\right) = \sum_{k\geq 1}\psi_k^{L\pm}(y)W_\mu^{(k)\pm}(x) \tag{3.14d}$$

$$A_\mu^{R\pm}(x,z) = \frac{1}{\sqrt{2}}\left(A_\mu^{R1} \mp iA_\mu^{R2}\right) = \sum_{k\geq 1}\psi_k^{R\pm}(y)W_\mu^{(k)\pm}(x) \tag{3.14e}$$

The zero-mode of the Z tower has been made explicit. As the Kaluza-Klein spectrum of $A_5^{R,La}$ and B_5^a decouples without leaving physical zero-modes, attention is no longer payed to these fields.

Masses and wave functions can be determined by plugging (3.13) into the boundary conditions (3.12), which yields a linear system of equations for the coefficients $a_k^{(A)}$ and $b_k^{(A)}$. For reasons of lucidity, the definitions

$$\kappa = \frac{g_5}{\tilde{g}_5} \qquad R_i = \frac{Y_i(MR)}{J_i(MR)} \quad \tilde{R}_i = \frac{Y_i(MR')}{J_i(MR')} \tag{3.15}$$

will be used. The $W^{\pm}$ masses can then be inferred by solving the system of linear equations

$$
\begin{aligned}
&a_k^{L\pm} + a_k^{R\pm} + \tilde{R}_0 b_k^{L\pm} + \tilde{R}_0 b_k^{R\pm} = 0 && \text{(3.16a)}\\
&a_k^{L\pm} - a_k^{R\pm} + \tilde{R}_1 b_k^{L\pm} - \tilde{R}_1 b_k^{R\pm} = 0 && \text{(3.16b)}\\
&a_k^{L\pm} \qquad\quad + R_0 b_k^{L\pm} \qquad\qquad\quad = 0 && \text{(3.16c)}\\
&\qquad a_k^{R\pm} \qquad\qquad\quad + R_1 b_k^{R\pm} = 0 && \text{(3.16d)}
\end{aligned}
$$

which yields the mass defining equation

$$
(R_0 - \tilde{R}_1)(\tilde{R}_0 - R_1) - (R_0 - \tilde{R}_0)(R_1 - \tilde{R}_1) = 0 \tag{3.17}
$$

Similarly, the Z/B-like states result from

$$
\begin{aligned}
&a_k^{L3} + a_k^{R3} + \tilde{R}_0 b_k^{L3} + \tilde{R}_0 b_k^{R3} = 0 && \text{(3.18a)}\\
&a_k^{L3} - a_k^{R3} + \tilde{R}_1 b_k^{L3} - \tilde{R}_1 b_k^{R3} = 0 && \text{(3.18b)}\\
&\kappa a_k^{B} + a_k^{R3} + R_0 b_k^{R3} + \kappa R_0 b_k^{B} = 0 && \text{(3.18c)}\\
&a_k^{B} + \tilde{R}_0 b_k^{B} = 0 && \text{(3.18d)}\\
&a_k^{B} - \kappa a_k^{R3} - \kappa R_1 b_k^{R3} + R_1 b_k^{B} = 0 && \text{(3.18e)}\\
&a_k^{L3} + R_0 b_k^{L3} = 0 && \text{(3.18f)}
\end{aligned}
$$

For $\tilde{R}_0 = R_0$, (3.18) obviously has a nontrivial solution: (3.18c) $- \kappa \times$ (3.18d) equals (3.18a) $-$ (3.18f), roots of this equation are more photon-like states. In addition, there is a second tower of states, given by the roots of the equation

$$
\kappa^2 \left\{ (\tilde{R}_0 - R_0)(\tilde{R}_1 - R_1) + (\tilde{R}_1 - R_0)(\tilde{R}_0 - R_1) \right\} + 2(\tilde{R}_1 - R_0)(\tilde{R}_0 - R_1) = 0 \tag{3.19}
$$

Effective $4d$ Feynman Rules

With the masses at hand, the gauge bosons' wave functions along the fifth dimension are known in terms of a single parameter that is fixed by normalization. The effective $4d$ interactions are provided by terms trilinear and quartic in the fields

$$
\begin{aligned}
\int_R^{R'} \mathrm{d}y \, \frac{R}{4y} F^{a\mu\nu} F^a_{\mu\nu}\Big|_{>2} &= \int_R^{R'} \mathrm{d}y \, \frac{Rg}{y} f^{abc} \partial_\mu A^a_\nu(x,y) A^{b\mu}(x,y) A^{c\nu}(x,y) \\
&\quad + \int_R^{R'} \mathrm{d}y \, \frac{Rg^2}{4y} f^{eab} f^{ecd} A^a_\mu(x,y) A^b_\nu(x,y) A^{c\mu}(x,y) A^{d\nu}(x,y) \\
= g \sum_{k,l,m} &\left\{ \int_R^{R'} \mathrm{d}y \, \left(\frac{R}{y}\right) \psi_k^{(a)} \psi_l^{(b)} \psi_m^{(c)} \right\} f^{abc} \partial_\mu A^{(k)a}_\nu(x) A^{(l)b\mu}(x) A^{(m)c\nu}(x) \\
+ g^2 \sum_{k,l,m,n} &\left\{ \int_R^{R'} \mathrm{d}y \, \left(\frac{R}{y}\right) \psi_k^{(a)} \psi_l^{(b)} \psi_m^{(c)} \psi_n^{(d)} \right\} f^{eab} f^{ecd} A^{(k)a}_\mu(x) A^{(l)b}_\nu(x) A^{(m)c\mu}(x) A^{(n)d\nu}(x)
\end{aligned}
$$

This implies ordinary Feynman rules for non-abelian gauge theories with countably infinite gauge bosons and coupling constants that are given by an integral over the warped down product of the gauge boson's wave functions along y-direction.

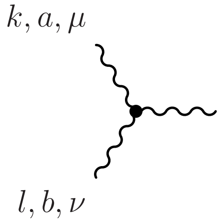

$$= \left\{ \int_R^{R'} \mathrm{d}y \, \frac{R}{y} \psi_k^{(a)} \psi_l^{(b)} \psi_m^{(c)} \right\} \times \tag{3.20a}$$

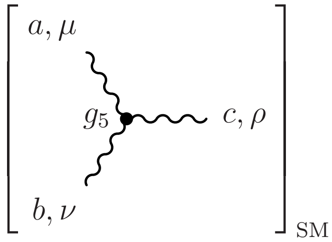

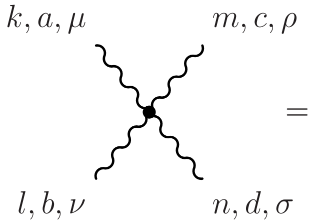

$$= \left\{ \int_R^{R'} \mathrm{d}y \, \frac{R}{y} \psi_k^{(a)} \psi_l^{(b)} \psi_m^{(c)} \psi_n^{(d)} \right\} \times \tag{3.20b}$$

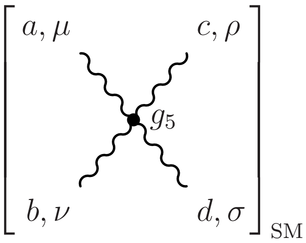

After proper normalization $\int \mathrm{d}y \, (R/y) \psi_k^2 \equiv 1$ the propagator is

$$= \delta^{kl} \times \tag{3.20c}$$

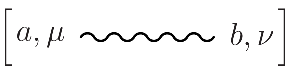

Writing the Feynman rules in terms of the mass eigenstates (3.14) yields Standard Model vertices times integrals over the corresponding wave functions $\psi^\pm$, ψ^3. The model includes two non-abelian and one abelian gauge group, so one has to sum over the group's contributions keeping the Kaluza-Klein decomposition in mind, e.g. the WWZ-coupling is

$$g_{klm}^{WWZ} = g_5^2 \int_R^{R'} \mathrm{d}y \, \frac{R}{y} \sum_{i=L,R} \left\{ \psi_k^{(i)\pm}(y) \psi_l^{(i)\pm}(y) \psi_m^{(i)3} \right\} \tag{3.21}$$

The normalizations are chosen such that

$$\begin{aligned} Z\text{-like} \int_R^{R'} \mathrm{d}y \, \frac{R}{y} \left(\left(\psi^{L3}\right)^2 + \left(\psi^{R3}\right)^2 + \left(\psi^{B}\right)^2 \right) &= 1 \\ W\text{-like} \int_R^{R'} \mathrm{d}y \, \frac{R}{y} \left(\left(\psi^{L\pm}\right)^2 + \left(\psi^{R\pm}\right)^2 \right) &= 1 \end{aligned} \tag{3.22}$$

Modified fermion sector and consistency with oblique corrections

As mentioned earlier this section, consistency with measurements of the oblique corrections can be attained by modifications of the theory's fermion sector. The presented argument persists to the enlarged set of oblique parameters by Barbieri *et al.* [17, 15] that accounts for additional four-fermi operator measurements at LEP2. For this reason, S, T and U are considered only.

After Randall and Sundrum's proposal, it has been quickly realized that localizing fermions either on the Planck- or the TeV-brane results in positive or negative S-parameters of order 1, respectively. This value is typical for models of electroweak symmetry breaking more complicated than a $4d$ Higgs doublet. But recently, it was argued that promoting the fermions to the bulk points to a solution to experimentally observed $S \approx 0$ [1, 15, 22].

However, fermions in the model fig. 3.1 introduce additional difficulties due to the curved background and the vector character of fermions in odd dimensions. The aspects of realistic fermion spectra in this framework, e.g. getting a left-handed chiral low energy limit, have been worked out in [23] and are of minor importance to this thesis' study, except for the size of the oblique corrections. In a nutshell, a low-energy chiral spectrum can be constructed by assigning boundary conditions to the two Weyl spinors forming the vector-like Dirac fermion that only allow for a left- or right-handed zero mode living in $(2,1)_{1/6}$ and $(1,2)_{1/6}$, respectively. Then, the zero modes can be lifted by adding a TeV brane-located Dirac masses (the theory is non-chiral there) to match the Standard Model content of the light fermions.

Identifying the fermion-fermion-gauge boson couplings of the lowest Kaluza-Klein states of the $4d$ effective theory with the Standard Model's couplings shifts the oblique corrections into mass and wave function renormalizations. It turns out that for an approximately flat profile of the light fermions (that is controlled by the $5d$ Dirac bulk mass) with respect to the fifth dimension, the S parameter can be made arbitrarily small while $T, U \approx 0$ as rather generic features of the model. The reason behind this is intuitive: The lowest Kaluza-Klein states have an approximately flat wave function and they are orthogonal to the higher modes, therefore, a flat fermion profile minimizes

Figure 3.2: Oblique corrections from the Higgsless model fig. 3.1 [22]. c_L corresponds to the $5d$ bulk Dirac mass with boundary conditions for the fermions chosen such that the Kaluza-Klein zero mode is left-handed. The contours are $|S| = 0.5$ (dashed), 0.25 (solid), and $|T| = 0.5$ (dashed), 0.3 (solid), 0.1 (dotted). The right side shows the suppression of the coupling of left-handed down-type fermion $(-\frac{1}{2}, 0, \frac{1}{6})$ to the Kaluza-Klein Z_2 with respect to the Standard Model coupling.

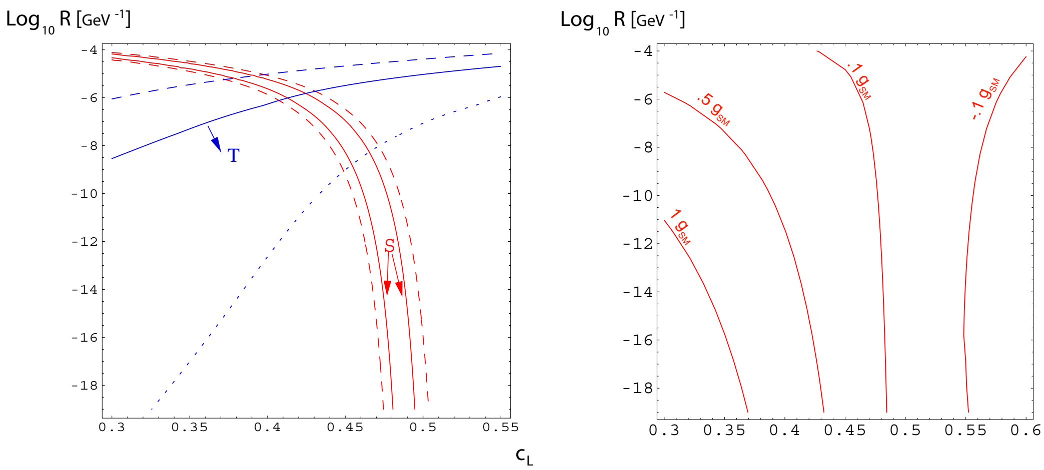

the interaction of the fermions with the Kaluza-Klein bosons that manifests itself in the oblique corrections, and due to to the AdS setup mainly the S parameter is affected. The Kaluza-Klein gauge bosons are 'fermiophobic' and weaker bounds on Kaluza-Klein production are an immediate consequence as the production cross section of heavy Standard Model-like gauge bosons from fermions is $\sim g^2 M^{-2}$. Whilst the S parameter can be made sufficiently small, there is a residual dependence of the T parameter on the Planck brane localization as custodial symmetry gets violated there. This dependence, together with bounds on Kaluza-Klein production provides an upper bound of $R \lesssim 10^{-7}\text{GeV}^{-1}$ [22].

So far, the third generation has not been included in the discussion. This has been a major obstacle of the Higgsless model. With the fermions delocalized towards the UV brane like it is done with the light generations, it is impossible to have a top quark mass larger than $\sim m_W$. The third generation has to be located via the bulk Dirac mass in the vicinity of the TeV brane, but still a large boundary Dirac mass that mixes left and right handed fermions must be added to account for the top mass. Therefore, the left-handed bottom has a component in the right-handed doublet and its experimentally well-established coupling to the Z will change. A way to protect the $b_L\bar{b}_L Z$ coupling is to abandon the ordinary assignment of the left- and right-handed particles of the third family in favor of a

$$\begin{aligned} (2,2)_{2/3} &\supset t_\ell, b_\ell \\ (1,1)_{2/3} &\supset t_r \\ (1,3)_{2/3} \oplus (1,3)_{2/3} &\supset b_r \end{aligned} \tag{3.23}$$

representation. This arises from the fact that a discrete $L \leftrightarrow R$ symmetry-enhanced custodian conserves L, R charges individually [24].

3.3 (De)Constructed models

The model class considered so far reveals its five dimensional character when it is probed at energies larger than the inverse size of the extra dimension that is typically $\sim$ TeV^{-1}. However, for fivedimensional gauge theories $[g_5] = -1/2$, and a cut-off is needed. The cut-off may be as large as the fundamental, fivedimensional Planck scale, where zero-mode gravity becomes strong. Yet, the model of figure 3.1 offers only an effective description at comparatively low scales with gravity completely unrelated to the critical UV-behavior of non-renormalizable gauge theories. To have a credible description of beyond-the-cut-off physics a UV-completion of the model into a more fundamental theory is needed.

A possible way to UV-complete higherdimensional gauge theories, which motivates another class of Higgsless models was presented in [25]. Starting with a renormalizable, fourdimensional gauge theory, it is possible to 'build' an additional dimension by strong dynamics. The basic idea of constructing dimensions is reviewed in the next section along with its application to electroweak symmetry breaking.

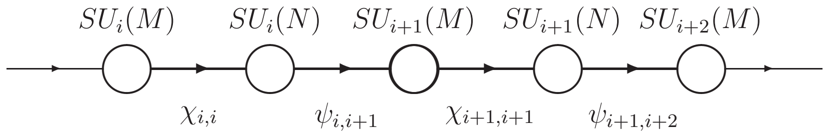

Figure 3.3: A linear moose or quiver diagram.

3.3.1 (De)constructing dimensions and linear moose models

The idea of dimensional (de)construction is based on a product gauge group setup of fig. 3.3 with $\Lambda^i \ll \Lambda_s^i$ the strong coupling scales of the $SU(M)_i$ and $SU(N)_i$, respectively. The gauge groups are linked by fermions that transform

$$\chi_{i,i} = (M, \bar{N}, 1) \qquad \psi_{i,i+1} = (1, N, \bar{M})$$

under adjacent groups $(i, i+1)$. Below Λ_s the fermions will condense similar to chiral symmetry breaking in QCD. A parametrization consistent with naive dimensional analysis [26] is

$$\langle \chi_{i,i} \psi_{i,i+1} \rangle \sim \frac{{\Lambda_s^i}^3}{(4\pi)^2} U_{i,i+1} \in (M \otimes \bar{M})$$

$U_{i,i+1}$ is a unitary $M \times M$ matrix. All 'hadronic' $SU(N)$ bound states acquire a mass $\sim \Lambda_s$ so that they can be neglected at the scales where $SU(M)$ is still weakly coupled. In that intermediate energy range the linear moose can be described by non-linear sigma fields $U_{i,i+1}$ coupled to a $\prod_i SU_i(M)$ gauge theory.

$$D_\mu U_{i,i+1} = \partial_\mu U_{i,i+1} - i g_i A_i^a t_i^a U_{i,i+1} + i g_{i+1} A_{i+1}^a U_{i,i+1} t_{i+1}^a \tag{3.24}$$

The effective action reads

$$S = -\frac{1}{4} \sum_i F_{\mu\nu}^i F^{i\mu\nu} - \frac{1}{4} \sum_i f_i^2 \mathrm{Tr}\{(D_\mu U_{i,i+1})^\dagger D^\mu U_{i,i+1})\} \tag{3.25}$$

which yields the gauge boson mass matrix

$$\frac{1}{8} \begin{pmatrix} \ddots & & & & & \\ & \tilde{g}_{i-1} g_i & (f_{i-1}^2 + f_i^2) g_i^2 & -\tilde{g}_i g_{i+1} & 0 & \\ & 0 & -\tilde{g}_i g_{i+1} & (f_i^2 + f_{i+1}^2) g_{i+1}^2 & \tilde{g}_{i+1} g_{i+2} & \\ & & & & & \ddots \end{pmatrix}, \tilde{g}_j = f_{s,j}^2 g_j \tag{3.26}$$

The vacuum expectation value $\langle U \rangle = 1$ breaks the symmetry down to to the diagonal subgroup $SU(M)_D$, there will be M massless linear combinations of the gauge bosons (3.24). The mass matrix (3.26) is symmetric and diagonalizable, hence.

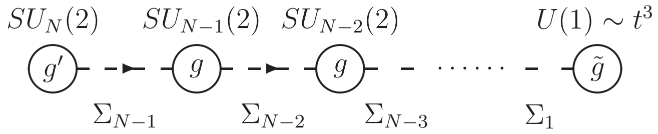

Figure 3.4: A 'condensed' linear moose model for higgsless electroweak symmetry breaking

3.3.2 Application to electroweak symmetry breaking

To arrive at another realization of Higgsless symmetry breaking that has been argued to be a UV-Completion of fig. 3.1 [27] , a $\prod_{i=1}^{N} SU_i(2)$ moose in large N limit has been suggested [28]. The symmetry breaking should leave a gauged $U(1)$ unbroken, which is incorporated by gauging a single direction of another rigid $SU(2)$, fig. 3.4. An additional benefit is the conservation of an approximate custodial $SU(2)$. Following (3.24), (3.25), and (3.26) the mass matrix of the uncharged gauge Z boson can be formulated, with the mass matrix of the charged gauge bosons $W^{\pm} = 1/\sqrt{2}(A^1 \mp iA^2)$ as the lower $N \times N$ matrix. Upon diagonalizing, there are N W-solutions and $N+1$ Z-solutions which includes a massless eigenstate. One can write the action in terms of the mass eigenstates using the spectral theorem

$$A_\mu^{(j)\pm} = \sum_{i=1}^{N} (\psi_i^W)_j W_\mu^{(i)\pm} \qquad A_\mu^{(j)3} = \sum_{i=1}^{N+1} (\psi_i^Z)_j Z_\mu^{(i)} \tag{3.27}$$

and it is straightforward to write down the gauge boson couplings according to the method laid out in section 3.2.1.

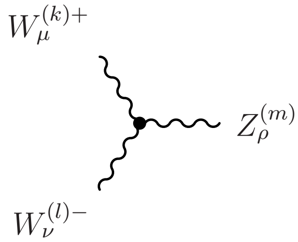

$$= g_{klm}^{WWV} \times$$

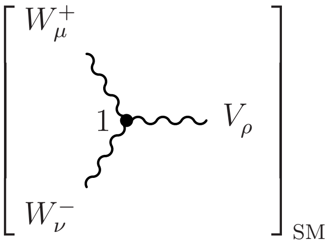

(3.28a)

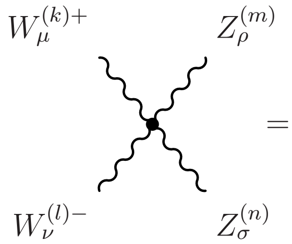

$$= g_{klmn}^{WWVV} \times$$

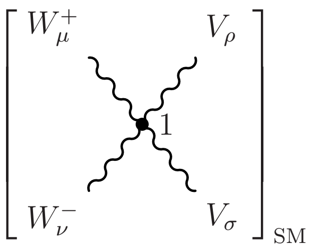

(3.28b)

with coupling constants

$$\begin{aligned} g_{klmn}^{WWZZ} &= g^2 \sum_{j=1}^{N-1} (\psi_k^W)_j (\psi_l^W)_j (\psi_m^Z)_j (\psi_n^Z)_j + g'^2 (\psi_k^W)_N (\psi_l^W)_N (\psi_m^Z)_N (\psi_n^Z)_N \\ g_{klm}^{WWZ} &= g^2 \sum_{j=1}^{N-1} (\psi_k^W)_j (\psi_l^W)_j (\psi_m^Z)_j + g'^2 (\psi_k^W)_N (\psi_l^W)_N (\psi_m^Z)_N \end{aligned} \tag{3.28c}$$

For larger N the action (3.25) takes the form of gauge theory with an extra latticed dimension [25] of length $Na = 2N/(gf)$ and fivedimensional coupling $g_5 = 2g/f$. The continuum limit $N \to \infty, Na$ fixed, is well-defined. At the ends of the extra dimension there are boundary kinetic terms corresponding to the $U(1)$ and $SU_N(2)$ groups of fig. 3.4. The lacking kinetic terms on the right boundary of the extra dimension should be interpreted as Dirichlet boundary conditions $A^a_\mu = 0$ for the continuum $5d$ gauge fields $a \neq 3$. The present gauge kinetic terms are to be interpreted as conditions for the gauge fields' derivative along the extra dimension as a consequence of the limiting process. Because the continuum limit is well-defined, the only consistent boundary conditions for the derivatives are Neumann-type (see chapter 4). But this is just a more realistic analogue of the flat space toy model that led to (3.11). Therefore, a 'coarser' copy of fermion delocalization (section 3.2.1) where fermions will receive their $SU(2)$ properties from more than one site of the moose can control the size of the oblique corrections [30]. Gauge theories on an anti-de Sitter background have also been deconstructed from a product gauge group on fourdimensional Minkowski space [27] by modulating the link fields's vacuum expectation value.

Chapter 4

Kaluza-Klein Scattering

So far, only a symmetry breaking mechanism has been constructed. With the Kaluza-Kleins in the spectrum and the Higgs vanished, the theory's high energy behavior will be different from the Standard Model. With the decoupling of the Higgs as a limiting process, one expects a good high energy behavior up to the theory's intrinsic $5d$ cut-off in the light of [31].

'Benchmark' tests of the trustability of a theory at high energies are elastic scattering processes of longitudinally polarized gauge bosons. The longitudinal polarization vector of a gauge boson with fourmomentum k_μ is characterized by

$$\varepsilon_L^2 = -1 \qquad \varepsilon_L^\mu k_\mu = 0$$

It becomes increasingly parallel to k_μ at energies E larger than their masses

$$\varepsilon_L^\mu(k) = \frac{k^\mu}{m} + \mathcal{O}\left(\frac{m}{E}\right) \tag{4.1}$$

Therefore, each diagram in fig. 4.1 contributes parts growing with $\sim E^2$ and $\sim E^4$. Unless this growth is cancelled, the unitarity violation bounds $|\Re a_\ell| < 0.5$ [32] are violated immediately[1].

$$\mathcal{M}_{fi} \overset{E\to\infty}{\longrightarrow} \infty \quad \Longrightarrow \quad a_\ell = \frac{1}{32\pi}\int_{-1}^{1} \mathrm{d}\cos\theta \; \mathcal{M}_{fi} P_\ell(\cos\theta) \to \infty \tag{4.2}$$

Hence, such a cancellation is a conditio sine qua non for the theory to be trustable. In the Standard Model these cancellations are a consequence of the underlying, spontaneously broken gauge symmetry. As it turns out, this is also true for the Higgsless scenarios, where the $5d$ gauge symmetry protects the effective $4d$ theory from the bad high energy behavior.

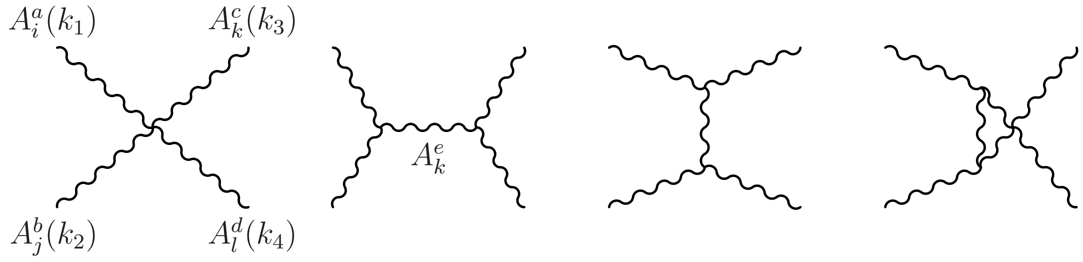

Figure 4.1: Tree level gauge boson scattering topologies.

[1] Here P_ℓ is the ℓth Legendre Polynomial. As all gauge boson helicities are equal no reduced Wigner functions are to be included.

4.1 Longitudinal Kaluza-Klein scattering

Massive *SU(2)* gauge boson scattering

To work out the high energy behavior of elastic longitudinal gauge boson scattering only bosons' energies far larger than their masses are considered. In addition to the gauge group index, the gauge bosons carry a Kaluza-Klein index n. An ansatz consistent with crossing symmetry and $SU(2)$ gauge symmetry is

$$\begin{aligned}\mathcal{M}(A_n^a A_n^b \to A_n^c A_n^d) = \mathcal{A}^{abcd}(s,t,u)\delta^{ab}\delta^{cd} \\ + \mathcal{A}^{acbd}(t,s,u)\delta^{ac}\delta^{bd} + \mathcal{A}^{adbc}(u,t,s)\delta^{ad}\delta^{bc}\end{aligned} \tag{4.3}$$

s, t, u are the ordinary Mandelstam variables. The result of (4.3) can be converted to the charge eigenstate basis using $|Z_k\rangle = |A_k^3\rangle$ and $\left|W_k^\pm\right\rangle = 1/\sqrt{2}\,|A_k^1 \mp iA_k^2\rangle$ for the S matrix elements

$$\mathcal{M}(W_n^+ W_n^- \to Z_n Z_n) = \mathcal{A}(s,t,u) \tag{4.4a}$$
$$\mathcal{M}(W_n^+ W_n^- \to W_n^+ W_n^-) = \mathcal{A}(s,t,u) + \mathcal{A}(t,s,u) \tag{4.4b}$$
$$\mathcal{M}(Z_n Z_n \to Z_n Z_n) = \mathcal{A}(s,t,u) + \mathcal{A}(t,s,u) + \mathcal{A}(u,t,s) \tag{4.4c}$$

All other scattering processes can be obtained from (4.4) by crossing. The expansion of $\mathcal{A}$ into powers of the center of mass energy at energies larger then m_n is most easily performed in the center of mass frame (for details see appendix A) and yields

$$\mathcal{A}(s,t,u) = \mathcal{A}^{(2)}(s,t,u)s^2 + \mathcal{A}^{(1)}(s,t,u)s^1 + \mathcal{A}^{(0)}(s,t,u) + \mathcal{O}\left(m_n^2 s^{-1}\right) \tag{4.5}$$

The amplitude parts growing with E^4 and E^2 are given by (color indices are dropped from now on)

$$\begin{aligned}16m_n^4\mathcal{A}^{(2)} &= 2\Big(g_{nnnn} - \sum_k g_{nnk}^2\Big)\cos^2\theta - 6\Big(g_{nnnn} - \sum_k g_{nnk}^2\Big) \\ 16m_n^4\mathcal{A}^{(1)} &= 4m_n^2 g_{nnnn} - 3\sum_k m_k^2 g_{nnk}^2\end{aligned}$$

with scattering angle θ. Thus, unitarity conservation requires the couplings to obey the sum rules

$$0 = g_{nnnn} - \sum_k g_{nnk}^2 \tag{4.6a}$$
$$0 = 4m_n^2 g_{nnnn} - 3\sum_k m_k^2 g_{nnk}^2 \tag{4.6b}$$

Indeed, these sum rules turn out to be a consequence of the Sturm-Liouville problem with Neumann and Dirichlet boundary conditions (see appendix A). This special set of boundary conditions is the only one consistent with unbroken and non-explicitly broken gauge theories on compactified extra dimensions that does not involve boundary localized scalars (chapter 3). In this way the higherdimensional gauge theory protects the fourdimensional effective theory from a bad UV behavior. The resulting completeness relation for every gauge index is also an a posteriori justification for dropping the gauge indices in (4.6)[2]. Although the convergence of the sum rules is found to be rapid in the AdS continuum, the cancellation of (4.6) requires all, infinitely many Kaluza-Klein states to be taken into account. Together with the intrinsic cut-off of the underlying higherdimensional gauge theory, this means summing over an infinite number of unphysical states. The Kaluza-Klein spectrum will be cut at the $5d$ cut-off at the latest, with new physics entering that possibly resolves the 'moose' structure. The cut on the eigenspectrum is going to result in a residual growth $\sim E^2$ for the heaviest state with Kaluza-Klein index N. If the four-gauge boson-coupling is *defined* in the Higgsless scenario

$$g_{NNNN} = \sum_{k \lesssim \Lambda} g^2_{NNk}$$

the second sum rule (4.6b) reads

$$g_{NNNN} = \sum_{k \lesssim \Lambda} g^2_{NNk} \frac{3m_k^2}{4m_N^2} < \sum_{k \lesssim \Lambda} g^2_{NNk}$$

because $m_N > m_k$ and $k < N$ by construction. The highest Kaluza-Klein scattering amplitude can not be unitarized within the model and is therefore sensitive to the UV-completion. However, measuring the UV-completion via this state in Weak Boson Fusion processes is unlikely, given the constraints of the measurement of the oblique corrections.

Scattering of physical states: Initial and final state mass splitting

Last section only dealt with the elastic scattering of gauge bosons with equal masses. This applies for WW scattering, but the situation changes slightly when mass differences of initial or final state Ws and Zs are accounted for. The modified sum rules are worked out in appendix A.1.1. The first one $\sim E^4$ is similar to (4.6a)

$$g_{WWZZ} = \sum_{k \geq 1} g^2_{W_k WZ} \tag{4.7a}$$

and the second one $\sim E^2$ differs only by the mass difference of the initial states

$$2(m_Z^2 + m_W^2) g_{WWZZ} = \sum_{k \geq 1} g^2_{W_k WZ} \left(3m_k^2 - \frac{(m_Z^2 - m_W^2)^2}{m_k^2} \right) \tag{4.7b}$$

[2]For gauge field-dependent boundary conditions the Kaluza-Klein index can be interpreted as a double index, e.g. i is $\{i, a\}$.

4.2 Kaluza-Klein masses and couplings: Parameter space analysis

To analyse the model's parameter space and eventually implement the Higgsless scenario into a parton-level Monte-Carlo, a C++ program was created that provides masses and couplings of the gauge bosons according to (3.17), (3.18) and (3.20) using GNU Scientific Library's adaptive numerical integration routines `QAGS` and `QAG` [33]. For technical details on the program's realization the reader is referred to appendix B.

For the model of fig. 3.1, there is a single free parameter, which is chosen to be the location of the Planck brane R. The perturbative expansion in $\log^{-1}(R'/R)$ of (3.17) yields the lowest lying state

$$m_{W^1}^2 = \frac{1}{R'^2 \log(R'/R)} + \mathcal{O}\left(\log^{-2}(R'/R)\right) \tag{4.8}$$

which is to be identified as the Standard Model W. Whilst this is an unfeasible approximation as the logs can be significant, (4.8) clarifies that given the location of the UV brane, the location of the IR brane is fixed by the W mass and R. Then, the Kaluza-Klein W spectrum is entirely determined by (3.17). The coupling of the unbroken gauge group's massless state to these W bosons is identified as the QED coupling

$$g^{WW\gamma} = \frac{g_5 \tilde{g}_5 a}{\mathcal{N}_A} = e$$

where $\mathcal{N}_A$ is the photon normalization chosen such that the kinetic term is canonically normalized:

$$\mathcal{N}_A = \int_R^{R'} \mathrm{d}y \frac{R}{y} \left(2\tilde{g}_5^2 + g_5^2\right) a^2$$

This gives a relation between the coupling of the $SU(2)$s and the $U(1)$ coupling

$$e^2 = \frac{g_5^2 \tilde{g}_5^2}{(2\tilde{g}_5^2 + g_5^2) R \log(R'/R)}$$

The Z mass, taken to be (3.18)'s first zero, eventually fixes the absolute values of the couplings g_5, $\tilde{g}_5$ as functions of R, which leaves the entire Z mass spectrum determined.

Kaluza-Klein mass spectrum

The dependence of R' on R is shown in fig. 4.2 along with the Kaluza-Klein masses of the first few $W^\pm$ and Z states for the considered parameters $R \in [10^{-19}\mathrm{GeV}^{-1}, 10^{-7}\mathrm{GeV}^{-1}]$. The mass spectrum exhibits a curious property: Three nearly degenerate gauge boson states are followed by two nearly degenerate $W^\pm$ and Z bosons, the masses differ only by a few percent. The specific form of the mass spectrum is a consequence of the symmetry breaking's heavy mixing of the $SU(2)$ and $U(1)$ gauge bosons on the boundaries of the extra dimension. The Z tower divides into two sets: One is determined by the unbroken gauge groups condition $\tilde{R}_0 = R_0$, the other one by (3.18). Thus, one of the Zs of the $W^{\pm}, Z, Z$ mass 'triplet', generically the heavier one, is a Standard Model-like photon copy in the sense that it is part of the unbroken gauge group's tower. The $W^{\pm}, Z$ mass 'doublet' can be considered Standard Model-like as the W is lighter than the doublet's Z, which is opposite to the triplet's W and lighter Z. The W and the non-photon-like Z of the triplet correspond to mixtures of the gauge fields that cannot be interpreted as Standard Model-related states.

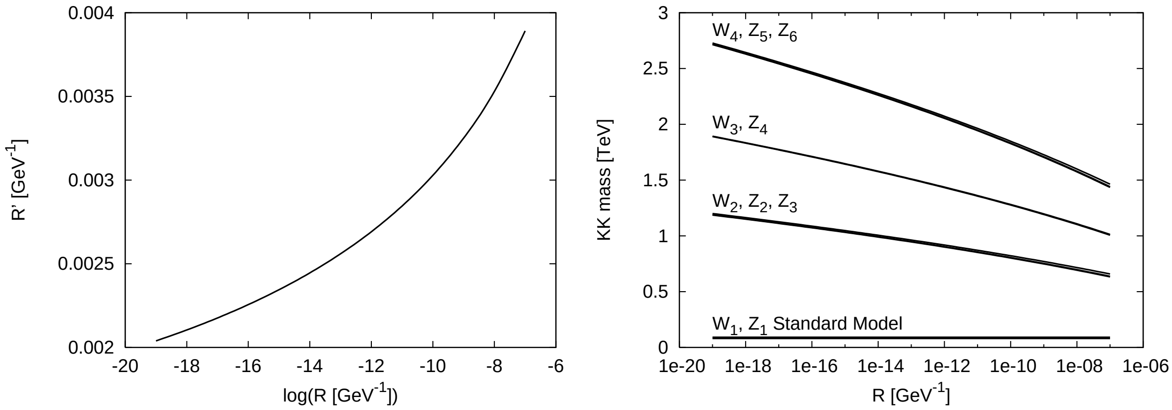

Figure 4.2: Left: Location of the infrared brane as a function of the ultraviolet brane's location for fixed W_1 mass. Right: Kaluza-Klein Z_k and W_k mass spectrum as a function of R.

Kaluza-Klein couplings

The above distinction between different types of gauge bosons also persists to the couplings' characteristics, fig. 4.3. The states with strongly suppressed couplings are the Standard Model-like ones. The fast drop-off of the couplings with the Kaluza-Klein index number, along with the approximate linear growth of the Kaluza-Klein masses

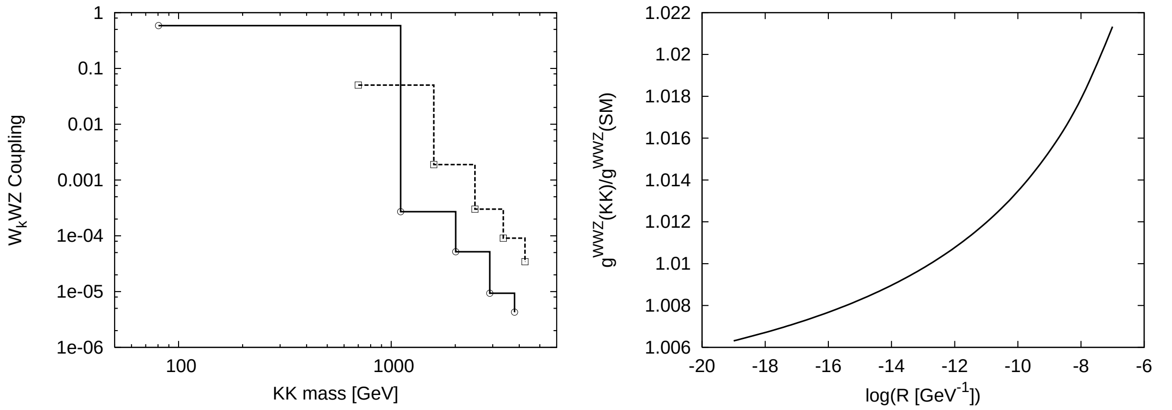

Figure 4.3: Left: Couplings of the Kaluza-Kleins W_k to the Standard Model W and Z for $k \leq 10$. Right: Comparison of the WWZ coupling in the Higgsless model with the Standard Model value. $R \approx 10^{-8}\mathrm{GeV}^{-1}$ is chosen such that the $k = 2$ Kaluza-Klein W has a mass of 700GeV. The steps distinguish between SM-like and SM-unlike states.

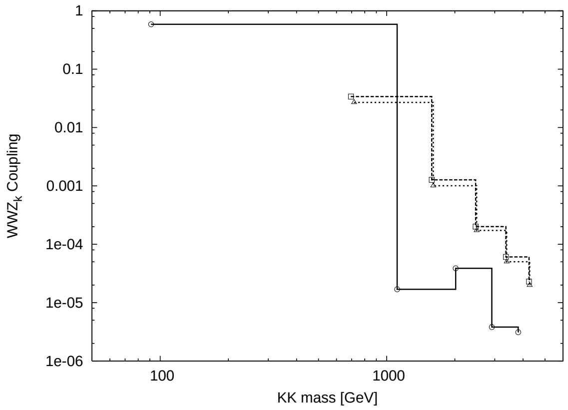

Figure 4.4: Couplings of the Kaluza-Kleins Z_k to the Standard Model W for $R = 10^{-8}\mathrm{GeV}^{-1}$. The steps again distinguish between the The SM-like and SM-unlike states. Additionally, the photon tower (dots) is distinguished from the Z tower (dashes).

with the same number does not depend on the chosen value of R and leads to invisibly small contributions of Kaluza-Klein excitations with $k > 2$ to cross sections and distributions. Thus, detecting states at collider experiments higher than the first non-Standard Model one is impossible in this scenario. Because of the the R dependence of g_5, the WWZ coupling also depends on the Planck brane localization and differs from the the Standard Model value, fig. 4.3. The difference, however, is still in accordance with measurements over the whole parameter range of R [1].

4.2.1 Higgsless models and unitarity violation

For deconstructed models with a finite number of sites, the first sum rule (4.6a) is automatically fulfilled by orthonormality of the mass matrices' eigenvectors (3.28c). However, the second sum rule is violated as the part of the amplitude that grows with E^2 is only suppressed by N^{-1}, which is a consequence of the tridigonal form of the real mass matrices resulting from the aliphatic moose structure. For this reason finite sized deconstructed models provide a simple approach to study the extra dimension's *generic* properties, e.g. effects of fermion (de)localization on oblique corrections etc., but they do not exhibit phenomenologically reasonable results for a smaller number of moose sites without modifications at typical LHC center of mass energies. The three-sited version of fig. 3.4 violates unitarity at < 2.5TeV and should not be considered as a reliable candidate for electroweak symmetry breaking in the advent of LHC. For

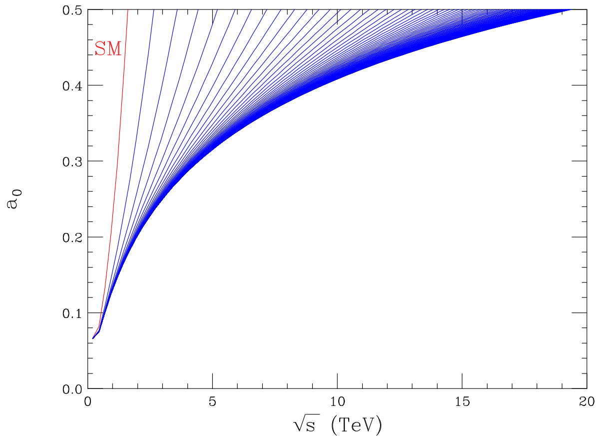

Figure 4.5: $J = 0$ partial wave for longitudinal $WW \to WW$ scattering in the deconstructed model, section 3.3.2, with $N \leq 100$, and Standard Model without Higgs boson [28]. The parameters are chosen such that the second Kaluza Klein W has a mass $m_{W^2} = 500\mathrm{GeV}$.

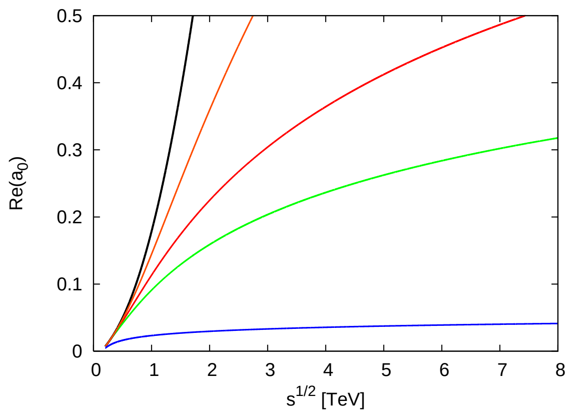

Figure 4.6: J=0 partial wave for longitudinal WZ scattering with m_{W^2}=500GeV (green), 700GeV (red), 1200GeV (orange, $R\simeq M_{\rm Pl}^{-1}$), Standard Model without Higgs boson (black), and Standard Model Higgs $m_h = 120$GeV (blue).

a larger number of sites $\gtrsim 100$ unitarity violation converges at values ~ 20TeV for $m_W^2 = 500$GeV, yet, the bounds of figure 4.5 give only a very rough upper estimates of the theory's UV cut-off and the model can not be considered valid up to these scales (section 4.2.2).

To perform the partial wave analysis of the longitudinal gauge boson scattering in the continuum model, a FORTRAN77 program was created, which uses the Helicity Amplitude Subroutines `HELAS` [34] generated by `Madgraph` [35] for the Standard Model case and a modified version of the `Madgraph` subroutines for the extra dimension scenarios. Additionally, the FORTRAN code is interfaced with the previously mentioned C++ code. The integration over the scattering angle is performed numerically with FORTRAN using NUMERICAL RECIPES' `qromb` subroutine [36], and we focus on WZ scattering because of the absence of t channel photon exchange. The crossed channels require a separate analysis, however, the estimate of the unitarity violation scale that is given at the end of section 4.2.2 is rather process-independent. For details, particularly concerning the implementation of the gauge bosons, the reader is referred to appendix B and section 5.2. The $J = 0$ partial amplitudes are shown in fig. 4.6 for configurations with Kaluza-Klein $W^\pm$ masses 500GeV, 700GeV, and 1200GeV, the higher partial waves $J = 1, 2, 3$ are shown in fig. 4.7. The T-Parameter bound of $R \leq 10^{-7}\text{GeV}^{-1}$ of the anti-de Sitter background model exhibits a gauge mass bound

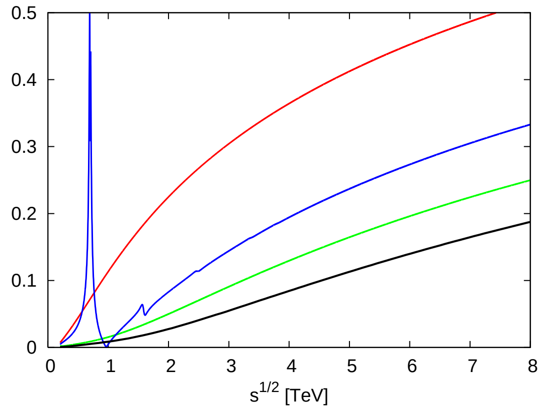

Figure 4.7: J=0 (red), 1 (blue), 2 (green), 3 (black) partial waves for longitudinal WZ scattering with $m_{W^2} = 700$GeV. Partial wave unitarity violation is set by the zeroth partial wave.

$m_{W^2} \gtrsim 630$ GeV and the partial wave unitarity bound from figure 4.6 is approximately 7.5TeV for $m_{W^2} = 700$GeV. Towards a more 'fundamental' model parameter $R \simeq M_{\rm Pl}^{-1}$ the scale decreases to 2.8TeV. This trend is intuitive as, by kinematics, a heavier Kaluza Klein spectrum can not prevent the longitudinally polarized amplitude from blowing up around 1TeV.

For R values leading to light second Kaluza-Klein modes $\simeq 700$ GeV the unitarity violation scale inferred from the partial wave analysis presented above overestimates the violation scale. As in the Standard Model, where t-channel photon exchange gives an infinite contribution to forward scattering, the forward region gives a logarithmic enhancement at energies larger than the exchanged Kaluza-Klein in the Higgsless model. These logs arise from t and u channel propagators, respectively, and lead to the depicted partial wave unitarity violation, figs 4.6 and 4.7. Thus, for light Kaluza-Klein spectra this bound can not give a reliable estimate of the unitarity violation scale. The logs become sizeable at energies where inelastic channels open up and must not be neglected in the determination of the unitarity violation scale. This contrasts to heavy spectra with $m_{W^2} \sim 1$TeV. For these parameter choices, partial wave unitarity is violated at center of mass energies, where inelastic channels are barely accessible. Thus, the bound inferred from partial wave analysis gives a reliable scale estimate.

4.2.2 Unitarity constraints and Naive Dimensional Analysis

Unitarity constraints on scattering processes of particles with spin can be found in [32], the ℓth partial wave was already given in (4.2)

$$a_\ell^{fi} = \frac{1}{32\pi} \int_{-1}^{1} \mathrm{d}\cos\theta \; \mathcal{M}_{fi}(\cos\theta) P_\ell(\cos\theta)$$

with P_ℓ the ℓth Legendre Polynomial. $\mathcal{M}_{fi}$ is related to the T matrix element

$$S = \mathbb{1} + iT \qquad \mathcal{M}_{fi} = (2\pi)^4 \delta(p_f - p_i) \langle f|T|i\rangle$$

and unitarity of the S matrix $S^\dagger S = \mathbb{1}$ leads to the Optical Theorem

$$2\Im\{\mathcal{M}_{ii}\} = \sum_{f(\sqrt{s})} \int \mathrm{d}\phi_2^f |\mathcal{M}_{fi}|^2 \tag{4.9}$$

where $f(\sqrt{s})$ are the accessible final states at center of mass energies $\sqrt{s}$. For $2 \to 2$ processes this simplifies in the notation of the partial waves (appendix A.2).

$$\Im\{a_\ell^{ii}\} = \sum_f |a_\ell^{fi}|^2 \quad \Longrightarrow \quad \sum_f \frac{|a_\ell^{fi}|^2}{|a_\ell^{ii}|} \le 1 \tag{4.10}$$

For the Standard Model with only one accessible state i this is a weaker bound than the previously applied $\Re\{a_0\} \le 0.5$ constraint, however, it becomes clear that unitarity violation is determined by the inelastic channels opening up.

A feasible and model-independent method to estimate the scale, at which a theory is supposed to enter the strong coupling regime, is Naive Dimensional Analysis (NDA) [26, 37]. NDA provides a powerful tool to evaluate the factors multiplying effective operators generated by strongly-interacting dynamics, taking into account loops and geometrical factors. This method is 'naive' in the sense that it neglects $\mathcal{O}(1)$ prefactors, arising from the fact that NDA provides an upper limit instead of an exact scale prediction. In a d dimensional theory, a loop typically has the form

$$g_d^2 \int \frac{\mathrm{d}^d p}{(2\pi)^d} f(p^2) = \frac{g_d^2}{2(2\pi)^d} \int \mathrm{d}\Omega_d \int \mathrm{d}p^2 p^{d-2} f(p^2)$$

with the area of the d dimensional unit sphere $2\pi^{d/2}\left[\Gamma(d/2)\right]^{-1}$ this is

$$= \frac{g_d^2}{2^d \pi^{d/2} \Gamma(d/2)} \int \mathrm{d}p^2 p^{d-2} f(p^2)$$

In NDA the coupling is chosen such that each loop order gives an equal contribution, so that in $d = 5$ the equation

$$1 \sim \frac{g_5^2 \Lambda}{24\pi^3} \tag{4.11}$$

leads to the strong coupling scale Λ up to a factor $\mathcal{O}(1)$. For Randall-Sundrum-related models, this scale depends on the localization along the additional warped dimension because of the scaling behavior mentioned in section 3.2. The smallest estimate can be attained by warping the scale (4.11) down to the TeV brane

$$\Lambda_{\mathrm{NDA}} \sim \frac{24\pi^3}{g_5^2} \frac{R}{R'} \tag{4.12}$$

For $R = 10^{-19}\mathrm{GeV}^{-1}$ the $\mathcal{O}(1)$ factor is found to be approximately

$$\frac{\Lambda_{\mathrm{PWA}}}{\Lambda_{\mathrm{NDA}}} \approx 0.12 \tag{4.13}$$

Upon extrapolation this means a cut-off of ~ 4.6TeV for the scenario with $m_{W^2} \approx 700$GeV. Probing invariant masses larger than 3TeV in weak boson scattering will be difficult at the LHC. We note that the cut-off can be pushed to higher scales ~ 7TeV by adding a large brane-localized $U(1)_Y$ gauge kinetic term [29].

4.3 Higgsless cross sections

To conclude this section about Kaluza-Klein scattering, and especially about Standard Model WW and WZ scattering by Kaluza Klein W and Z exchange, figures 4.8 and 4.9 compare the total cross sections for weak gauge boson scattering in the Standard Model and in the Higgsless model. The cross section for a general $2 \to 2$ process, e.g. $W^+(p_1)Z(p_2) \to W^+(q_1)Z(q_2)$, can be obtained by integrating [12]

$$\mathrm{d}\sigma = \frac{1}{4\sqrt{(p_1 \cdot p_2)^2 - m_1^2 m_2^2}} \left|\mathcal{M}_{fi}\right|^2 \frac{1}{16\pi^2} \frac{|\boldsymbol{p}_{\mathrm{CM}}|}{\sqrt{s}} \mathrm{d}\Omega \tag{4.14}$$

The squared amplitude was calculated with `HELAS`, while the integral over the scattering angle is again performed using Numerical Recipes' `qromb` subroutine.

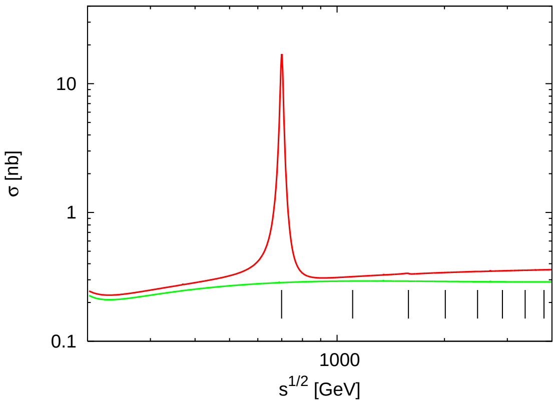

Figure 4.8: Comparison of the total cross sections for WZ scattering by Kaluza-Klein exchange (red, $m_{W^2} = 700\text{GeV}$) and Standard Model Higgs (green, $m_h = 700\text{GeV}$). The vertical black line segments mark the masses of the Kaluza-Klein Ws.

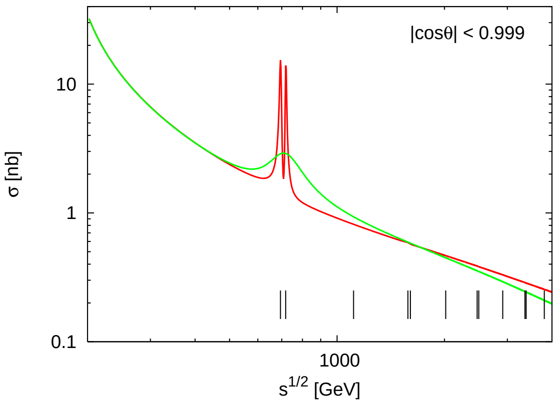

Figure 4.9: Comparison of the total cross sections for WW scattering by Kaluza-Klein exchange (red, $m_{W^2} = 700\text{GeV}$) and Standard Model Higgs (green, $m_h = 700\text{GeV}$). The vertical black line segments mark the masses of the Kaluza-Klein Zs. The phase space integral is cut at $|\cos\theta| < 0.999$ to avoid the singularity arising from t channel photon exchange.

Chapter 5

Implementation into vbfnlo

5.1 The program vbfnlo

VBFNLO [38] is a next-to-leading order QCD parton-level Monte-Carlo for vector boson fusion processes (VBF) created by D. Zeppenfeld *et al.* This thesis focuses on weak boson fusion processes, figure 5.1:

$$
\begin{aligned}
pp &\longrightarrow W^+ + W^- + \left\{ \begin{array}{c} 2j \\ 3j \end{array} \right\} + X \longrightarrow e^+ + \nu_e + \mu^- + \bar{\nu}_\mu + \left\{ \begin{array}{c} 2j \\ 3j \end{array} \right\} + X && \text{(5.1a)} \\
&\longrightarrow W^\pm + Z + \left\{ \begin{array}{c} 2j \\ 3j \end{array} \right\} + X \quad \longrightarrow e^\pm + \nu_e + \mu^\pm + \mu^\mp + \left\{ \begin{array}{c} 2j \\ 3j \end{array} \right\} + X && \text{(5.1b)} \\
&\longrightarrow Z + Z + \left\{ \begin{array}{c} 2j \\ 3j \end{array} \right\} + X \qquad \longrightarrow e^+ + e^- + \mu^+ + \mu^- + \left\{ \begin{array}{c} 2j \\ 3j \end{array} \right\} + X && \text{(5.1c)}
\end{aligned}
$$

The third jet arises from additional gluons radiated off the quark legs in figure 5.1. It is also possible to switch to $p\bar{p}$ as initial state.

Figure 5.1: Weak boson fusion topology calculated by VBFNLO. The shaded area contains the topologies of figure 4.1 in the physical basis and corresponds to the leptonic tensor, cf. section 5.2.

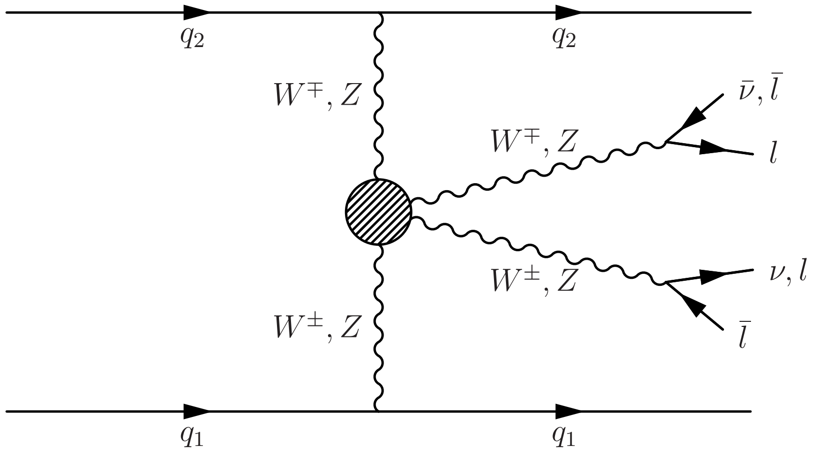

NLO-QCD corrections and model characteristics

There are several other topologies besides fig. 5.1 to be considered for the full processes (5.1), e.g. graphs where one gauge boson is radiated off the quark leg and subsequently decays leptonically. In the discussed limit $S = 0$ with fermiophobic Kaluza-Klein excitations, however, these topologies are heavily suppressed compared to the Standard Model-mode exchange diagrams due to small Kaluza-Klein-fermion couplings (chapter 3). They are neglected in the following, that is, the model of fig. 3.1 is supposed to contain an ideally delocalized fermion sector that resembles the Standard Model content. If there is a modification of the Higgsless model that allows for vanishing oblique corrections while a sizeable overlap of the zero-mode fermions with higher order Kaluza-Kleins is retained, one will focus on Drell-Yan production and related processes to analyse the model's phenomenology.

Although the code provides the next-to-leading order QCD calculations as an option, the details of their implementation will not be discussed as the NLO-QCD corrections factorize from the model-specific modifications. This can be understood from fig. 5.1: The depicted topology can be written

$$\mathcal{M}_{fi} = \mathcal{J}^{\varepsilon}_{q_1}\mathcal{J}^{\delta}_{q_2}\mathscr{L}_{\varepsilon\delta} \tag{5.2}$$

and all other topologies accordingly. The *leptonic tensor* $\mathscr{L}_{\varepsilon\delta}$ is defined to be the part of the amplitude, which is left after cutting the gauge boson propagators that connect the shaded area with the quark legs. This leaves all QCD-corrections to the *hadronic tensor* $\mathcal{J}^{\varepsilon}_{q_1}\mathcal{J}^{\delta}_{q_2}$ with the leptonic tensor unaffected, cf. [38, 39]. Consequently, all considered effects beyond the Standard Model are contained in the leptonic tensor for the discussed model.

Weak boson fusion signatures

Weak boson fusion processes (WBF) are sensitive to the mechanism of electroweak symmetry breaking as they involve longitudinal gauge boson scattering. In the Standard Model, WBF is a prominent Higgs production channel as it offers the second largest production cross section after gluon fusion with smallest relative error. The branching ratios for Higgs masses larger than 140GeV are dominated by decays into weak gauge bosons. WBF is also sensitive to strongly-coupled physics beyond the Standard Model [40] and is most promising for the Higgsless model sketched in fig. 3.1.

Other arguments in favor of WBF processes are their specific and clean signatures that arise from special kinematics and the processes' color structure [41]:

(i) The vector bosons radiated off the quark legs tend to carry small momentum fractions x. Additionally, the valence quark distribution peaks around $x = 0.1 - 0.2$, so there are two energetic jets that can be used to tag the event.

(ii) The W or Z boson masses act as cut-offs on the bosons' propagators, the two tagging jets have comparatively small transverse momenta $p_T \sim m_{Z,W}$. Along with the high energy of the scattered quark, this is tantamount to small scattering angles of the quarks, or large rapidity y or pseudorapidity η differences between the tagging jets.

$$y = \frac{1}{2}\ln\frac{E+p_z}{E-p_z} = \frac{1}{2}\ln\frac{1+\beta\cos\theta}{1-\beta\cos\theta} \xrightarrow[m\to 0]{\beta\to 1} \frac{1}{2}\ln\frac{1+\cos\theta}{1-\cos\theta} = \eta \tag{5.3}$$

Here $\beta = p/E$, and the limit $\beta \to 1$ corresponds to $m \to 0$.

(iii) Weak boson fusion proceeds without color exchange between the two incident quarks. Similar to photon bremsstrahlung in QED, additional gluon radiation will be preferentially emitted at small angles in the forward and backward directions, between the tagging jets and the beam axis. Thus, there is only few hadronic activity in the central region.

(i)-(iii) are in sharp contrast to QCD-mediated backgrounds, and can be used to enhance the significance by imposing cuts (section 6.1) and a central jet veto.

5.2 Redesigned leptonic tensors

The implementation of the model for the different decay channels requires modified versions of the leptonic tensors '`tozz.f`', '`towz.f`', and '`toww.f`' of VBFNLO, which consist of various subroutines for the different topologies. As already argued, only the fusion topologies vv`toww`, vv`towz`, and vv`tozz` need to be modified. v ranges over the allowed set of Standard Model gauge bosons. Exemplarily, the Feynman graphs for the part of the leptonic tensor $\mathscr{L}_{\varepsilon\delta}$ of $W^+W^- \to e^+\bar{\nu}_e\mu^-\nu_\mu$, where the Ws are radiated off the quark legs in fig. 5.1, are given in the following. As mentioned earlier, only the $WW\gamma$ coupling is taken to be the Standard Model value, the remaining three- and four-gauge boson-couplings (highlighted with a dot in the diagrams) differ from the SM. Note also, that there are no diagrams with Higgs exchange, but sums over the Kaluza-Klein intermediate states, that is all BSM-related physics is part of $\mathscr{L}_{\varepsilon\delta}$

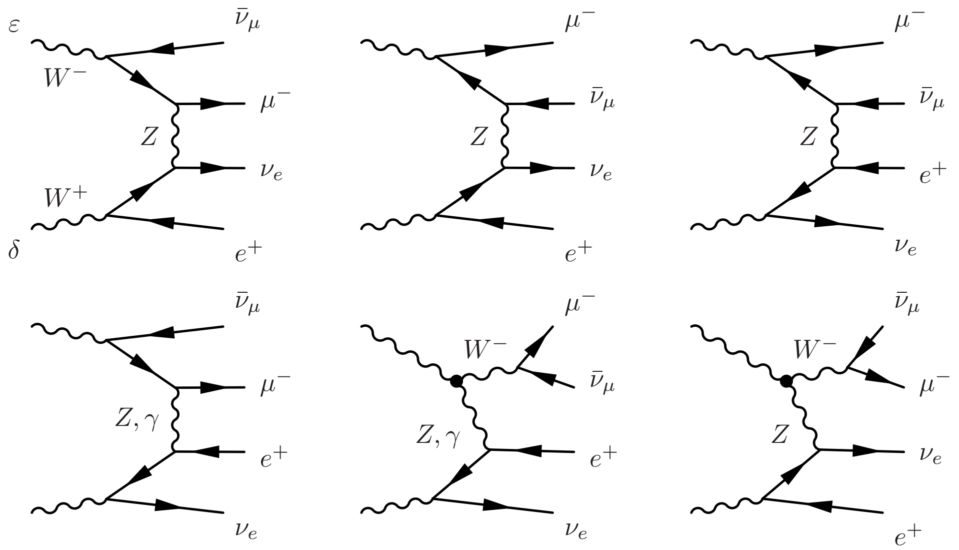

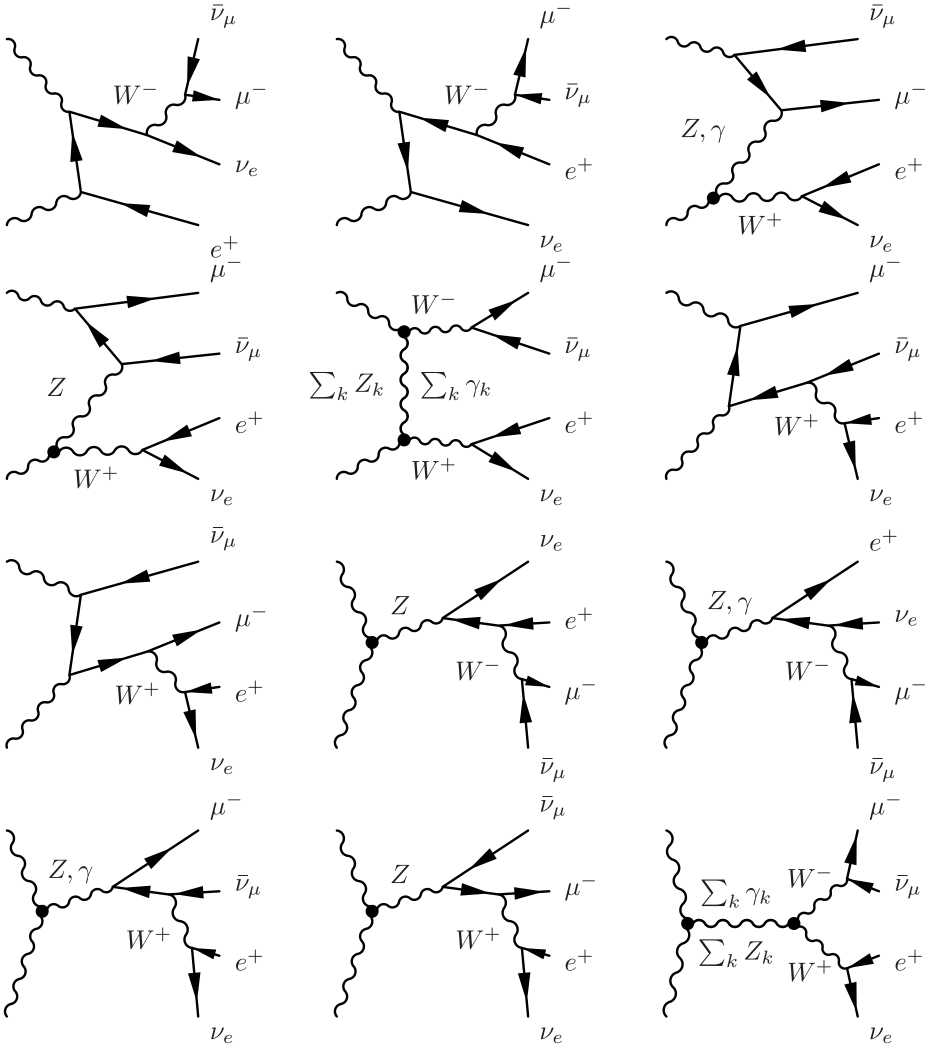

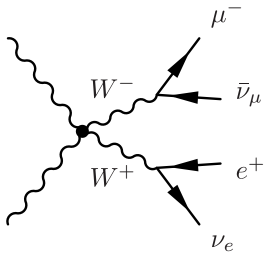

To include the additional gauge bosons, a new common block `coupl_kk` was created, which contains the number of Kaluza-Klein states to be included, their masses and couplings. This common block is filled by calling the subroutine `kk_coupl_inp` right after the Standard Model couplings, masses and widths are calculated with VBFNLO's `koppln` subroutine. `kk_coupl_inp` globally changes the WWZ-coupling and provides the gauge boson widths by calling the subroutine `widthkk`, which sums all the partial decay widths of the kinematically accessible Kaluza-Klein states using the coupling constants from the common block `coupl_kk`. The modified versions of the leptonic tensors contain internal loops over the Kaluza-Klein-related `HELAS` subroutines, e.g.

```
      call JVVXXX(w(1,1),w(1,2),gwwz_k(k),
     &         kkmass(k),kkwidth(k),kk1(1,k))
      call VVVXXX(w(1,3),kk1(1,k),w(1,4),
     &                     gwwa_k(k),ampk(k))
```

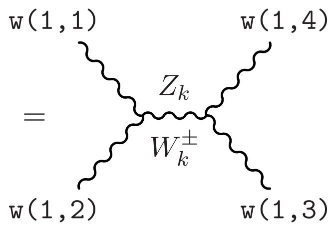

Here the `w(1,i)` are complex sixdimensional arrays that consist of the fusing vector bosons' off-shell wave functions and their fourmomenta calculated by VBFNLO's `VCARTX` subroutine. `JVVXXX` returns the off-shell vector current from the effective VVV_k vertex with the Kaluza-Klein's Breit-Wigner propagator included. Finally, the subroutine `VVVXXX` calculates the vertex function given the effective coupling and the wave functions and fourmomenta of the Kaluza-Klein `kk1(1,k)` and the two decay gauge bosons `w(1,3)`, `w(1,4)`. The *vv*`toww`, *vv*`towz` and *vv*`tozz` subroutines return the amplitude of a specific subprocess summed over the Kaluza-Klein states with the Standard Model contribution included to the `m2s` subroutines where the leptonic tensors are contracted (5.2) and the squared matrix element is calculated. The decay vector bosons' effective polarization vectors are determined from the massless decay leptons' fourmomenta q_i^μ, their fixed helicities, and $f\bar{f}V$ coupling g, e.g.

```
  call IXXXX(q1,zero,
&           l1hel,-1,wv1)
  call OXXXX(q2,zero,
&           l2hel,+1,wv2)
  call JIOXXX(wv1,wv2,g,
& gbmass,gbwidth,w(1,3))
```

$=$ `w(1,3)`

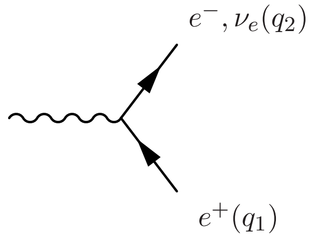

5.2.1 Couplings in `kk_coupl_inp.f` and sum rule saturation

By only taking a finite number of Kaluza-Klein states into account, the sum rules (4.6), (4.7) will be violated to a small extent. This has been checked numerically for 10 Kaluza-Klein states and the violation is found to be $\simeq 10^{-7}\%$ for the first and $\simeq 10^{-3}\%$ for the second sum rules (masses are typically $\sim 10^3$GeV), which is found to be in agreement with the numerical integration's relative error. However, the violation of the first sum rule ($\sim s^2$) is still large enough to spoil the cross sections and distributions[1]. The required agreement of the left and right side of (4.6), (4.7) is found to be at a level of $\lesssim 10^{-10}\%$, which is beyond the attainable precision of the effective couplings' integration with a sensible number of Kaluza-Klein states included. To 'saturate' the sum rules, given the small violation of the first one, the effective four-vertex coupling during a calculation with $n+1$ Kaluza-Klein states is *defined* to be equal to the right side of (4.6a), (4.7a), e.g.

$$g_{WWWW} \equiv \sum_{k=0}^{n} g_k^2 + g_{n+1}^2$$

with $g_k = g_{WWZ_k}$. Inserted in the second sum rule this yields

$$g_{n+1}^2 = \frac{4m_W^2 \sum_{k=0}^{n} g_k^2 - 3\sum_{k=0}^{n} m_k^2 g_k^2}{3m_{n+1}^2 - 4m_W^2}$$

[1]Using the couplings without further modification leads to a change in magnitude of the cross section.

Taking the couplings of the n Kaluza-Klein states to the Standard Model modes to be the ones from the numerical integration, `kk_coupl_inp` fixes the coupling g_{n+1} given the mass m_{n+1}. This guarantees small numerical sum rule violations $\lesssim 10^{-14}\%$ with the cross section and the phenomenology unaffected due to the fast convergence of the sum rules (cf. the exponential drop-off in figures 4.3, 4.4). All Kaluza-Klein related information including the relative sum rule violations are written to a text file for later checks and comparisons.

5.2.2 Tests

Most of the testing was done with code that provides couplings and masses. The calculated masses were checked against numerical results from MATHEMATICA for different R parameters. The convergence of the first sum rules marks another powerful test of the couplings' code as it is tantamount to the wave functions orthonormality, which was also checked by explicit integration. The feasibility to redesign the leptonic tensors by implementing additional `HELAS` subroutines combined with sum rules simplified VBFNLO's testing to a large extent. On the one hand, if implemented correctly, the cross sections will be consistent with gauge symmetry and Lorentz invariance by design. On the other hand, if the `HELAS` subroutines are implemented in a false way, this will be immediately reflected in the high energy behavior $\sim E^8$ of the squared matrix elements as the sum rules are no longer fulfilled. After fixing the sum rules by the previously described method, each $2 \to 2$ subamplitude was checked this way and afterwards implemented into the respective VBFNLO subroutines.

For consistency, the programs' results were also tested against existing predictions [20, 42].

Chapter 6

Higgsless cross sections and distributions at the LHC

With a center-of-mass energy of 14TeV, the LHC is going to test gauge boson pair invariant masses $\lesssim$ 3TeV in weak boson fusion. Figure 4.6 suggests that this should be sufficient to decide among different electroweak symmetry breaking mechanisms, in particular between breaking by the Standard Model Higgs or the geometric symmetry breaking mechanism arising from extra dimensions. Although the Higgsless model's deviations from the Standard Model are heavily constrained by electroweak precision measurements, the two models exhibit an extraordinarily different phenomenology. The appearance of additional charged gauge bosons are testable predictions on their own and as heavy s-channel states, they will leave footprints in numerous differential distributions. The numerical results are discussed in this chapter.

6.1 Weak boson fusion cuts

To identify the weak boson fusion processes, two hard jets need to be identified

$$p_{T,j} \geq 20\text{GeV}, \qquad |y_j| \leq 4.5 \tag{6.1a}$$

The k_T-algorithm with parameter $D = 0.8$ is used to construct jets from the final state partons. The visible decay leptons have to be hard, central, and isolated from each other and the jets to be observable

$$p_{T,l} \geq 20\text{GeV}, \qquad |\eta_l| \leq 2.5, \qquad R_{ll} \geq 0.2, \qquad R_{jl} \geq 0.4 \tag{6.1b}$$

where R_{jl} is the distance of the lepton from the jet in the azimuthal angle-pseudorapidity-plane (Lego-Plot). In addition, the leptons are required to fall into the rapidity gap between the two tagging jets

$$\min\{y_{j_1}, y_{j_2}\} \leq \eta_l \leq \max\{y_{j_1}, y_{j_2}\} \tag{6.1c}$$

In case of neutrinos in the final state, a cut on the missing transverse momentum

$$\not{p}_T \geq 30\text{GeV} \tag{6.1d}$$

is applied. To enhance the signal to (QCD) background ratio for weak boson fusion processes, the rapidity gap is chosen to be large and the jets are required to be measured in opposite detector hemispheres with a cut on their invariant mass

$$|y_{j_1} - y_{j_2}| > 4, \qquad y_{j_1} \times y_{j_2} < 0, \qquad m_{j_1 j_2} \geq 600\text{GeV} \tag{6.1e}$$

	Resonance structure			Cross section [fb]				
Process	Higgsless	(MS)SM	decay mode	(i)	(ii)	(iii)	(iv)	(v)
W^+Z	+	-	$3l + \not{p}_T$	1.05	0.69	0.50	0.50	0.53
W^-Z	+	-	$3l + \not{p}_T$	0.53	0.34	0.25	0.25	0.26
W^+W^-	+	+	$2l + \not{p}_T$	7.56	6.72	7.13	5.54	8.47
ZZ	-	+	$2l + \not{p}_T$	0.89	0.89	0.77	0.71	1.56
	-	+	$4l$	0.20	0.20	0.16	0.16	0.40

Table 6.1: Comparisons of the leading order cross sections and resonance structure of the Higgsless Model $m_{W^2} = 700$GeV and the SM (two Higgs doublet model) with cuts (6.1). The '+' denotes the appearance, the '$-$' the absence of a resonance in the respective model. The contributions of the different lepton generations have been summed while the small interference of identical final states is neglected. Statistical errors of the Monte-Carlo integration are smaller than 0.5%.

These cuts are very efficient in reducing the backgrounds.

6.2 SM and Higgsless model: LHC comparisons

To compare and eventually distinguish between Standard Model's electroweak symmetry breaking mechanism and the AdS$_5$ scenario, the following cases are considered:

(i) Warped Higgsless model with $m_{W^2} = 700$GeV, $m_{Z^2} = 695$GeV, and $m_{Z^3} = 718$GeV. This corresponds to a model parameter $R \approx 10^{-8}\text{GeV}^{-1}$ with a UV cutoff ~ 4.6TeV.

(ii) Warped Higgsless model with $m_{W^2} = 1190$GeV, $m_{Z^2} = 1187$GeV, and $m_{Z^3} = 1200$GeV. This corresponds to a model parameter $R = 10^{-19}\text{GeV}^{-1}$ and a UV cutoff ~ 2.7TeV. This is the smallest R parameter considered, and from a pessimistic perspective, the LHC will not be able to test the model's UV-completion to full extend.

(iii) Standard Model with $m_h = 120$GeV, which is the preferred Higgs mass from fits of the Standard Model to existing data.

(iv) Standard Model with $m_h = 120$GeV and invariant mass cut $m_{VV} \geq 130$GeV. This corresponds to a unitarized 'Higgsless Standard Model', which acts as an estimate of the irreducible Standard Model background, i.e. the SM gauge boson continuum.

(v) Standard Model with $m_h = 700$GeV for comparisons of the resonant channels. This mass is close to the upper bound on the Standard Model Higgs mass of 800GeV, arising from triviality bounds with higher order corrections taken into account.

The cross sections for (i)-(v) are listed in table 6.1. The program's important input parameters are to be found in appendix D.

The evident phenomenological difference of the two models is the occurrence of a charged, spin one resonance in the $W^\pm Z$ channel and the lack of resonances in ZZ fusion, which contrasts to the Standard Model and left-right symmetric extensions thereof. This is indeed a 'smoking gun' of the Higgsless models. While there are similar scalar s-channel contributions in two-Higgs-doublet models, these are strongly suppressed as they involve (pseudo)scalar Higgs couplings to the fermion legs, which are proportional to the fermions' masses. In Technicolor-like theories the exchanged bound states (techni-ρs or techni-σs) are in general heavy and very broad (typically several 100GeV) as the theory is strongly coupled. This again contrasts to the considered Higgsless model, where the first Kaluza-Klein W appears below 1TeV with perturbative couplings and widths of typically 10s of GeV so that they appear as sharp resonances in the invariant mass distributions[1]. For this reason, the $W^\pm Z$ channel's phenomenology is particularly interesting, section 6.2.3.

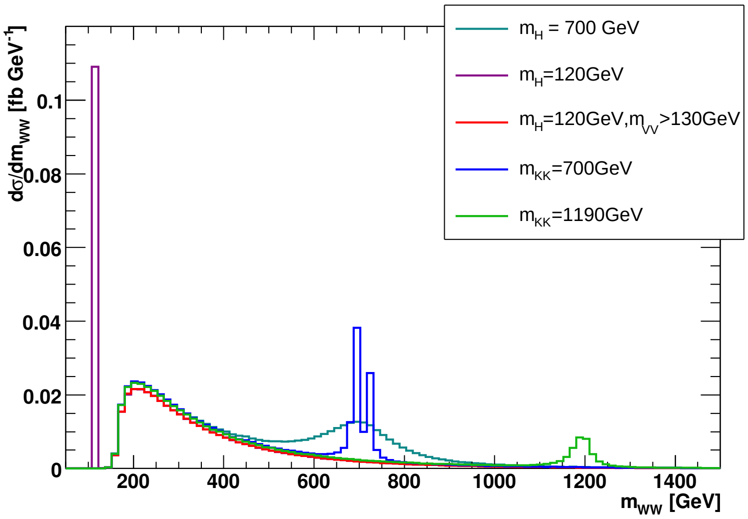

Figure 6.1: Invariant mass distribution for $WW \to 2l\not{p}_T$. Effects of the detector resolution are discarded.

6.2.1 $pp \to W^+W^- \to 2j + 2l + \not{p}_T$

This channel exhibits a resonance in the Standard Model as well as two resonances in the Higgsless model, which, however, are difficult to disentangle. The reconstruction of the invariant WW mass (fig. 6.1) requires hadronic W decays and is not possible for the considered final state. For the massive and sharp resonances a reconstruction similar to $h \to \tau\tau$ [43] where the decaying W pair is taken to be massless with respect to the Kaluza-Klein W_2 is promising but fails because of the small Kaluza-Klein masses. For heavier Kaluza-Klein spectra, the coupling is controlled by the second sum rule, so that the second mode is weaker coupled to the SM modes ($g_{WWZ_2} \sim m_2^{-1}$). Numerically, the coupling of scenario (ii) is only 57% of the coupling of scenario (i). That is, for Kaluza-Klein masses large enough to improve the approximation, the Kaluza-Klein is too weakly coupled and kinematically suppressed. In addition, the integrated Higgsless

[1]In fact, from AdS/CFT correspondence, the Kaluza-Klein states are techni-ρs of the strongly coupled CFT.

cross section decreases with a heavier Kaluza-Klein mass spectrum. Without the possibility to reconstruct the neutrino's momenta, one is forced to rely on observables in the transverse plane. The definition of the transverse mass of the $2l\not{p}_T$ system

$$m_T^2(WW) = \left(\sqrt{m_{ll}^2 + \vec{p}_{T,ll}^{\,2}} + |\not{p}_T|\right)^2 - (\vec{p}_{T,ll} + \vec{\not{p}}_T)^2 \tag{6.2}$$

allows for a reconstruction (fig. 6.2) of the comparatively light resonances and does not yield a clean reconstruction of the Kaluza Klein or the heavy Higgs. The different distributions between the two latter cases is due to their different widths.

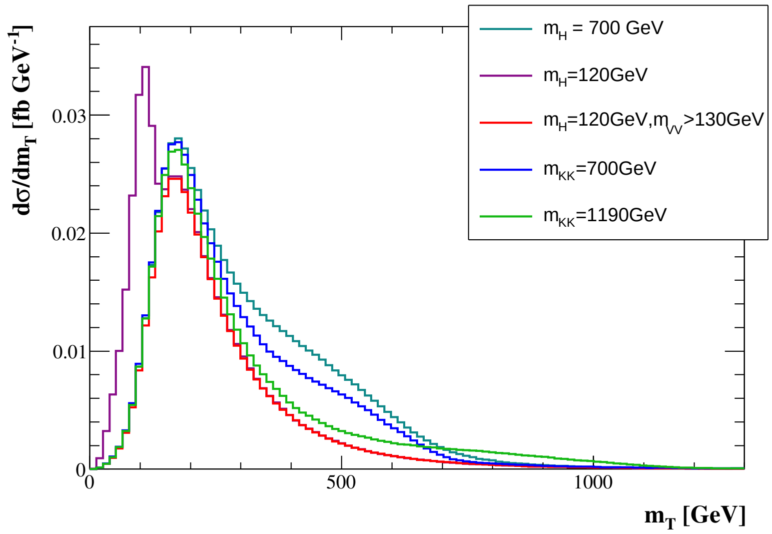

Figure 6.2: Transverse mass distribution (6.2) of the two decay lepton in $W^+W^- \to 2l\not{p}_T$.

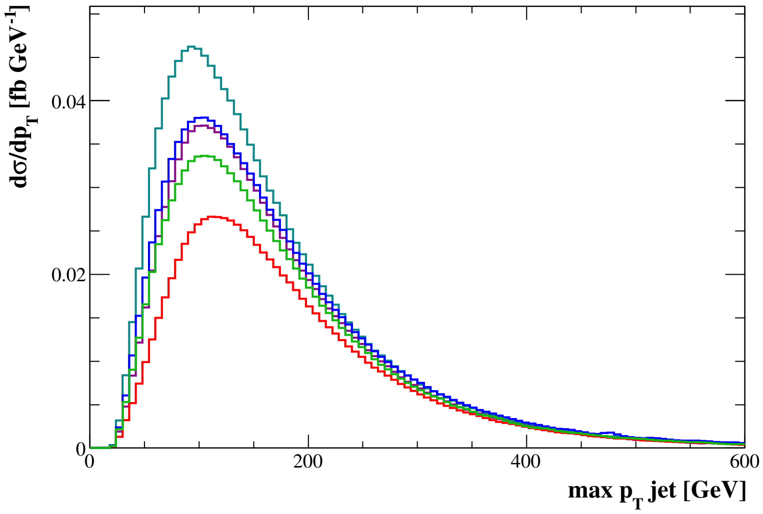

Figure 6.3: p_T spectrum of the hardest jet in $W^+W^- \to 2l\not{p}_T$.

The hadronic observables remain rather unaffected except for the change in the cross section. Figures 6.3 and 6.4 show the p_T spectrum of the hardest jet and the azimuthal distribution of the two tagging jets for the 2 jet final state, respectively. The jets peak at slightly different p_T values and the Higgsless model 'interpolates' between the heavy Higgs and the Standard Model with invariant mass cut.

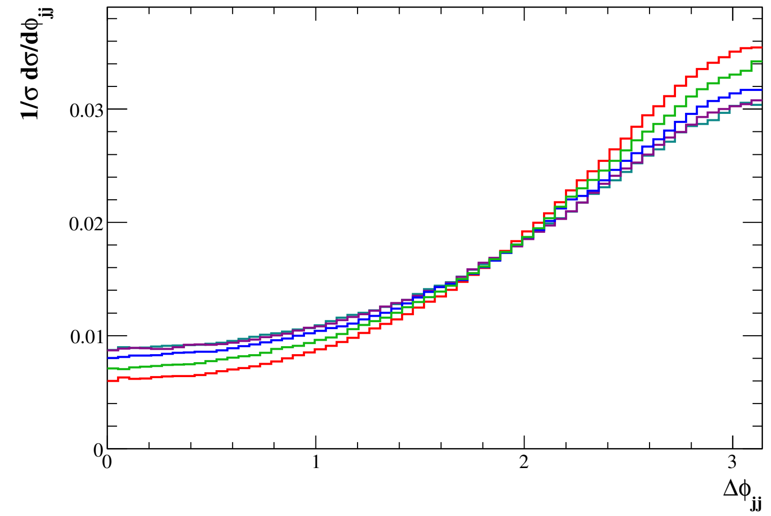

Figure 6.4: Distribution of the azimuthal angle between the two tagging jets.

A heavy particle in the s-channel mainly affects the angular correlations of the visible leptons depicted in fig. 6.5-6.8. The leptonic observables are quite robust against detector effects (C.1b), and are unlikely to be spoiled by parton showering and hadronization (which also holds for tag jet observables after additional central jet vetoing). The charged leptons tend to be back-to-back in case of the heavy resonances as they undergo large boosts that stem from the large momenta of the W bosons in the Kaluza-Klein Z or heavy Higgs rest frame. Along with the distribution of the leptons' rapidity difference peaking at small values, this explains the LEGO Plot separation in fig. 6.6.

$$R_{ll} = \sqrt{\Delta\phi_{ll}^2 + \Delta\eta_{ll}^2}$$

The reconstructed transverse mass (6.2) and the angular distributions figs. 6.5, 6.8 clearly provide distinctions between the resonances mass. The characteristics of the angular distributions then bear information about the particle's spin. For the large masses these correlations are, however, blurred as the Ws from the particle's decay do undergo the Lorentz boosts. But still, the Kaluza Klein scenario exhibits 20% less back-to-back leptons than the heavy Higgs distribution.

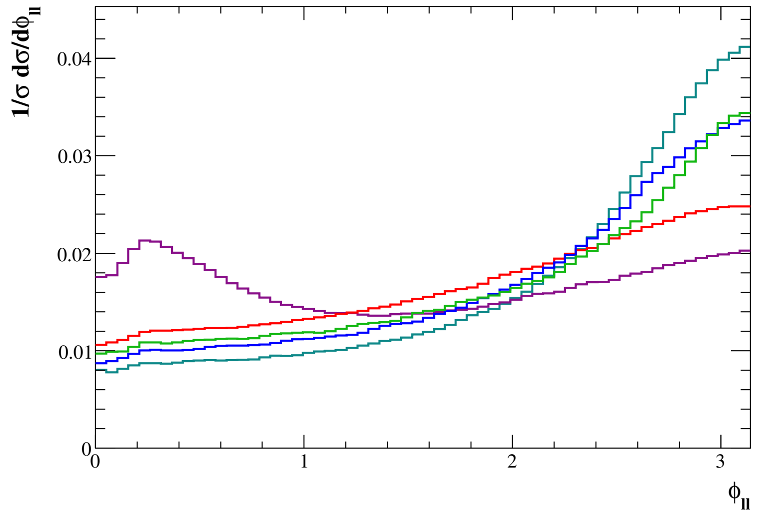

Figure 6.5: Distribution of the azimuthal angle between the two decay leptons.

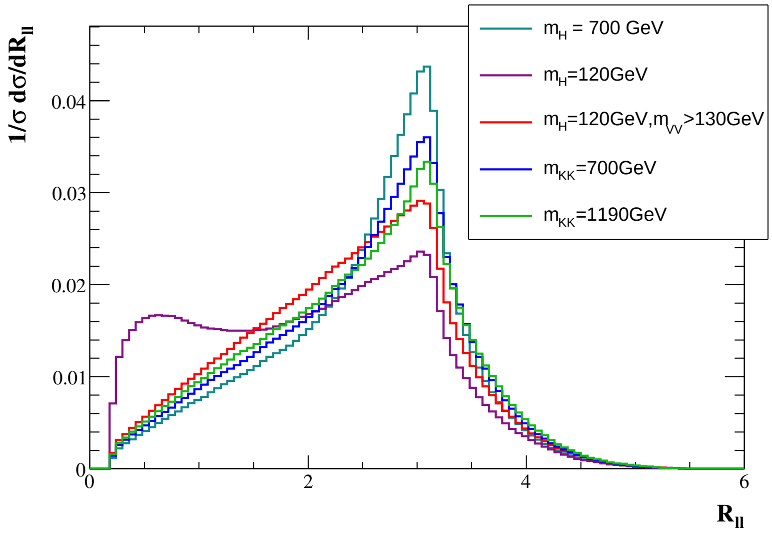

Figure 6.6: Lego Plot separation of the two decay leptons.

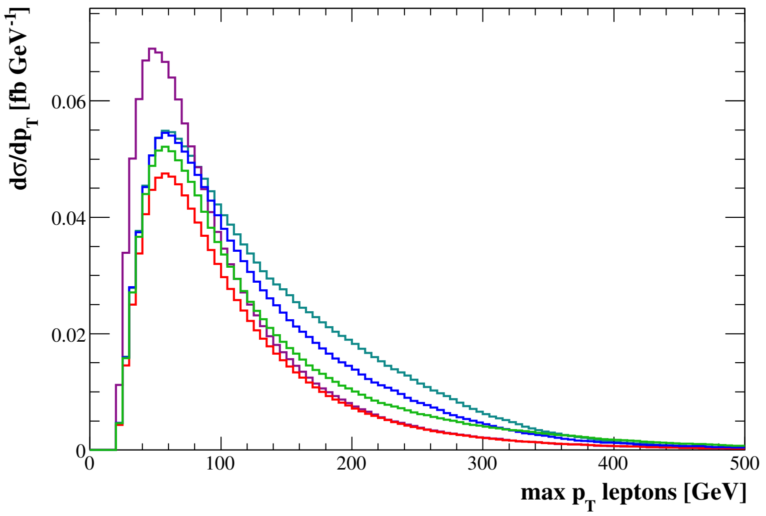

Figure 6.7: $\max p_T$ distribution of the two decay leptons.

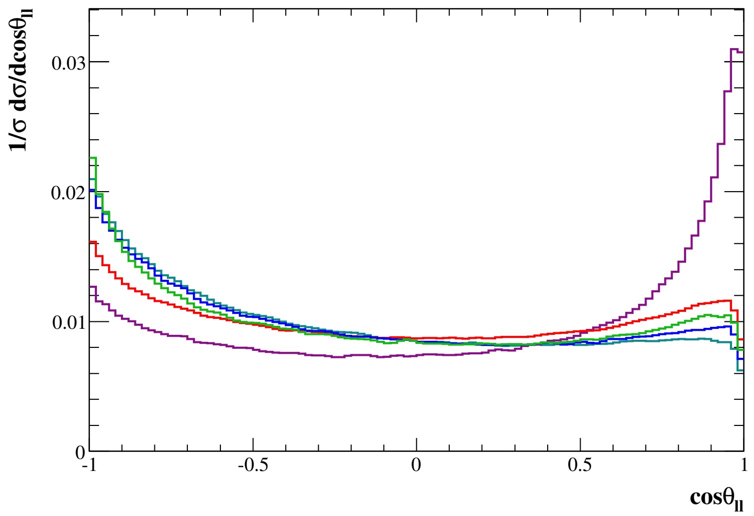

Figure 6.8: $\cos\theta$ of the two decay leptons.

6.2.2 $pp \to ZZ \to 2j + 2l + \not{p}_T$ and $pp \to ZZ \to 2j + 4l$

The distribution of the Higgsless model in these channels will resemble the ones from (iv) to some extent but should not be considered equal: Without a Higgs in the particle spectrum, there is no $ZZ \to ZZ$ scattering. Formally, this corresponds to a decoupled Standard Model Higgs, while $m_{ZZ} \geq 130$GeV still gives small contributions to Higgs-sensitive lepton distributions from s, t and u channel off-shell Higgs exchange. The higher cross section in the Higgsless cases partly arises from the larger WWZ-coupling, but mainly from the lack of the scalar Higgs exchange, which differs in sign with respect to the gauge boson graphs in the Standard Model. The comparison of the resonance structures (which is accompanied by sizeable change in the cross sections) of the ZZ and $W^{\pm}Z$ processes at the LHC (table 6.1) is going to provide a powerful test of the Higgsless scenarios against the Standard Model and the two Higgs doublet models. The W^+W^- channel exhibits no information about wether the resonance that controls the distributions is a heavy Higgs or a Kaluza-Klein except for the impact of the particles' widths. In contrast to the W^+W^- channel, however, the invariant mass of the process $ZZ \to 4l$ can be fully reconstructed, being the cleanest channel for Higgs discovery for $m_h \geq 180$GeV and thus the resonance structure of this channel (fig. 6.9) can be measured very accurately for heavy Higgses but also for the Higgsless model. The modifications of the distribution's shapes from light Higgs particles are mediocre. The jets' max p_T distribution again resemble in shape (except for similar shifts fig. 6.3) and is plotted in figure 6.10.

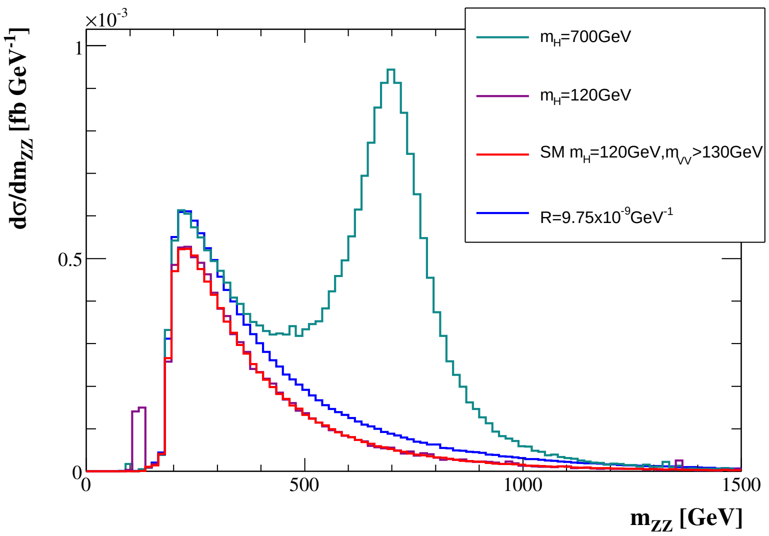

Figure 6.9: Invariant mass distribution for $ZZ \to 4l$.

The explanation of the W^+W^- angular distributions also persists to the $2l\not{p}_T$ final state via ZZ. The heavy Higgs leaves its footprints in terms of two strongly collimated charged leptons that stem from the heavily boosted Z decays. This marks another indirect test of the ZZ resonance structure with an approximately quadrupled cross section compared to the clean $4l$ decay mode. The Kaluza-Klein distribution for different Kaluza-Klein masses do only differ by the changed WWZ coupling. For this reason only the 700GeV Kaluza-Klein scenario is depicted.

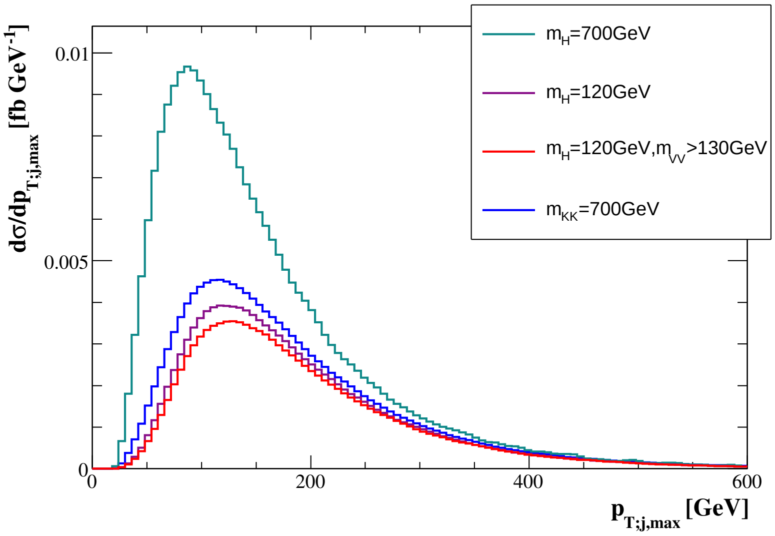

Figure 6.10: $\max p_T$ distribution of the tagging jets.

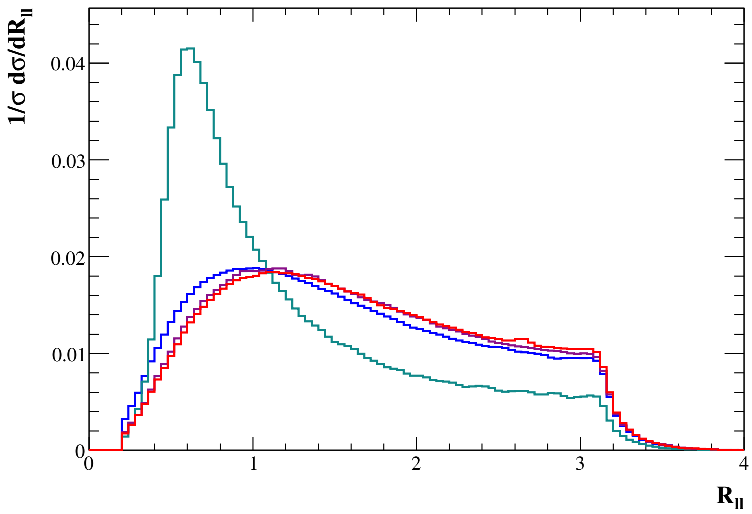

Figure 6.11: LEGO Plot separation of $ZZ \to 2l\not{p}_T$.

6.2.3 $pp \to W^{\pm}Z \to 2j + 3l + \not{p}_T$

This channel is the most exceptional one compared to other models of electroweak symmetry breaking. The resonance structure depicted in table 6.1 and figure 6.12 is a striking feature of the models' electroweak sector. Because in the Standard Model there are only t and u channel Higgs exchanges, the cross section and the distributions are rather indifferent to variations of the Higgs' mass. For this reason only scenarios (i)-(iii) are plotted in the following.

The invariant mass distribution can not be reconstructed directly, in contrast to $ZZ \to 4l$. However, the W^2 can be reconstructed by measuring the momenta of the charged leptons and the missing transverse momentum. By demanding that two of the charged leptons lie close to the Z mass shell, the neutrino momentum can be determined up to a twofold ambiguity by the requirement

$$2p_\nu \cdot p_l \equiv 2\not{p} \cdot p_l = m_W^2 \tag{6.3}$$

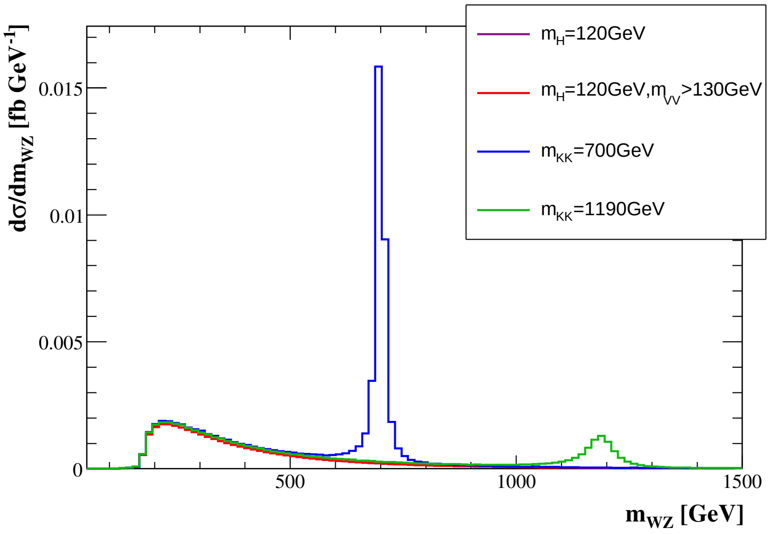

Figure 6.12: Invariant mass distribution for $W^+Z \to 3l\not{p}_T$. Effects from the detector's resolution are discarded. The invariant mass distribution of the W^-Z channel is identical except for the smaller cross section.

This ambiguity leads to a theoretical uncertainty that is negligible compared to combinatorial errors in recombining the Z mass. Nevertheless, the largest effect on the distribution figure 6.13 stems from the finite detector resolution, in particular for $\not{p}_T$ (cf. appendix C).

Alternatively, the W_k peak can be reconstructed from the transverse cluster mass fig. 6.14, which is defined by

$$m_T^2(WZ) = \left(\sqrt{m_{lll}^2 + \vec{p}_{T,lll}^{\,2}} + |\not{p}_T|\right)^2 - (\vec{p}_{T,lll} + \vec{\not{p}}_T)^2 \tag{6.4}$$

and also the invariant mass distribution of the visible leptons shows characteristics of the additional resonance.

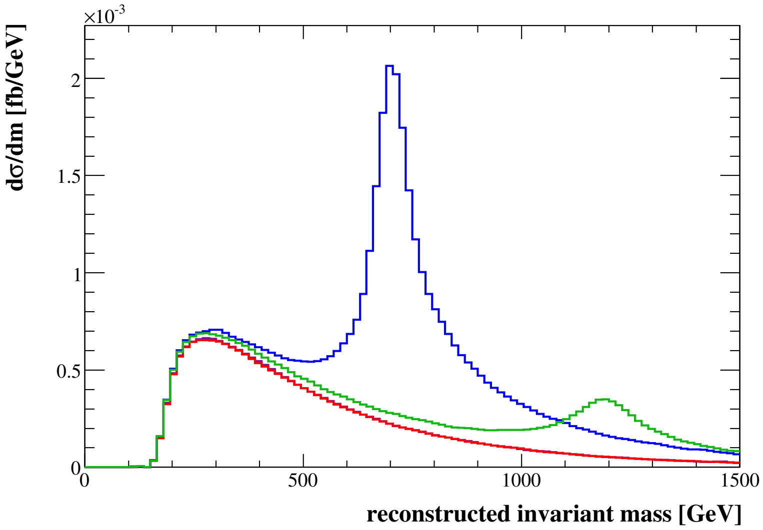

Figure 6.13: Reconstructed mass m_{W+Z} (6.3). The leptons required to reconstruct the Z boson are chosen such that their invariant mass differ at most 5GeV from the Z mass for half of the statistics. The other half is supposed to be identified by the leptons' different family type (e^- vs. μ^-).

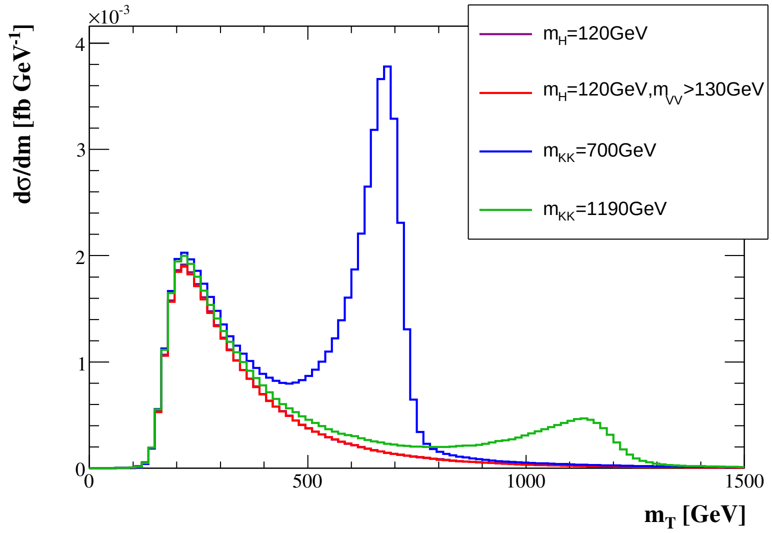

Figure 6.14: Transverse cluster mass distribution for $W^+Z \to 2l\not{p}_T$.

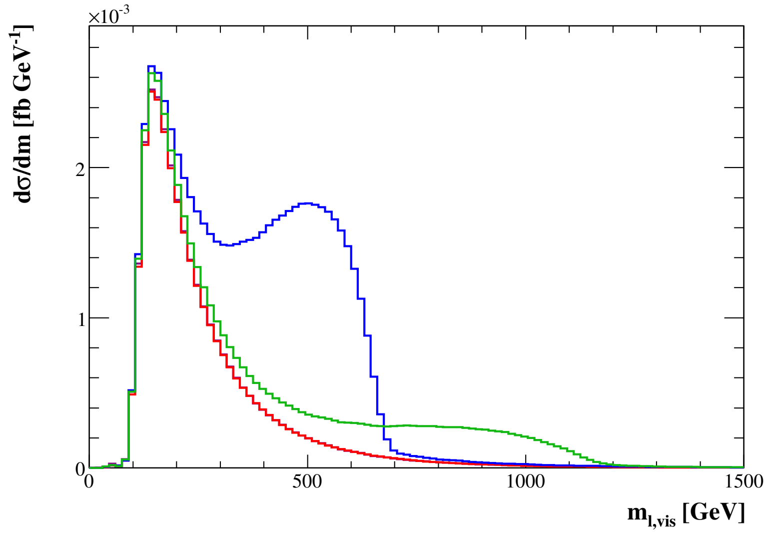

Figure 6.15: Distribution of the invariant mass of the visible leptons.

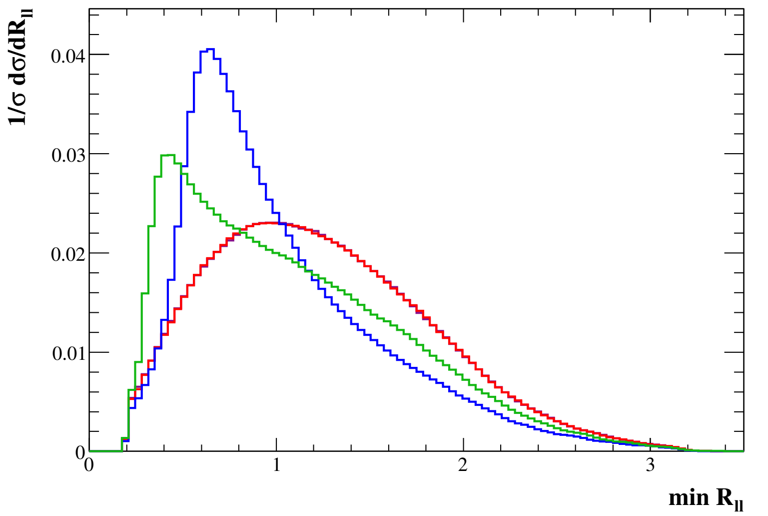

Figure 6.16: Distribution of the minimal LEGO-Plot separation of the three leptons.

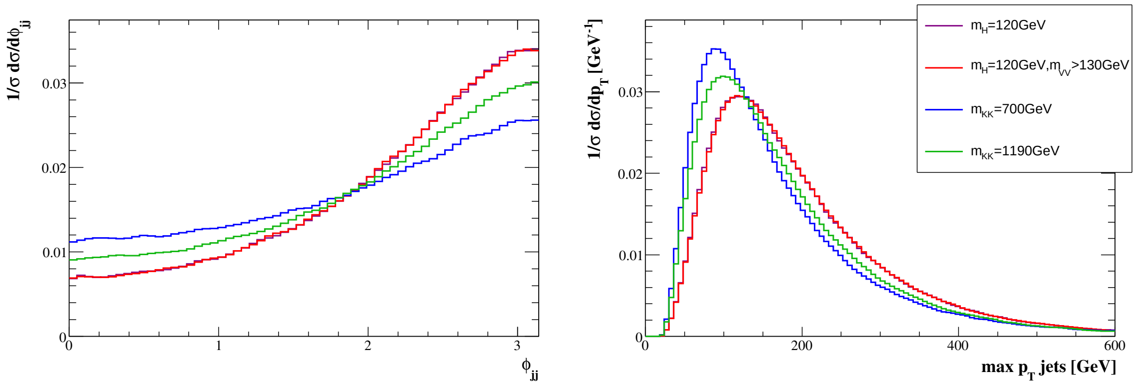

Figure 6.17: *Left*: Azimuthal angle between the two tagging jets. *Right*: p_T distribution of the hardest jet.

Due to the steep drop-off of the Jacobian peak in the transverse mass, the detector resolution does not affect the distribution too much. This is why, the reconstruction via (6.4) yields a cleaner result than than the methode (6.3).

Again, the angular distributions are dominated by large boosts. In contrast to the previously discussed channels, there are quite sizeable modifications of the jet distributions compared to the Standard Model ones, figure 6.17, which can not be the result of a heavy Higgs as in the W^+W^- channel. The limits $\Delta\phi_{jj} = 0, \pi$ exhibit differences of approximately 20% and the azimuthal angle between the tagging jets flattens out in the Higgsless scenario approaching the Higgsless Standard Model with an increasing decoupling of the Kaluza Klein states. Also the p_T distribution peaks at a $\approx$ 25GeV smaller value. The maximum of the rapidity-difference distribution of the jets is shifted to larger y, which also holds for the maximum lepton-jet rapidity difference, figure 6.18. This is because the rapidity-difference distribution of the leptons peaks at small values due to the boost (that is, the leptons are produced slightly more central).

Another consequence of the heavy Kaluza-Klein W is the changed shape of the $\not{p}_T$ distribution, figure 6.19. The distribution peaks at larger $\not{p}_T$ and does not exhibit the steep drop-off encountered in the Standard model. This is because the neutrino

Figure 6.18: *Left*: Absolute rapidity difference between the tagging jets normalized to the cross sections. *Right*: Normalized, maximal jet-lepton rapidity difference.

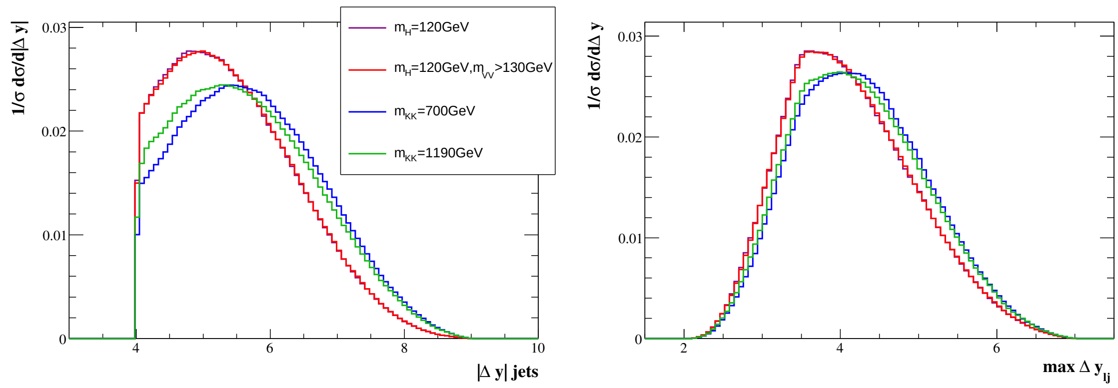

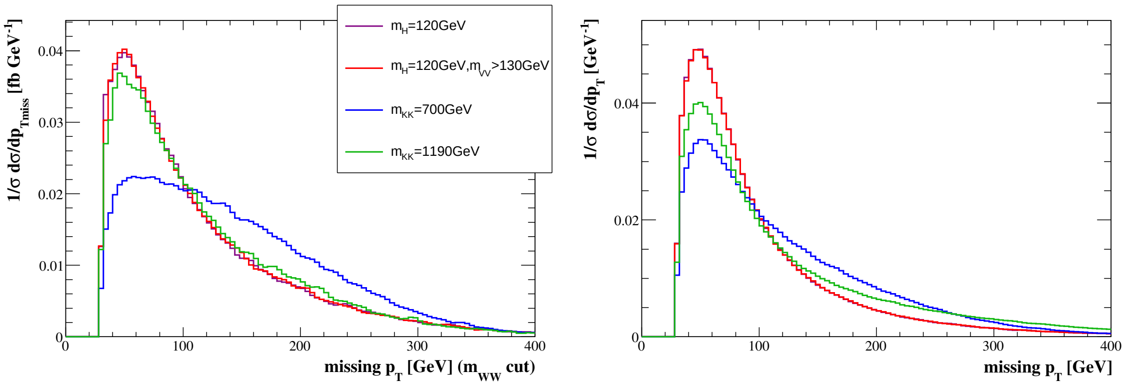

Figure 6.19: *Left*: Normalized $\not{p}_T$ distribution of the resonance scan 650GeV$< m_{WZ} <$ 750GeV with detector effects discarded. *Right*: Full $\not{p}_T$ distribution including detector effects, normalized to the cross section.

receives sizable momentum fractions from the heavy intermediate state. This effect is blurred when detector effects are switched on and the full Standard Model background is included. From the 1200GeV scenario's shape in fig. 6.19, it is also suggestive that the final state is hardly influenced by the Kaluza-Klein exchange in invariant mass regions away from the resonance.

6.3 QCD corrections to Higgsless WBF

QCD in Higgsless models

Including the unbroken gauge group $SU(3)_C$ into the bulk of the model sketched in fig. 3.1 leads to testable predictions: As a consequence of both-sided Neumann boundary conditions, the gluon-tower is similar to the photon-tower and the appearance of gluons with masses $\mathcal{O}$(TeV), coupling only to colored fermions, leads to characteristic signatures in quark-quark scattering, which then provides a test of the structure of the fermion sector proposed by the constraints from the oblique corrections (chapter 3). By including the next-to-leading order contributions to the hadronic tensors in Vbfnlo's calculation, the loop effects of the $\mathcal{O}$(TeV) Kaluza-Klein gluons are omitted, thus, the following QCD corrections are to be understood as zero-mode corrections. Nevertheless, the contributions of the massive gluons should be negligible compared to the Standard Model gluon corrections as the massive loops will be heavily suppressed by the rather large Kaluza-Klein gluon mass and it's small coupling. As the $W^\pm Z$ channel is most decisive for the Higgsless models, the next-to-leading order corrections are studied exemplarily for this process. The results turn out to be comparable to the Standard Model [38] and rather generic for all the considered weak boson fusion processes, table 6.2.

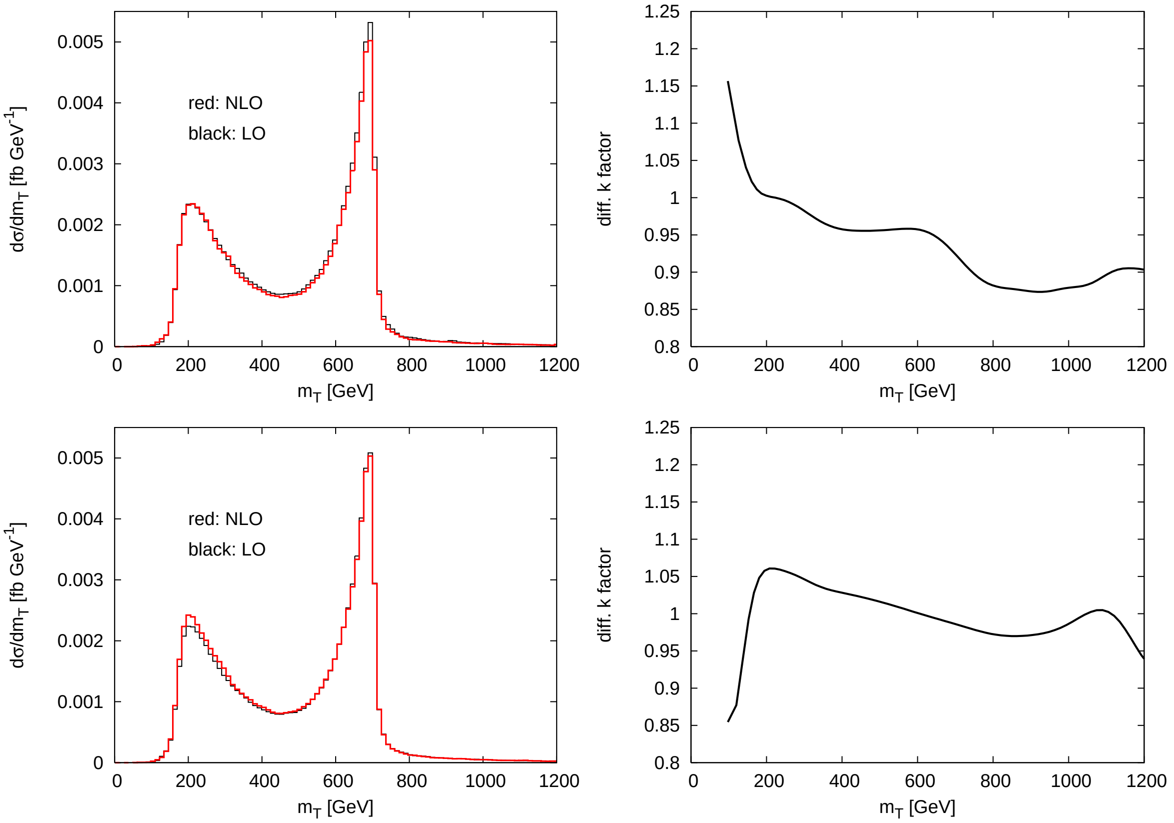

Figure 6.20: Leading and next-to-leading order distributions of the transverse cluster mass and the differential $k(m_T)$-factor (6.5) for $m_{W^2} = 700$GeV in W^+Z, respectively. Effects from detector resolution are neglected. *Top*: Fixed factorization scale $\mu_F = (m_W + m_Z)/2$. *Bottom*: Factorization and normalization scales are chosen to be the t-channel momentum transfers of the incoming Standard Model W or Z in the VBF graphs.

QCD corrections to $W^\pm Z$

The color singlet structure of (5.2) hints at small QCD-induced corrections to the leptonic observables. This is only partly true as the differential k-factor

$$k(\hat{\mathcal{O}}) = \frac{\mathrm{d}\sigma^{\mathrm{NLO}}}{\mathrm{d}\mathcal{O}} \bigg/ \frac{\mathrm{d}\sigma^{\mathrm{LO}}}{\mathrm{d}\mathcal{O}} \tag{6.5}$$

of the transverse mass (6.20) (and all other distributions) ranges between 1.2 and 0.8, indicating a quite sizeable deviation of the distributions' shapes. This also applies for the NLO-corrections to the jet observables, figure 6.21. In [38] it was pointed out that a 'proper' choice of the factorization scale, namely the momentum transfer of the t channel electroweak Standard Model gauge bosons Q in VBF graphs, improves the leading order shapes with respect to the full NLO calculation. This was checked and also confirmed for Higgsless weak boson fusion (cf. figures 6.20, 6.21), independent of the underlying Kaluza-Klein mass spectrum. The overall k factors of the Higgsless cross sections with these different scale choices are

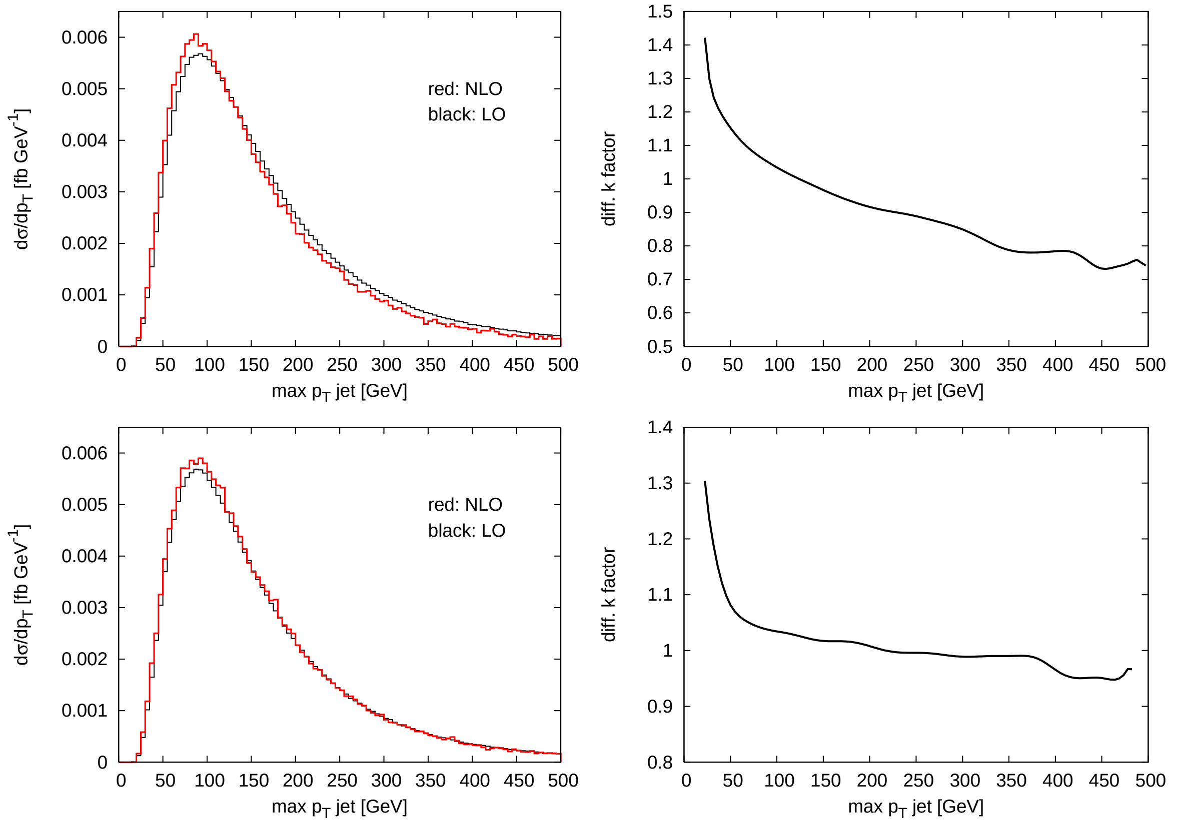

Figure 6.21: Leading and next-to-leading orderdistribution of the tagging jets' maximum transverse momentum. Detector effects are neglected. *Top*: Fixed factorization scale $\mu_F = (m_W + m_Z)/2$. *Bottom*: Factorization and renormalization scales are again chosen to be Q.

W^+Z	$k = 0.965$	μ_F, μ_R fixed $\mu = (m_W + m_Z)/2$
	$k = 1.021$	$\mu_F = \mu_R = Q$, LO result $\sigma = 1.01$fb
W^-Z	$k = 0.985$	μ_F, μ_R fixed $\mu = (m_W + m_Z)/2$
	$k = 1.043$	$\mu_F = \mu_R = Q$, LO result $\sigma = 0.51$fb

The next-to-leading order results differ by $\lesssim 0.5\%$ due to the residual scale dependence. This small value signalizes a very good perturbative control over the Higgsless weak boson fusion.

Summary

Table 6.2 summarizes the NLO-QCD corrections to the various weak boson fusion processes (5.1). As already mentioned, ZZ scattering in different Kaluza-Klein scenarios differs only by a percent-level change of the WWZ coupling and does not contain any further information. Thus, the ZZ results for only the Kaluza-Klein scenario with $m_{W^2} = 700$GeV are given. The overall k factors are found to be few percent, while the corrections to the distributions are typically $\lesssim 7\%$.

fixed scale (k factor)	scales = Q (k factor)	process	model
7.34 (0.97)	7.41 (1.05)	W^+W^-	
1.02 (0.97)	1.02 (1.02)	W^+Z	$m_{W^2} = 700\text{GeV}$
0.52 (0.98)	0.52 (1.04)	W^-Z	
0.89 (0.99)	0.88 (1.06)	$ZZ \to 2l\not{p}_T$	
0.21 (1.02)	0.20 (1.05)	$ZZ \to 4l$	
6.66 (0.99)	6.50 (1.05)	W^+W^-	
0.66 (0.97)	0.66 (1.03)	W^+Z	$m_{W^2} = 1190\text{GeV}$
0.33 (0.98)	0.33 (1.04)	W^-Z	

Table 6.2: NLO-QCD results of the total Higgsless weak boson fusion cross sections summed over the leptonic final states with identical final state-interference neglected.

6.4 Discussion

The previous section 6.2 elucidated the Higgsless model's different phenomenology compared to the various Standard Model scenarios that exhibit similar resonance structures or that are favored by electroweak fits. The differences in the leptonic angular correlations are evident and dominated by the boosts from the heavy Kaluza-Klein resonance. Particularly, the $W^\pm Z$ channel exhibits striking and model-specific signatures as expected. The combined analysis of the four different channels, along with perturbative stability and small NLO-QCD corrections, leads to precise predictions of the model's weak boson fusion signatures at the LHC. However, a complete study of the Model requires a detailed analysis of the (modified) backgrounds to the corresponding VBF process, e.g. tZj and tWj production, respectively. This was not performed, so the numbers of table 6.3 must not be taken literally, but have to be considered as an upper bound at most. There, the significance is defined to be

$$\frac{\Delta S^{KK}}{\sqrt{S^{SM}}} = \frac{|\sigma^{KK} - \sigma^{SM}|}{\sqrt{\sigma^{SM}(m_{VV} > 130\text{GeV})}} \times \sqrt{\text{luminosity}}$$

The rather small numbers of the comparison to the $m_h = 120\text{GeV}$ Standard Model case is misleading because a light Higgs will be experimentally well-established within a short time. The mentioned ambiguity between a heavy resonance in the $2l\not{p}_T$ channel might become resolved within three years of running the LHC at high luminosity.

Furthermore, the distributions of the different channels offer good possibilities to enhance the signal-to-background ratio by imposing additional cuts. Particularly, due to the resonance in the $W^\pm Z$ channel, in a 100fb^{-1} sample, one expects

$$N(0.75 m_{W^2} \leq m_T^{WZ} \leq 1.25 m_{W^2}) = \begin{cases} 73 & 700\text{GeV Kaluza-Klein} \\ 18 & 1190\text{GeV Kaluza-Klein} \end{cases}$$

events in the mass range under the peak of the transverse cluster mass. These numbers are inferred from the leading order calculation $\mu_F = \mu_R = Q$ with the k parameter

Final state	Hypothesis SM m_h [GeV]	KK scenario	Luminosity 10fb^{-1}	100fb^{-1}	300fb^{-1}
$2j3l\not{p}_T$	120	(i)	3.0	9.6	16.6
		(ii)	1.0	3.2	5.6
$2j3l\not{p}_T$	700	(i)	2.8	9.1	15.8
		(ii)	0.9	2.8	4.8
$2j2l\not{p}_T$	120	(i)	0.7	2.2	3.9
		(ii)	0.4	1.1	1.9
$2j2l\not{p}_T$	700	(i)	2.0	6.2	10.9
		(ii)	3.0	9.6	16.7
$2j4l$	120	(i),(ii)	0.3	1.0	1.7
$2j4l$	700	(i),(ii)	1.6	5.0	8.7
		Significance	$\Delta S^{KK}/\sqrt{S^{SM}}$		

Table 6.3: Test of the Higgsless model against the various Standard Model expectations based on the cross sections of table 6.1, the small QCD corrections do not change the picture qualitatively. The scenarios (i) and (ii) represent $m_{W^2} = 700\text{GeV}$ and 1190GeV, respectively. 1fb^{-1} is the expected integrated luminosity of the first LHC run, 10fb^{-1} is an optimistic value for the end of 2009, while 100fb^{-1} is the per-year design luminosity of the CMS experiment.

varying over the considered mass range $0.99 \leq k \leq 1.04$, so they can be considered stable against NLO effects.

Given a good efficiency to reduce the backgrounds by cuts, requiring 10 events for the discovery of the $W^{\pm}$ [42], approximately one year of measuring at high luminosity will test the 'backbone' of the Higgsless model over the whole considered parameter range. At the same time measuring *no* 700GeV resonance in the $4l$ final state

$$N(0.75m_h \leq m_{4l}^{ZZ} \leq 1.25m_h) = \begin{cases} 20 & \text{700GeV Higgs} \\ 4 & \text{Higgsless} \end{cases}$$

can be considered as the exclusion of the Standard Model's electroweak symmetry breaking mechanism including left-right symmetric extensions in favor of the Higgsless model (the k parameter varies $0.99 \leq k \leq 1.03$ over the considered mass range). Full identification still needs a precise determination of the detected resonances' couplings to the Standard Model gauge bosons and their mass in order to check a possible violation of the sum rules, maybe already by the first non-Standard Model mode. Whilst this would rule out the Higgsless realization immediately, violations from higher modes can not be studied in weak boson fusion as they are too weakly coupled.

Another prediction of the Higgsless model is the new particles' spin. The processes' angular correlations, however, are completely spoiled by the large Lorentz boosts, which turns spin measurements into a challenging task. All considered channels do not show any noticeable change in forward-backward asymmetries compared to the Standard Model cases. Spin measurements from Drell-Yan processes are disfavored by precision data while $ZZ \to 4l$, which can be used to determine the Higgs' spin in the Standard Model, does not exhibit a resonance.

Chapter 7

Summary

The mechanism of electroweak symmetry breaking remains the most urgent issue to be solved at the Large Hadron Collider. The Standard Model's Higgs mechanism (chapter 2), while being incredibly good in agreement with measurements so far, does not solve the remaining caveats in a completely satisfying way.

Thus, alternative approaches have been and will be developed to obtain an answer at a more fundamental level. Today, particularly theories with extra dimensions are considered as appealing candidates as they provide a natural interpretation of the Hierarchy problem in terms of additional, compactified dimensions, chapter 3. These models originally utilized the existence of branes to include the full Standard Model by confining it to a fourdimensional subspace in the higherdimensional framework. However, it was pointed out recently, that particularly the Randall-Sundrum scenarios, along with their dual interpretation driven by the AdS/CFT conjecture, allow for a symmetry breaking mechanism, consistent with measurements of the obilque corrections, while turning the Higgs field into a redundant degree of freedom. This Higgsless symmetry breaking provides a geometric alternative to the Standard Model Higgs mechanism and leads to a distinct and testable phenomenology at the LHC. The properties of the considered model sketched in figure 3.1, that is, the model's particle spectrum and its unitarity behavior, have been discussed in chapter 4. Also a preliminary discussion of the model's phenomenology and its differences compared to the SM was presented in terms of the comparison of the Higgless and the Standard Model $W^{\pm}Z$ and WW cross sections, figures 4.9 and 4.8.

While being perturbatively under good control, weak boson fusion processes provide insight into the nature of electroweak symmetry breaking mechanism as they access longitudinal gauge boson scattering, discussed in chapter 4 and appendix A, via distinct and clean signatures. Therefore, they are supposed to be excellent candidates to test the Higgsless model's phenomenology. In order to make quantitative predictions, the framework of the NLO-QCD parton-level monte carlo program VBFNLO was used and extended, to arrive at a fully-flexible and fast FORTRAN77 code that enabled the study of the Higgsless phenomenology in detail. For the sake of speed and numerical stability, a full FORTRAN77 implementation, based on available software, was relaxed in favor of a much faster numerical C++ integration, which then was interfaced with VBFNLO. As a byproduct the user can switch from the automatically and rather model-dependent generated masses and couplings, to her or his own set of calculated parameters. The details of the implementation have been presented in chapter 5.

Chapter 6 analyzes the model's phenomenology in detail, applying the modified version of Vbfnlo. Cross sections and significant distributions are compared to similar-appearing Standard Model scenarios. Generically, the Higgsless scenario exhibits a larger cross section than the fit-preferred light Higgs Standard Model and a smaller one compared to the Standard Model with an equally heavy Higgs. The lepton distributions' shapes are dominated by the heavy Kaluza-Klein states, whereas the jet distributions' shapes do not change considerably, except for the $W^{\pm}Z$ channel.

The impact of the NLO (zero mode) QCD corrections are found to be small, while the scale dependence is highly reduced. In fact, the characteristics of the NLO QCD corrections, which were presented in a series of publications for the SM case [38] generalize to the Higgsless scenario and weak boson fusion is perturbatively under excellent control, also in the Higgsless case. Consequently, the presented qualitative predictions are very stable.

With reservation concerning the lacking background study, the LHC requires approximately one year of running at high luminosity to detect the Kaluza-Klein resonance over the considered parameter range.

Appendix A

Gauge Boson Scattering

A.1 Unitarity Sum Rules

Kinematics

To work out the expansion of $\mathcal{A}$ in (4.3) we use the center of mass frame kinematics, fig. A.1

$$k^{\mu}_{1/2} = \begin{pmatrix} E_n \\ 0 \\ 0 \\ \pm p \end{pmatrix}, \quad k^{\mu}_{3/4} = \begin{pmatrix} E_n \\ 0 \\ \pm p \sin\theta \\ \pm p \cos\theta \end{pmatrix}$$

and longitudinal polarizations

$$\varepsilon^{\mu}(k_{1/2}) = \begin{pmatrix} p/m_n \\ 0 \\ 0 \\ \pm E_n/m_n \end{pmatrix}, \quad \varepsilon^{\mu}(k_{3/4}) = \begin{pmatrix} p/m_n \\ 0 \\ \pm E_n \sin\theta/m_n \\ \pm E_n \cos\theta/m_n \end{pmatrix}$$

with momentum $p^2 = E_n^2 - m_n^2$. Expressed in terms of the center of mass energy squared s and the scattering angle θ, energy and momentum read

$$E_n = \frac{\sqrt{s}}{2} \qquad p = \sqrt{\frac{s}{4} - {m_i}^2}$$

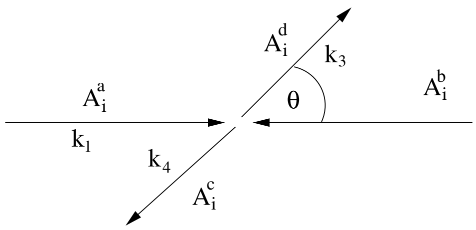

Figure A.1: Center-of-mass frame kinematics of $2 \to 2$.

Sum rules $\sim E^4$

Sum rules (4.6a), (4.6b) result from the completeness of the Kaluza-Klein wave functions along the fifth dimension, regardless of the gauge index.

$$\sum_k \psi^a_k(y)\psi^a_k(z) = \delta(y-z) \quad \text{no sum over } a \tag{A.1}$$

Consequently, dropping the gauge indices,

$$
\begin{aligned}
g_{ijkl} &= g_5^2 \int \mathrm{d}y\, \psi_i \psi_j \psi_k \psi_l = g_5^2 \int \mathrm{d}y \int \mathrm{d}y' \psi_i(y)\psi_j(y)\psi_k(y')\psi_l(y')\delta(y-y') \\
&= g_5^2 \sum_n \left(\int \mathrm{d}y\, \psi_i(y)\psi_j(y)\psi_n(y) \right) \left(\int \mathrm{d}y' \psi_k(y')\psi_l(y')\psi_n(y') \right) \\
&= \sum_k g_{ijn} g_{kln}
\end{aligned}
\tag{4.6a}
$$

R/y factors for anti-de Sitter models are absorbed into the definition of the measure $\mathrm{d}y$. Note that the sum rule does not depend on the chosen boundary conditions.

Sum rules $\sim E^2$

The sum rules (4.6b) are sensitive to the chosen boundary conditions and depend on the bulk equations of motion with respect to the extra dimension $\partial_y^2 \psi_n + m_n^2 \psi_n = 0$. In fact, they are only satisfied for either Dirichlet or Neumann boundary conditions. Completeness is again a key ingredient:

$$
\begin{aligned}
3 \sum_k m_k^2 g_{nnk}^2 &= 3 \sum_k m_k^2 g_{nnk} \int \mathrm{d}y\, \psi_n^2(y) \psi_k(y) \\
&\overset{\text{eqm}}{=} -3 \sum_k g_{nnk} \int \mathrm{d}y\, \psi_n^2(y) \psi_k''(y) \\
&\overset{\text{pi}}{=} -3 \sum_k g_{nnk} \int \mathrm{d}y\, \left[\psi_n^2(y)\right]'' \psi_k(y) \\
&= -6 \sum_k g_{nnk} \int \mathrm{d}y\, \left[\psi_n'(y)\right]^2 \psi_k + 6 m_n^2 g_{nnnn} \\
&= -6 \int \mathrm{d}y\, \left[\psi_n'(y)\right]^2 \psi_n^2(y) + 6 m_n^2 g_{nnnn}
\end{aligned}
$$

The first term in the last line can be simplified using the bulk equation of motion and partial integration:

$$
\begin{aligned}
\int \mathrm{d}y\, \left[\psi_n'\right]^2 \psi_n^2 &= -\int \mathrm{d}y\, \left[\psi_n^2 \psi_n'\right]' \psi_n = -2 \int \mathrm{d}y\, \left[\psi_n'\right]^2 \psi_n^2 - \int \mathrm{d}y\, \psi_n^3 \psi_n'' \\
&= -2 \int \mathrm{d}y\, \left[\psi_n'\right]^2 \psi_n^2 + m_n^2 \int \mathrm{d}y\, \psi_n^4
\end{aligned}
$$

Hence,

$$
3 \sum_k m_k^2 g_{nnk}^2 = 4 m_n^2 g_{nnnn} \tag{4.6b}
$$

The restriction to either Neumann or Dirichlet boundary conditions in Higgsless models can not be relaxed as terms arising from partial integration would spoil the sum rule.

A.1.1 Sum Rules in Physical Basis

So far mass splittings between W and Z have been neglected. The sum rules for WW scattering are the same as (4.6), however, the second sum rule for WZ scattering slightly changes. With E, the energy of the incoming W boson, and $\cos\theta = c$, the cosine of th scattering angle, the contribution of gauge boson s and u channel exchange is (an overall factor $m_Z^{-2} m_W^{-2}$ is omitted)

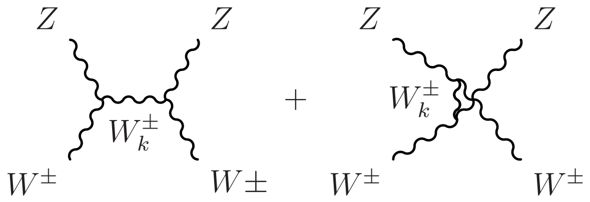

$$\sim -g^2_{W_k WZ}\Big\{ \big(c^2 - 6c - 3\big)\, E^4 \;\; - \big(c^2 - 10c - 3\big)\, m_W^2 E^2 + \big(c^2 - 2c - 3\big)\, m_Z^2 E^2 + (1-c)\left(\frac{3}{2} m_k^2 - \frac{(m_Z^2 - m_W^2)^2}{2m_k^2}\right) E^2 \Big\} + \mathcal{O}(E^0)$$

Together with the fourvertex

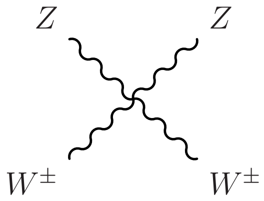

$$\sim g_{WWZZ}\Big(\big(c^2 - 6c - 3\big)\, E^4 - \big(c^2 - 9c - 4\big)\, m_W^2 E^2 + \big(c^2 - 3c - 2\big)\, m_Z^2 E^2\Big) + \mathcal{O}(E^0)$$

The modified WZ sum rules are

$$g_{WWZZ} = \sum_{k\geq 1} g^2_{W_k WZ} \tag{4.7a}$$

$$2(m_Z^2 + m_W^2) g_{WWZZ} = \sum_{k\geq 1} g^2_{W_k WZ}\left(3m_k^2 - \frac{(m_Z^2 - m_W^2)^2}{m_k^2}\right) \tag{4.7b}$$

A.2 Kaluza Klein Unitarity Constraints

Using the inverse of the definition of the ℓth partial wave

$$\mathcal{M}_{fi}(\cos\theta) = 32\pi \sum_\ell a_\ell^{fi} P_\ell(\cos\theta)$$

(the Legendre Polynomials are complete as solutions of a Sturm-Liouville problem) one can write

$$
\begin{aligned}
&\sum_{f(\sqrt{s})}\sum_{\ell} a_\ell^{fi}(a_\ell^{fj})^\star \\
&= \frac{1}{(32\pi)^2}\sum_{f(\sqrt{s})}\sum_{\ell}\iint \mathrm{d}\cos\theta\,\mathrm{d}\cos\theta' \mathcal{M}_{fi}(\cos\theta)\mathcal{M}^\star_{fj}(\cos\theta')P_\ell(\cos\theta)P_\ell(\cos\theta') \\
&= \frac{1}{2\pi(32\pi)^2}\sum_{f(\sqrt{s})}\int \mathrm{d}\Omega\,\mathcal{M}_{fi}\mathcal{M}^\star_{fi}
\end{aligned}
$$

Weighting the left side with $\tilde{\phi}_2^f = \phi_2/(4\pi)$ yields

$$
\sum_{f(\sqrt{s})}\sum_{\ell}\tilde{\phi}_2^f a_\ell^{fi}\left(a_\ell^{fj}\right)^\star = \frac{1}{4(32\pi)}\int \mathrm{d}\phi_2\,\mathcal{M}_{fi}\mathcal{M}^\star_{fi} = \frac{-i}{4(32\pi)}\left(\mathcal{M}_{ji}-\mathcal{M}^\star_{ij}\right) \tag{A.2}
$$

The Optical Theorem (4.9) was used in the last step. For a $2 \to 2$ process crossing symmetry yields

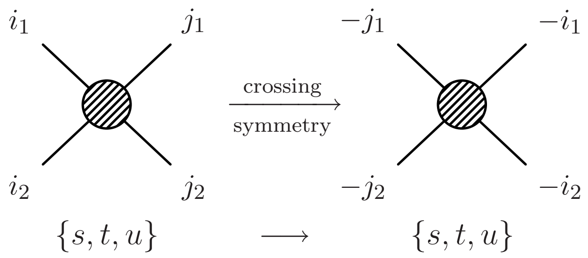

That is, $\cos\theta$ is invariant under the fully crossed longitudinal amplitude. Using again the inverse of the partial wave expansion, for forward scattering (A.2) reads

$$
\sum_{\ell}\left(\sum_{f(\sqrt{s})}\tilde{\phi}_2^f a_\ell^{fi}\left\{a_\ell^{fj}\right\}^\star - \frac{1}{2}\Im\{a_\ell^{ij}\}\right) = 0
$$

and as ℓ is conserved,

$$
\frac{1}{2}\Im\{a_\ell^{ij}\} = \sum_{f(\sqrt{s})}\tilde{\phi}_2^f a_\ell^{fi}\left\{a_\ell^{fj}\right\}^\star \tag{A.3}
$$

Writing $a_\ell^{ii} = |a_\ell^{ii}|\exp\{i\delta_\ell^{ii}\}$ and performing the relativistic limit $\tilde{\phi}_2(\sqrt{s}\to\infty) = 1/2$ yields

$$
\sum_{f(\sqrt{s})}\frac{|a_\ell^{fi}|^2}{|a_\ell^{ii}|} \leq 1 \tag{4.10}
$$

Appendix B

Programs

B.1 Masses and Couplings

Gauge boson masses

The mass defining equations (3.17), (3.18) are sinoidal functions with respect to the Planck brane localization R and the mass m. Thus, their zeros can be determined by *regula falsi* in a fast and accurate way. This is done for the determination of the TeV brane localization R' (4.8) given the W mass and R, and for the determination of the Kaluza-Klein masses given R and R'. The masses are stored in arrays `massw`, `massz`, and `massg`:

```
for (i=0;i<10;i++){
if (i==0) {a=77;}
else {a=mass[i-1]+50.;}
b=a;
do {b=b+10.;}
    while (Zeros(b,rup,rdwn)*Zeros(a,rup,rdwn)>0);
do {
  d=c;
  c=a-(b-a)/(Zeros(b,rup,rdwn)-Zeros(a,rup,rdwn))
       *Zeros(a,rup,rdwn);
  if(Zeros(a,rup,rdwn)*Zeros(c,rup,rdwn) > 0) {a=c;}
  if(Zeros(b,rup,rdwn)*Zeros(c,rup,rdwn) > 0) {b=c;}
    }
while (fabs(d-c) > 1e-10);
mass[i]=c;
}
```

Here, `Zeros` is the mass defining function and `mass` the respective array to be filled. For consistency, the code will abort if the input parameters m_W and m_Z are evaluated incorrectly as first massive modes of the towers.

Width-dependent sum rule violations

In fact, as `HELAS` uses Breit-Wigner propagators and VBFNLO involves off-shell gauge bosons, the sum rules have to be modified

$$m_n^2 \to m_n^2 - i\Gamma_n m_n \tag{B.1}$$

and the couplings and widths have to be calculated in a self-consistent way, eventually leading to small phase shifts between the different Feynman graphs. This also holds for the Standard Model implementation. However, the scattering processes are suppressed by kinematics at energy scales, at which the breaking of the second sum rule becomes sizable, which leaves negligible deviations from the 'straightforward' implementation. Nevertheless, the effect of (B.1) has been studied for a simplified scenario with only one additional Kaluza-Klein Z, fully saturated to the Standard Model WWZ coupling. The first sum rule balances the imaginary part of the couplings, thus, the overall effect is found to be negligible.

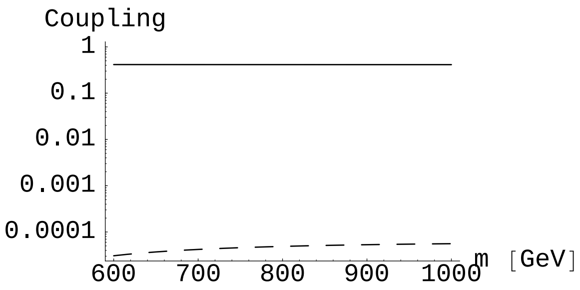

Figure B.1: Real and imaginary part of the saturated models' four vertex coupling plotted solid and dashed, respectively.

Effective couplings and normalizations

For the numerical integration several integration routines have been tested and compared. Adaptive algorithms like GNU Scientific Library's `QAG` and `QAGS` provide fast and accurate methods to evaluate the integrals (3.20), while non-adaptive algorithms like Numerical Recipes' `qromb` turned out to be either non-converging or extremely slow for the considered integrands. `Cernlibs`' integration routines are no longer fully maintained, so they do not offer a reliable option to Vbfnlo users and have been discarded in the comparison.

The Bessel Functions' coefficients are determined in terms of a single parameter using the masses from the arrays. This parameter is fixed by the numerically calculated normalization of the gauge boson wave function (3.22). The effective three- and fourvertices are calculated by integrating (3.21) and

$$g_{1111}^{WWVV} = g_5^2 \int_R^{R'} \mathrm{d}y \, \frac{R}{y} \sum_{i=L,R} \left\{ \psi_{W_1}^{(i)}(y) \psi_{W_1}^{(i)}(y) \psi_{V_1}^{(i)}(y) \psi_{V_1}^{(i)}(y) \right\} \qquad V = W, Z$$

The generalized $W_i W_j Z_k$ couplings needed for the partial widths are calculated accordingly. Throughout the integration is performed with small relative errors $< 10^{-7}\%$.

B.2 Partial Wave Analysis

The partial wave analysis was performed using modifications analogous to section 5.2. The Kaluza-Klein masses and couplings are included by calling `kk_coupl_inp`. For the cross section, the squared matrix elements, multiplied by the appropriate phase space factor, defines a function, which is integrated over the scattering angle by NUMERICAL RECIPES' `qromb` integration subroutine. The center of mass energy as the remaining free parameter is stored in a common block and is increased after every integration. For the partial waves, a function is defined that calls the modified `Madgraph` amplitude for longitudinal gauge boson polarizations and multiplies the corresponding Legendre polynomial. The center of mass energy is again inferred from the common block and the function's integration is performed with `qromb`.

Appendix C

Detector Resolution

To attain more realistic characteristics, the finite detector resolution has to be included into the analysis. These effects have major impact, not only on the distributions themselves, but also on the application of cuts. During the ROOT analysis this is respected by re-application of the cuts after 'smearing' the event. To mimic the effect of the detector resolution on the distributions, the event is multiplied by a detector acceptance function that is taken to be a Gaussian distribution with variances based on the CMS technical notes [44]. The variance for jets is

$$\frac{\Delta E}{E} = \begin{cases} 5.6\, E_{T,\mathrm{MC}}^{-1} \oplus 1.25\,\sqrt{E_{T,\mathrm{MC}}^{-1}} \oplus 0.033 & |\eta| < 1.4 \\ 4.8\, E_{T,\mathrm{MC}}^{-1} \oplus 0.89\,\sqrt{E_{T,\mathrm{MC}}^{-1}} \oplus 0.043 & 1.4 \leq |\eta| \leq 3.0 \\ 3.8\, E_{T,\mathrm{MC}}^{-1} \oplus 0.089 & 3.0 < |\eta| \leq 5.0 \end{cases} \tag{C.1a}$$

The variance for charged leptons is

$$\frac{\Delta E}{E} = 0.02 \tag{C.1b}$$

and for the $\not{E}_T$ measurements

$$\frac{\Delta \not{p}_{x,y}}{\not{p}_{x,y}} = 0.63\,\sqrt{\sum E_{T,\mathrm{MC}}} \tag{C.1c}$$

is applied. All components of the fourvectors are multiplied with equal factors to leave the invariant mass unchanged. $\not{p}_T$ is calculated by balancing the momenta in the transverse plane and is attributed to the neutrinos.

Appendix D

Important Input Parameters

The Standard Model particle masses and widths are

$$\begin{aligned} m_W &= 80.423\text{GeV} & \Gamma_W &= 2.100\text{GeV} \\ m_Z &= 91.188\text{GeV} & \Gamma_Z &= 2.510\text{GeV} \\ m_t &= 174.000\text{GeV} & \Gamma_t &= 1.380\text{GeV} \end{aligned}$$

Standard Model couplings are chosen

$$\begin{aligned} g_{WWZ}^{\text{SM}} &= 0.57615 \\ \alpha_{\text{QED}} &= 1/132.54 \\ \alpha_s(m_Z) &= 0.13244 \end{aligned}$$

The factorization scales of the CTEQ6l1 parton distribution functions [45] are chosen to fixed

$$\mu_F = \begin{cases} m_W & W^+W^- \text{ channel} \\ m_Z & ZZ \text{ channel} \\ \frac{1}{2}(m_W + m_Z) & W^\pm Z \text{ channel} \end{cases}$$

and for the NLO-QCD calculations the parton distributions of CTEQ6M are used.

Bibliography

[1] W. M. Yao *et al.* [Particle Data Group], "Review of particle physics," J. Phys. G **33** (2006) 1.

[2] J. Fuchs und C. Schweigert, "Symmetries, Lie Algebras and Representations," *Cambridge University Press, Cambridge, UK (2003)*

[3] C. Quigg, Lecture series on Electroweak Theory, University of Karlsruhe, 2006.

[4] L. Susskind, "Dynamics of spontaneous symmetry breaking in the Weinberg-Salam theory," Phys. Rev. D **20** (1979) 2619.
M. J. G. Veltman, "The infrared - ultraviolet connection," Phys. Rev. D **66** (2002) 010001.
A. A. Andrianov and N. V. Romanenko, "Vacuum fine tuning and empirical estimations of masses of the top quark and Higgs boson," Phys. Rev. D **66** (2002) 010001 [arXiv:`hep-ph`/9305252].

[5] S. P. Martin, "A supersymmetry primer," [arXiv:`hep-ph`/9709356].

[6] M. Schmaltz and D. Tucker-Smith, "Little Higgs review," Ann. Rev. Nucl. Part. Sci. **55** (2005) 229 [arXiv:`hep-ph`/0502182].
T. Han, H. E. Logan, B. McElrath and L. T. Wang, "Phenomenology of the little Higgs model," Phys. Rev. D **67** (2003) 095004 [arXiv:`hep-ph`/0301040].

[7] N. Arkani-Hamed, S. Dimopoulos and G. R. Dvali, "The hierarchy problem and new dimensions at a millimeter," Phys. Lett. B **429** (1998) 263 [arXiv:`hep-ph`/9803315].

[8] L. Randall and R. Sundrum, "A large mass hierarchy from a small extra dimension," Phys. Rev. D **66** (2002) 010001 [arXiv:`hep-ph`/9905221].

[9] T. Kaluza, "On the problem of unity in physics," Sitzungsber. Preuss. Akad. Wiss. Berlin (Math. Phys.) **1921** (1921) 966.
O. Klein, "Quantum theory and five-dimensional theory of relativity," Z. Phys. **37**, 895 (1926) [Surveys High Energ. Phys. **5**, 241 (1986)].

[10] R. Rattazzi, "Cargese lectures on extra dimensions," [arXiv:`hep-ph`/0607055].
M. J. Duff, "Kaluza-Klein Theory in perspective," [arXiv:`hep-th`/9410046].

[11] W. D. Goldberger and M. B. Wise, "Modulus stabilization with bulk fields," Phys. Rev. Lett. **83** (1999) 4922 [arXiv:`hep-ph`/9907447].

[12] M. Böhm, A. Denner and H. Joos, "Gauge theories of the strong and electroweak interaction," *Teubner, Stuttgart, Germany (2001)*
M. E. Peskin and D. V. Schroeder, "An Introduction To Quantum Field Theory," *Addison-Wesley, Reading, USA (1995)*

[13] K. Fujikawa, B. W. Lee and A. I. Sanda, "Generalized Renormalizable Gauge Formulation Of Spontaneously Broken Gauge Theories," Phys. Rev. D **6** (1972) 2923.

[14] C. Csaki, C. Grojean, H. Murayama, L. Pilo and J. Terning, "Gauge theories on an interval: Unitarity without a Higgs," Phys. Rev. D **69** (2004) 055006 [arXiv:hep-ph/0305237].

[15] R. Sekhar Chivukula, E. H. Simmons, H. J. He, M. Kurachi and M. Tanabashi, "Ideal fermion delocalization in Higgsless models," Phys. Rev. D **72** (2005) 015008 [arXiv:hep-ph/0504114].
G. Cacciapaglia, C. Csaki, C. Grojean and J. Terning, "Oblique corrections from Higgsless models in warped space," Phys. Rev. D **70**, 075014 (2004) [arXiv:hep-ph/0401160].

[16] H. Georgi, A. K. Grant and G. Hailu, "Brane couplings from bulk loops," Phys. Lett. B **506**, 207 (2001) [arXiv:hep-ph/0012379].

[17] R. Barbieri, A. Pomarol, R. Rattazzi and A. Strumia, "Electroweak symmetry breaking after LEP1 and LEP2," Nucl. Phys. B **703** (2004) 127 [arXiv:hep-ph/0405040].

[18] J. M. Maldacena, "The large N limit of superconformal field theories and supergravity," Adv. Theor. Math. Phys. **2** (1998) 231 [Int. J. Theor. Phys. **38** (1999) 1113] [arXiv:hep-th/9711200].
E. Witten, "Anti-de Sitter space and holography," Adv. Theor. Math. Phys. **2** (1998) 253 [arXiv:hep-th/9802150].
O. Aharony, S. S. Gubser, J. M. Maldacena, H. Ooguri and Y. Oz, "Large N field theories, string theory and gravity," Phys. Rept. **323** (2000) 183 [arXiv:hep-th/9905111].

[19] N. Arkani-Hamed, M. Porrati and L. Randall, "Holography and phenomenology," JHEP **0108** (2001) 017 [arXiv:hep-th/0012148].
R. Rattazzi and A. Zaffaroni, "Comments on the holographic picture of the Randall-Sundrum model," JHEP **0104** (2001) 021 [arXiv:hep-th/0012248].

[20] C. Csaki, C. Grojean, L. Pilo and J. Terning, "Towards a realistic model of Higgsless electroweak symmetry breaking," Phys. Rev. Lett. **92** (2004) 101802 [arXiv:hep-ph/0308038].

[21] M. E. Peskin and T. Takeuchi, "Estimation of oblique electroweak corrections," Phys. Rev. D **46** (1992) 381.

C. P. Burgess, S. Godfrey, H. Konig, D. London and I. Maksymyk, "Model Independent Global Constraints On New Physics," Phys. Rev. D **49** (1994) 6115 [arXiv:hep-ph/9312291].

[22] G. Cacciapaglia, C. Csaki, C. Grojean and J. Terning, "Curing the ills of Higgsless models: The S parameter and unitarity," Phys. Rev. D **71**, 035015 (2005) [arXiv:hep-ph/0409126].

[23] C. Csaki, C. Grojean, J. Hubisz, Y. Shirman and J. Terning, "Fermions on an interval: Quark and lepton masses without a Higgs," Phys. Rev. D **70** (2004) 015012 [arXiv:hep-ph/0310355].

[24] K. Agashe, R. Contino, L. Da Rold and A. Pomarol, "A custodial symmetry for Z b anti-b," Phys. Lett. B **641** (2006) 62 [arXiv:hep-ph/0605341].
G. Cacciapaglia, C. Csaki, G. Marandella and J. Terning, "A new custodian for a realistic Higgsless model," Phys. Rev. D **75** (2007) 015003 [arXiv:hep-ph/0607146].

[25] N. Arkani-Hamed, A. G. Cohen and H. Georgi, "(De)constructing dimensions," Phys. Rev. Lett. **86** (2001) 4757 [arXiv:hep-th/0104005].

[26] A. Manohar and H. Georgi, "Chiral Quarks And The Nonrelativistic Quark Model," Nucl. Phys. B **234** (1984) 189.
Z. Chacko, M. A. Luty and E. Ponton, "Massive higher-dimensional gauge fields as messengers of supersymmetry breaking," JHEP **0007** (2000) 036 [arXiv:hep-ph/9909248].

[27] H. Abe, T. Kobayashi, N. Maru and K. Yoshioka, "Field localization in warped gauge theories," Phys. Rev. D **67** (2003) 045019 [arXiv:hep-ph/0205344].

[28] R. Foadi, S. Gopalakrishna and C. Schmidt, "Higgsless electroweak symmetry breaking from theory space," JHEP **0403** (2004) 042 [arXiv:hep-ph/0312324].
E. H. Simmons, R. S. Chivukula, H. J. He, M. Kurachi and M. Tanabashi, "Higgsless models: Lessons from deconstruction," AIP Conf. Proc. **857** (2006) 34 [arXiv:hep-ph/0606019].

[29] H. Davoudiasl, J. L. Hewett, B. Lillie and T. G. Rizzo, "Higgsless electroweak symmetry breaking in warped backgrounds: Constraints and signatures," Phys. Rev. D **70** (2004) 015006 [arXiv:hep-ph/0312193].

[30] R. S. Chivukula, E. H. Simmons, H. J. He, M. Kurachi and M. Tanabashi, "Deconstructed Higgsless models with one-site delocalization," Phys. Rev. D **71** (2005) 115001 [arXiv:hep-ph/0502162].
R. Foadi, S. Gopalakrishna and C. Schmidt, "Effects of fermion localization in Higgsless theories and electroweak constraints," Phys. Lett. B **606** (2005) 157 [arXiv:hep-ph/0409266].

[31] J. M. Cornwall, D. N. Levin and G. Tiktopoulos, "Derivation Of Gauge Invariance From High-Energy Unitarity Bounds On The S Matrix," Phys. Rev. D **10** (1974) 1145 [Erratum-ibid. D **11** (1975) 972].

[32] M. Jacob and G. C. Wick, "On the general theory of collisions for particles with spin," Annals Phys. **7** (1959) 404 [Annals Phys. **281** (2000) 774].

[33] M. Galassi *et al.*, "GNU Scientific Library Reference Manual (2nd Ed.)," *Network Theory Limited, Bristol, UK (2003)*

[34] H. Murayama, I. Watanabe and K. Hagiwara, "HELAS: HELicity amplitude subroutines for Feynman diagram evaluations," [KEK-91-11]

[35] T. Stelzer and W. F. Long, "Automatic generation of tree level helicity amplitudes," Comput. Phys. Commun. **81** (1994) 357 [arXiv:hep-ph/9401258].

[36] W. H. Press, S. H. Teukolsky, W. T. Vetterling and B. P. Flannery "Numerical Recipes in Fortran 77 (2nd Ed.)," *Cambridge University Press, Cambridge, UK (1992)*

[37] M. Papucci, "NDA and perturbativity in Higgsless models," [arXiv:hep-ph/0408058].

[38] G. Bozzi, B. Jager, C. Oleari and D. Zeppenfeld, "Next-to-leading order QCD corrections to W^+Z and W^-Z production via vector-boson fusion," Phys. Rev. D **75** (2007) 073004 [arXiv:hep-ph/0701105].
B. Jager, C. Oleari and D. Zeppenfeld, "Next-to-leading order QCD corrections to Z boson pair production via vector-boson fusion," Phys. Rev. D **73** (2006) 113006 [arXiv:hep-ph/0604200].
B. Jager, C. Oleari and D. Zeppenfeld, "Next-to-leading order QCD corrections to W^+W^- production via vector-boson fusion," JHEP **0607** (2006) 015 [arXiv:hep-ph/0603177].

[39] K. Hagiwara and D. Zeppenfeld, "Amplitudes for Multiparton Processes Involving a Current at $e^+e^-, e^\pm p$, and Hadron Colliders," Nucl. Phys. B **313** (1989) 560.

[40] J. Bagger *et al.*, "The Strongly interacting W W system: Gold plated modes," Phys. Rev. D **49** (1994) 1246 [arXiv:hep-ph/9306256].
J. Bagger *et al.*, "LHC analysis of the strongly interacting W W system: Gold plated modes," Phys. Rev. D **52** (1995) 3878 [arXiv:hep-ph/9504426].

[41] D. Zeppenfeld, "Collider physics," [arXiv:hep-ph/9902307].
D. L. Rainwater, "Intermediate-mass Higgs searches in weak boson fusion," [arXiv:hep-ph/9908378].

[42] A. Birkedal, K. Matchev and M. Perelstein, "Collider phenomenology of the Higgsless models," Phys. Rev. Lett. **94** (2005) 191803 [arXiv:hep-ph/0412278].

[43] T. Plehn, D. L. Rainwater and D. Zeppenfeld, "A method for identifying $H \to \tau\tau \to e^\pm\mu^\mp \not{p}_T$ at the CERN LHC," Phys. Rev. D **61** (2000) 093005 [arXiv:hep-ph/9911385].

[44] H. Pi *et al.* [CMS Collaboration], "Measurement of Missing Transverse Energy with the CMS Detector at the LHC," [CMS Note 2006/035]
A. Heister *et al.* [CMS Collaboration], "Measurement of Jets with the CMS Detector at the LHC," [CMS Note 2006/036]

[45] J. Pumplin, D. R. Stump, J. Huston, H. L. Lai, P. Nadolsky and W. K. Tung, "New generation of parton distributions with uncertainties from global QCD analysis," JHEP **0207** (2002) 012 [arXiv:hep-ph/0201195].

Zusammenfassung

Das Standardmodell der Elementarteilchenphysik (SM) beschreibt Quantenchromodynamik und elektroschwache Theorie konsistent vereint als eine auf der Eichgruppe $SU(3)_C \times SU(2)_L \times U(1)_Y$ basierende, spontan gebrochene chirale Quantenfeldtheorie. Auf den bisher zugänglichen Energieskalen erwies sich das Standardmodell als erstaunlich gutes Modell, das bislang allen experimentellen Tests standhalten konnte. Vorhersagen, wie die Existenz neutraler Ströme, ein durch Anomaliefreiheit motiviertes Auftreten von jeweils ganzen Generationen von Quarks und Leptonen und experimentell bestätigte Relationen zwischen den verschiedenen Kopplungskonstanten und Eichbosonmassen sind nur einige Gründe dafür, warum das Standardmodell als effektiver Niederenergielimes fest etabliert ist und an einer möglichen Beschreibung der Natur durch lokale Eichtheorien kaum noch gezweifelt wird.

Ein fundamentaler Bestandteil des Standardmodells jedoch, das Higgs-Boson, ein skalares Überbleibsel der elektroschwachen Symmetriebrechung, das unter anderem für Unitarität im Rahmen des Standardmodells verantwortlich ist, verbleibt bislang unentdeckt. Dies ist nur eines von vielen Argumenten, teils physikalischer, teils philosophischer Natur, die gegen den Standardmodell-Higgs-Sektor sprechen und in den letzten Jahren zu einer Vielfalt an Modellen jenseits des Standardmodells geführt haben.

Neben den klassischen Lösungen der elektroschwachen Symmetriebrechung wie dem Standardmodell, der minimal supersymmetrischen Erweiterung des Standardmodells und stark gekoppelten Technicolor-Modellen, haben vor allem sogenannte Little-Higgs Modelle und Szenarien mit extra Dimensionen viel an theoretischer Aufmerksamkeit gewonnen. Besonders drastisch erscheinen dabei Vorschläge, in denen das Higgs vollständig aus dem Teilchenspektrum verschwindet und Symmetrie geometrisch gebrochen wird. Diese Modellklasse umgeht Probleme des Standardmodell-Higgs und bietet Lösungen für einige noch unbeantwortete Fragen, wie z.B. Hierarchieproblem und Flavorhierarchie. Unitaritätsverletzung wird dabei durch den Austausch schwerer Kopien von $W^{\pm}$- und Z Bosonen zu einer wesentlich höheren Skala im Vergleich zum Standardmodell ohne Higgs verschoben. Das Auftreten dieser neuen Teilchen an der TeV Skala, verbunden mit den für sie charakteristischen Signaturen, stellt eine am *Large Hadron Collider* (CERN/Genf) überprüfbare Vorhersage dieser Modellklasse dar. Gegenstand dieser Arbeit ist die Vorhersagen dieser Modelle für Vektorbosonfusionsprozesse, die für eine modellunabhängige, phänomenologische Untersuchung der elektroschwachen Symmetriebrechung gut geeignet sind: Da sie als eigentliche Fusionskanäle (Abbildung 5.1) longitudinale Eichbosonstreuung beinhaltet, sind sie sensitiv auf den elektroschwachen Brechungssmechanismus. Bei entsprechenden Phasenraumschnitten (Kapitel 6.1) bieten sie ausserdem ein äusserst gutes Signal-zu-Hintergrundverhältnis und stellen daher Hauptentdeckungskanäle für das Higgs Boson am LHC dar.

Kapitel 2 gibt einen Überblick über die elektroschwache Symmetriebrechung im

Rahmen des Standardmodells und unterstreicht den experimentell nachgewiesenen und daher modelbauerisch notwendigen Aspekte einer ungefähr globalen, überbleibenden $SU(2)$ Symmetry des Higgssektors nach der Symmetriebrechung. Anschliessend wird das Hierarchie Problem vorgestellt, das die Hauptmotivation für Modellentwürfe jenseits des Standardmodells darstellt und diskutiert, in welcher Form insbesondere Theorien mit extra Dimensionen zu einer Lösung desselben führen können. Hier tritt speziell das sogenannte Randall-Sundrum Szenario RS1 [8] hervor, in dem die beobachtete Skalenhierarchie $\langle H \rangle \ll M_{\text{Planck}}$ durch Lokalisierung der Gravitation in ein experimentell bisher unzugänglichen Bereich des zugrunde liegenden fünfdimensionalen Raumes gelöst wird. Neben einer dualen Interpretation im Rahmen einer stark gekoppelten Konformen Feldtheorie, die Technicolor Theorien stark ähnelt, bietet das Randall-Sundrum Modell auch die Möglichkeit, das Higgsfeld in einen redundanten Freiheitsgrad zu verwandeln, indem den verbleibenden Standardmodellfeldern gestattet wird, in die zusätzliche, kompaktifizierte Dimension zu propagieren. Das Higgs verschwindet aus dem Teilchenspektrum, wobei es Randbedingungen an die Eichfelder an den Rändern der extra Dimension hinterlässt, die schlussendlich für die Symmetriebrechung verantwortlich sind. Zusammen mit den Bewegungsgleichungen entlang der fünften Dimension definieren diese Randbedingungen ein reguläres Sturm-Liouville Randwertproblem, d.h. das Teilchenspektrum wird durch abzählbar unendlich viele, zusätzliche Kaluza-Klein $W^{\pm}$ und Z Bosonen erweitert, die gerade den Hilbertraum der Lösungsmenge aufspannen.

Von besonderer Wichtigkeit sind dabei die Vollständigkeit der Lösungen und die durch die Higgs-Entkopplung resultierenden Randbedingungen die den Charakter einer spontanen Symmetrybrechung gewährleisten und für ein gutartiges Hochenergieverhalten von longitudinalen Eichbosonstreuprozessen verantwortlich sind.

Modelle mit komplizierterer Symmetriebrechung als mit Hilfe von Dubletts tendieren zu Konflikten mit elektroschwachen Präzissionsmessungen, und so bildet auch die higgslose Realisierung keine Ausnahme. Besonders die grosse Abweichung des S Parameters von ungefähr null, $|S| \approx 1$, die das higgslose Modell von seiner dualen Technicolor Interpretation erbt, können durch stark unterdrückte Kopplungen der Kaluza-Klein Bosonen an die Standard Modell Fermionmoden vermieden werden [1, 15]. In Kapitel 3 wurde dieses higgslose Symmetriebrechung ausführlich besprochen und die notwendigen Modifikation des Fermionsektors anhand des in dieser Arbeit betrachteten Modells (Abbildung 3.1) vorgestellt. Da höherdimensionale Eichtheorien intrinsisch nichtrenormierbar sind (Massendimension der Eichkopplungskonstanten $[g^{d>4}] < 0$) können Theorien mit zusätzlichen Raumdimensionen, in denen Eichfelder propagieren jedoch nicht ohne Vorbehalt als fundamental betrachtet werden. Eine UV-Erweiterung des Modells hin zu einer vollständig renormierbaren, vierdimensionalen Produktgruppeneichtheorie durch dimensionale (De)Konstruktion [25] bildet deshalb den Abschluss der Einführung in die higgslose Brechung.

Der Parameterbereich des vorgestellten Modells wurde mit Hilfe eines dafür erstellten C++ Programms untersucht und quantitative Vorhersagen an Kaluza-Klein Massen und - Kopplungen getroffen. Schranken an den Gültigeitsberich aufgrund von Unitaritätsverletzung in longitudinaler WZ-Streuung wurden ebenfalls vorgestellt. Es zeigt sich, dass dieser, anders als im Standard Modell, nicht durch Verletzen der

Schranke an die nullte Partialwellen $\Re|a_0| \leq 1/2$ gegeben ist, sondern durch die Zugänglichkeit inelastischer Kanäle bestimmt wird. Die Anwendung naiver dimensionaler Analyse [26] erlaubt eine quantitative Aussage über die Grösse der Skala der Unitaritätsverletzung $2.8\text{TeV} \lesssim \Lambda \lesssim 4.6\text{TeV}$ für $1200\text{GeV} \gtrsim m_{W^2} \gtrsim 630\text{GeV}$. Leichtere Kaluza-Klein Spektren besitzen dabei höhere Skalen, da sie kinematisch eher dazu in der Lage sind, den starken Anstieg longitudinaler Eichbosonstreuung bei ungefähr einem TeV abzuschwächen. Ein Vergleich von totalen higgslosen und Standardmodell $W^\pm Z$ und W^+W^- Wirkungsquerschnitten, Abbildungen 4.9 und 4.8, deutet die deutlich unterschiedliche Phänomenologie der beiden Modelle an.

Um diese Vermutungen letztlich konkretisieren zu können wurde das Fortran77 Programm Vbfnlo als Grundgerüst benutzt und der Fragestellung entsprechend erweitert. Um numerische Stabilität, Geschwindigkeit und Benutzerfreundlichkeit zu gewährleisten wurde auf eine komplette Fortran77 Umsetzung, auf Basis bestehender Software verzichtet und Vbfnlo mit oben genanntem C++ Programm verbunden. Als Nebeneffekt verbleibt dem Benutzer die Möglichkeit, die automatisch generierten Parameter durch eigens errechnete zu ersetzen. Die Details der Fortran77 Implementierung des Modells und des Kopplungs- und Massen C++ Programms wurden in Kapitel 5 besprochen.

Im Vergleich zum Standardmodell besitzt das higgslose Model eine deutlich unterschiedliche Phänomenologie (Kapitel 6), die in VBF Prozessen, wie das Standard Modell, pertubativ äusserst stabil ist. Besonders der Vergleich der Kanäle mit unterschiedlicher Resonanzstruktur erzeugt stark abweichende Vorhersagen an LHC Daten für einen kurzen Messungszeitraum. Die Auswirkungen von QCD Korrekturen in beide Modellen fallen vergleichsweise gering und ähnlich aus, d.h. die Ergebnisse früherer Standard Modell-bezogener Untersuchungen [38] verallgemeinern sich auf den higgslosen Fall.

Ein zweifelsfreie Identifizierung des higgslosen Modells durch die Messung des Kaluza-Klein Spektrums, allein in Vektorbosonfusion, wird durch durch die schnelle Konvergenz oben genannter Summenregeln unmöglich; höhere Moden sind schlichtweg zu schwach gekoppelt um Spuren in den Verteilung zu hinterlassen.

Unter Vorbehalt einer nicht durchgeführten Hintergrundstudie wird das LHC Experiment ungefähr ein Jahr Laufzeit bei hoher Luminosität benötigen, um die Kaluza-Klein Resonanz über den gesamten betrachteten Parameterbereich des vorgestellten Modells nachzuweisen oder auszuschliessen.

Danksagung

In erster Linie möchte ich mich bei Herrn Zeppenfeld für die Möglichkeit bedanken, meine Diplomarbeit auf einem genauso hochaktuellen wie spannenden Themengebiet anfertigen zu können. Dankbar bin ich auch für die gute Betreuung und den mir eingräumten Freiraum, der es mir stets gestattete, abseits meines Arbeitstitels viel über die aktuelle Teilchenphysik zu lernen.

Bei Herrn Nierste bedanke ich mich für seine Bereitschaft, das Koreferat zu übernehmen.

Allen Institutsangehörigen gilt mein Dank für die gleichermaßen ungezwungene wie professionelle Atmosphäre und natürlich auch für das Beantworten unzähliger Fragen. Besonders möchte ich mich dabei bei Manuel Bähr und Gunnar Klämke bedanken, von deren RooT Kenntnisse ich viel gelernt und profitiert habe. Bei meinen Mitdiplomanden und Bürokollegen Christoph Hackstein, Jan Germer und Matthias Werner möchte ich mich für die zahllosen und lehrreichen Diskussionen, auch ausserhalb der Universität, herzlich bedanken. Bei Jan Germer insbesondere für das Korrekturlesen.

Simon Plätzer danke ich, stellvertretend für die Systemadministratoren, für die Wartung und Bereitstellung einer funktionierenden IT-Infrastrukturt.

Zu guter letzt gilt mein größter Dank meinen Eltern, die mir ohne wenn und aber über mein gesamtes Studium Unterstützung und Rückhalt boten und mir damit diese Arbeit ermöglichten.